

Aus dem Bereich Physiologie
Theoretische Medizin und Biowissenschaften
der Medizinischen Fakultät
der Universität des Saarlandes, Homburg/Saar

**Identification of adenosine as an inflammatory mediator
triggering astrocyte reactivity to drive the pathogenesis of
sepsis-associated encephalopathy**

Dissertation

zur Erlangung des Grades eines Doktors der Naturwissenschaften

**der Medizinischen Fakultät
der Universität des Saarlandes**

2024

vorgelegt von: Qilin Guo
geb. am: 26. February 1990 in Shandong, China

Date of oral examination: 30. August 2024

Dean of the faculty: **Univ.-Prof. Dr. med. Michael D. Menger**

Examinants: **Prof. Dr. Frank Kirchhoff** - University of Saarland

Prof. Dr. Markus Hoth - University of Saarland

Prof. Dr. Thomas Volk - University of Saarland

This work was supported by grants from the Deutsche Forschungsgemeinschaft (HU 2614/1-1, Sino-German joint project KI 503/14-1), the Fritz Thyssen Foundation (10.21.1.021MN) and the Medical Faculty of the University of Saarland (HOMFORexzellent2016).

Contents

List of Abbreviations.....	i
List of Figures	iii
List of Tables.....	v
1. ABSTRACT	1
2. ZUSAMMENFASSUNG	3
3. INTRODUCTION.....	4
3.1. Sepsis and sepsis-associated encephalopathy	4
3.2. Animal model of septic inflammation	6
3.3. Main features of sepsis-associated encephalopathy	6
3.3.1. Blood-brain barrier dysfunction in sepsis-associated encephalopathy	6
3.3.2. Astrocyte reactivity in sepsis-associated encephalopathy.....	8
3.3.3. Microglia reactivity in sepsis-associated encephalopathy	9
3.4. Adenosine signaling in physiology and pathophysiology	11
4. AIMS OF THE STUDY	14
5. MATERIALS AND METHODS	15
5.1. Materials	15
5.1.1. Chemicals, reagents, and kits.....	15
5.1.2. Devices	15
5.1.3. Buffers and aqueous solutions	16
5.1.4. Enzymes	17
5.1.5. Drugs and Dyes.....	18
5.1.6. Antibodies.....	18
5.2. Methods.....	21
5.2.1. Animals	21
5.2.2. Genotyping.....	21
5.2.3. Tamoxifen and lipopolysaccharide preparation and administration	22
5.2.4. Plasma adenosine measurement	22
5.2.5. BBB permeability by Evans blue.....	22
5.2.6. Stereotactic injections of adeno-associated viruses.....	23
5.2.7. Pharmacological analysis of adenosine signaling	23
5.2.8. Cranial window implantation.....	23
5.2.9. <i>In vivo</i> imaging of extracellular adenosine levels	23
5.2.10. Reverse transcription-polymerase chain reaction (RT-PCR).....	24
5.2.11. Immunohistochemistry.....	24

5.2.12. Image acquisition and analysis.....	24
5.2.13. Ribosome immunoprecipitation (IP).....	25
5.2.14. Next-generation RNA sequencing	25
5.2.15. RNA-seq data processing.....	25
5.2.16. Cytokine expression analysis	26
5.2.17. Acute brain slice preparation	26
5.2.18. Ca ²⁺ imaging in hippocampal slices.....	26
5.2.19. Electrophysiology of brain slices (LTP).....	27
5.2.20. Behavior test	27
5.2.21. <i>In vivo</i> activation of hM4Di.....	27
5.2.22. Statistics and reproducibility	28
6. RESULTS.....	29
6.1. Systemic inflammation augmented adenosine levels in the blood and brain.	29
6.2. Peripheral administration of adenosine activated astrocytic A1ARs and induced neuroinflammation.	32
6.3. A1AR signaling promoted the inflammatory reactivity of astrocytes in the early phase of systemic inflammation.	37
6.4. Astrocyte reactivity in the early phase of systemic inflammation boosted the inflammatory response of microglia as well as global neuroinflammation.....	41
6.5. Astrocytic A1AR signaling activation impaired BBB integrity in systemic inflammation.	45
6.6. A1AR-mediated astrocyte activation promoted aberrant neuronal functions and depression-like behavior in systemic inflammation.....	46
6.7. Enhancing Gi signaling in A1AR-deficient astrocytes restored neuroinflammation upon peripheral LPS challenge.	48
7. DISCUSSION.....	51
7.1. Peripheral and central adenosine signaling involves neuroinflammation.....	51
7.1.1. Extracellular adenosine generation in neuroinflammation.....	51
7.1.2. Elevated humoral adenosine level directly enhances central extracellular adenosine level.....	Error! Bookmark not defined.
7.2. Adenosine signaling provokes neuroinflammation via astrocytic A1ARs.....	51
7.3. Loss of astrocytic A1ARs attenuate LPS induced neuroinflammation.....	52
7.3.1. A1AR activation was involved in fast astrocyte reactivity to systemic inflammation.	52
7.3.2. Astrocyte-microglia interaction in neuroinflammation.	53
8. CONCLUSION.....	55
9. APPENDIX.....	56
10. REFERENCES.....	66

11. ACKNOWLEDGEMENTS	81
12. CURRICULUM VITAE AND LIST OF PUBLICATIONS.....	82

List of Abbreviations

2P-LSM	Two-photon laser-scanning microscope
A1AR	Adenosine A1 receptor
AAV	Adeno-associated virus
ACSF	Artificial cerebral spinal fluid
AMPK	AMP-activated protein kinase
ANOVA	Analysis of variance
AR	Adenosine receptor
ATP	Adenosine triphosphate
BBB	Blood-brain barrier
BCA	Bicinchoninic Acid
BSA	Bovine serum albumin
CCL2	C-C motif chemokine ligand 2
cKO	Conditional knockout
CNS	Central nervous system
ctl	Control
CXCL1	Chemokine (C-X-C motif) ligand 1
CXCL8	Chemokine (C-X-C motif) ligand 8
ddH ₂ O	Ultrapure water
DEG	Differentially expressed gene
DNA	Deoxyribonucleic acid
ECM	Extracellular matrix
ENT	Equilibrative nucleoside transporter
F.I.	Fluorescence intensity
fEPSP	Field excitatory postsynaptic potentials
G-CSF	Granulocyte colony-stimulating factor
GFAP	Glial fibrillary acidic protein
GO	Gene ontology
GPCR	G protein-coupled receptor
GRAB _{ATP}	Genetically modified ATP sensor
ICAM1	Intracellular adhesion molecule 1
ICAM2	Intracellular adhesion molecule 2
IL-1 α	Interleukin-1 alpha
IL-1 β	Interleukin-1 beta
IL-6	Interleukin-6
iNOS	Inducible nitric oxide synthase
IP	Immunoprecipitation
KEGG	Kyoto Encyclopedia of Genes and Genomes
LCN-2	Lipocalin- 2
LPS	Lipopolysaccharide
LTP	Long-term potentiation
MMP	Matrix metalloproteinase
MS	Multiple sclerosis
n	Number
NGS	Next Generation Sequencing
NOD2	Nucleotide-binding oligonucleotide 2
PD	Parkinson disease

PECAM	Platelet endothelial cell adhesion molecule
PFA	Paraformaldehyde
PRR	Pattern recognition receptor
ROA	Regions of activity
ROI	Regions of interest
ROS	Oxygen-containing reactive species
RT	Room temperature
RT-PCR	Reverse transcription-polymerase chain reaction
SAE	Sepsis-associated encephalopathy
SLC	Solute carrier
TAM	Tamoxifen
TBS3	Triple θ -burst stimulation
TJ	Tight junction
TLR	Toll-like receptor
TNF- α	Tumor necrosis factor-alpha
VCAM-1	Vascular cell adhesion molecule 1
W	Week
wt	Wild-type

List of Figures

Figure 1. Global sepsis incidence in 2017 (Rudd et al., 2020).	4
Figure 2. Schematic pathophysiological alterations in sepsis-associated encephalopathy.	5
Figure 3. Blood-brain barrier dysfunction in sepsis-associated encephalopathy.	7
Figure 4. Roles of astrocyte in sepsis-associated encephalopathy	8
Figure 5. Roles of microglia in sepsis-associated encephalopathy	10
Figure 6. Extracellular and intracellular pathways regulating adenosine production, and clearance.	12
Figure 7. Transcriptomic profile of ARs gene expressions in CNS cells.	12
Figure 8. Peripheral LPS challenge altered the gene expression of glial markers as well as chemokines and cytokines.....	29
Figure 9. Peripheral LPS challenge increased adenosine levels in the blood.	30
Figure 10. Peripheral LPS challenge increased adenosine levels in the brain.	31
Figure 11. Plasma adenosine contributed to the increase of adenosine levels in the brain.....	32
Figure 12. Peripheral adenosine, NECA, CPA administration evoked inflammation-related genes expression in the brain.....	33
Figure 13. A1AR involved in upregulating inflammation-related genes in the brain.....	34
Figure 14. Generation and validation of astrocyte-specific A1AR deficient mice by qPCR and RNA-seq.....	35
Figure 15. Validation of astrocyte-specific A1AR deficient mice by Ca ²⁺ imaging.....	36
Figure 16. Astrocytic A1AR promoted inflammation-relative gene expression.....	37
Figure 17. A1AR-deficient astrocytes were less reactive to the peripheral LPS challenge.	37
Figure 18. Transcriptional profile of astrocyte after systemic LPS challenge.....	38
Figure 19. A1AR activation shaped the astrocytic transcriptional profile after systemic LPS challenge.	39
Figure 20. Expression changes of A1/A2 astrocyte marker gene expression in A1AR-deficient astrocytes post LPS injection.	40
Figure 21. Pathway analysis of RNA-seq data obtained from cortical astrocytes of A1AR-deficient and ctl mice post LPS injection.....	42
Figure 22. Astrocytic A1AR deficiency inhibited microglial p65 expression after LPS challenge.....	43
Figure 23. Astrocytic A1AR deficiency reduced microglial lysosomes after LPS challenge.	43
Figure 24. Astrocytic A1AR deficiency inhibited microglial activation and global neuroinflammation upon peripheral LPS challenge.....	44
Figure 25. Astrocytic A1AR deficiency inhibited global neuroinflammation at 6 hpi upon peripheral LPS challenge.	45

Figure 26. Astrocytic A1AR deficiency reduced BBB disruption and neutrophil infiltration post peripheral LPS injection.....	46
Figure 27. Astrocytic A1AR deficiency prevented aberrant neuronal hyperactivation after LPS treatment.	47
Figure 28. Astrocytic A1AR deficiency protected LTP of the mice after LPS treatment..	47
Figure 29. Astrocytic A1AR deficiency ameliorated depression-like behavior of the mice after LPS treatment.	48
Figure 30. Activation of Gi signaling in A1AR-deficient astrocytes restored the astrocytic and microglial response to peripheral LPS challenge.	49
Figure 31. Activation of Gi signaling in A1AR-deficient astrocytes restored global inflammation to peripheral LPS challenge.	50
Figure 32. Activation of Gi signaling in A1AR-deficient astrocytes restored the depression-like behavior of mice to peripheral LPS challenge.	50

List of Tables

Table 1. List of devices	15
Table 2. List of drugs	18
Table 3. List of primary antibodies	18
Table 4. List of secondary antibodies.....	19
Table 5. List of primers	20
Table 6. PCR reaction protocols	22

1. ABSTRACT

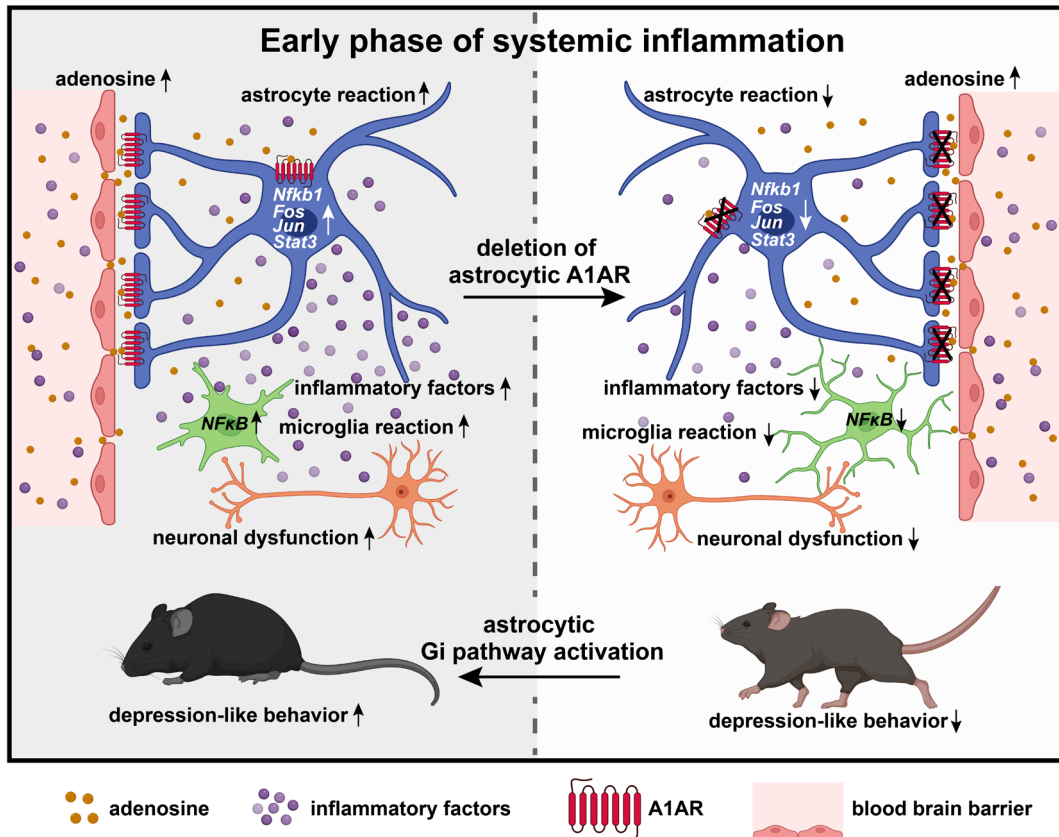
Infectious diseases, such as COVID-19, can cause severe systemic inflammation, which may even deteriorate to a life-threatening status called sepsis. Although it is immune-privileged due to its protection by the blood brain barrier, the central nervous system demonstrates rapid responses to systemic inflammation. Previous studies suggest immune signals of systemic inflammation can be mediated by increased humoral proinflammatory cytokines to induce inflammatory responses in the brain. In addition to cytokines, many metabolites such as purines are also upregulated when responding to systemic inflammation, though their contributions to neuroinflammation are still unclear.

Here, we show that systemic inflammation induced by peripheral endotoxin lipopolysaccharide (LPS) could rapidly elevate the plasma adenosine level with reaching its peak at 6 hours post LPS injection (hpi). Using *in vivo* 2P-LSM live imaging of a novel adenosine sensor GRAB_{Ado} expressed in astrocytes, we revealed that peripheral administration of adenosine could directly enhance the GRAB_{Ado} signal in the brain, suggesting that elevated blood levels of adenosine could increase the extracellular adenosine tone in the brain parenchyma. Furthermore, we detected elevated extracellular adenosine levels in terms of increased GRAB_{Ado} signal in the cortex of mice shortly after LPS injection which also peaked at 6 hpi. These results strongly suggest adenosine in the blood can contribute to the extracellular adenosine signal in the brain evoked by systemic inflammation. Combining pharmacological intervention, immunohistochemistry, genetic RiboTag technology and high-throughput RNA sequencing, cytokine array, quantitative PCR, Western blot, and IMARIS-assisted image analysis, we showed that increased adenosine could trigger astrocyte reactivity at the early phase (2-6 hpi) of the systemic inflammation.

Using transgenic mouse models, we deleted A1 adenosine receptors (A1ARs), which are Gi/o-coupled, specifically in astrocytes. After a peripheral injection of LPS into these mice, we observed inhibition of an early astrocyte reactivity and reduced expression of proteins related to neuroinflammation (such as CCL2, CCL5, and CXCL1). Subsequently, we found a decrease in microglial activation, less disruption of the blood-brain barrier, improved neuronal functions, and ultimately mitigated depression-like behavior induced by systemic inflammation. We further expressed CNO-mediated hM4Di DREADD stimulation in A1AR-deficient astrocytes at 2 and 4 hpi restored the neuroinflammation and depression-like behavior of the astrocytic-A1AR deficient mice, highlighting astrocytes rather than microglia as early drivers of neuroinflammation.

Taken together, our work unveils an important immune-mediated pathway, adenosine signalling via A1ARs, which provokes neuroinflammation by triggering early astrocyte reactivity in systemic inflammation of mice.

GRAPHICAL ABSTRACT



2. ZUSAMMENFASSUNG

Infektionskrankheiten wie COVID-19 können schwere systemische Entzündungen hervorrufen, die sich sogar zu einem lebensbedrohlichen Zustand, der Sepsis, ausweiten können. Obwohl es aufgrund des Schutzes durch die Blut-Hirn-Schranke (BHS) immunprivilegiert ist, reagiert das zentrale Nervensystem (ZNS) schnell auf systemische Entzündungen. Frühere Studien deuten darauf hin, dass Immunsignale einer systemischen Entzündung durch erhöhte humorale proinflammatorische Zytokine vermittelt werden können, um Entzündungsreaktionen im ZNS auszulösen. Neben Zytokinen werden auch viele Metabolite wie Purine als Reaktion auf systemische Entzündungen hochreguliert, obwohl ihr Beitrag zur Neuroinflammation nach wie vor nicht klar ist.

In dieser Studie zeigen wir, dass eine durch das Endotoxin Lipopolysaccharid (LPS) ausgelöste systemische Entzündung die Adenosinkonzentration im Plasma rasch ansteigen lässt und 6 Stunden nach der LPS-Injektion (hpi) ihren Höhepunkt erreicht. Unter Verwendung von in vivo 2P-LSM Live-Imaging eines neuartigen genetisch kodierten Adenosin-Sensors GRAB_{Ado}, der in Astrozyten exprimiert wird, konnten wir zeigen, dass die periphere Verabreichung von Adenosin das GRAB_{Ado}-Signal im Gehirn direkt verstärken kann, was darauf hindeutet, dass erhöhte Adenosinspiegel im Blut den extrazellulären Adenosin-Tonus im Gehirnparenchym erhöhen können. Darüber hinaus konnten wir kurz nach der LPS-Injektion erhöhte extrazelluläre Adenosinwerte in Form eines erhöhten GRAB_{Ado}-Signals in der Hirnrinde der Mäuse nachweisen, das ebenfalls um 6 hpi seinen Höhepunkt erreichte. Diese begleitenden pathologischen Ereignisse deuten stark darauf hin, dass Adenosin im Blutkreislauf zum gesamten zentralen Adenosin-Signal, das durch systemische Entzündungen hervorgerufen wird, beitragen kann. Durch die Kombination von pharmakologischen Eingriffen, Immunhistochemie, genetischer RiboTag-Technologie und Hochdurchsatz-RNA-Sequenzierung, Zytokin-Array, quantitativer PCR, Western Blot und IMARIS-unterstützter Bildanalyse konnten wir zeigen, dass eine erhöhte Adenosinmenge die Astrozytenreaktivität in der frühen Phase (2-6 hpi) der systemischen Entzündung auslösen kann.

In transgenen Mausmodellen haben wir A1-Adenosinrezeptoren (A1ARs), die Gi/ogekoppelt sind, speziell in Astrozyten ausgeschaltet. Nach einer peripheren Injektion von LPS in diese Mäuse beobachteten wir eine Hemmung der frühen Astrozytenreaktivität und eine verringerte Expression von Proteinen, die mit der Neuroinflammation zusammenhängen (wie CCL2, CCL5 und CXCL1). In der Folge stellten wir einen Rückgang der Mikroglia-Aktivierung, eine geringere Störung der Blut-Hirn-Schranke, verbesserte neuronale Funktionen und schließlich eine Abschwächung des durch die systemische Entzündung ausgelösten depressiven Verhaltens fest. Darüber hinaus haben wir den chemogenetischen hM4Di-Rezeptor in A1AR-defizienten Astrozyten exprimiert, um die Gi-Signalisierung nach CNO-Verabreichung bei 2 und 4 hpi zu induzieren, was die Neuroinflammation und das depressionsähnliche Verhalten der astrozytären-A1AR-defizienten Mäuse wiederherstellte und Astrozyten statt Mikroglia als frühe Treiber der Neuroinflammation hervorhob.

Unsere Forschung deckt einen bisher unbekanntem Signalweg auf, durch den Adenosin als Signalmolekül fungiert, um systemische Entzündungen zu vermitteln und Neuroinflammation durch die Initiierung einer frühen Reaktivität von Astrozyten zu induzieren. Zudem präsentiert diese Studie erstmalig den Nachweis, dass frühe reaktive Astrozyten eine treibende Kraft hinter der Neuroinflammation darstellen und nicht lediglich als Effektoren der reaktiven Mikroglia agieren.

3. INTRODUCTION

Sepsis is a life-threatening condition usually induced by unbridled systemic inflammatory response to injuries or bacterial infections, leading to dysfunctions of multiple organs (Hotchkiss and Karl, 2003). The elevated peripheral inflammation in septic patients could subsequently induce severe neuroinflammation, called sepsis-associated encephalopathy (SAE), leading to the impairments of the central nervous system (CNS) in terms of glial activation, neuronal dysfunction, and blood-brain barrier (BBB) breakdown (Gofton and Young, 2012). Notably, sepsis patients exhibit high levels of plasma purine metabolites such as adenosine which positively correlates with mortality, highlighting the importance of adenosine signaling in sepsis (Martin et al., 2000). However, the role of adenosine signaling in SAE remains unknown.

3.1. Sepsis and sepsis-associated encephalopathy

Sepsis is a life-threatening organ dysfunction characterized by systemic and disordered immune reaction to infections and injuries, which is the primary cause of preventable mortality, becoming one of the major and most urgent public health challenges worldwide (Reinhart et al., 2017; Singer et al., 2016). The features of sepsis essentially reflect the body's response to infection and include fever, hemodilution, tachycardia, hypotension, hypoperfusion, leukocytosis, and epinephrine-associated hyperlactatemia, as well as end-organ dysfunction, such as muscle degeneration, intestinal obstructions, acute lung injury, acute kidney injury, cardiomyopathy, and encephalopathy (Agapito Fonseca et al., 2020; Nunnally and Patel, 2019; Rocheteau et al., 2015).

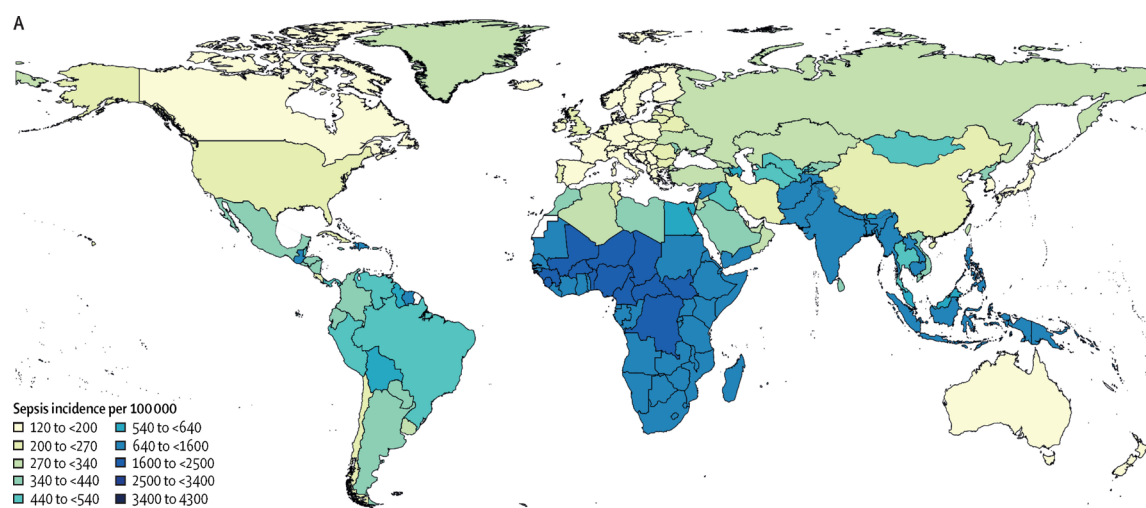


Figure 1. Global sepsis incidence in 2017 (Rudd et al., 2020).

A recent report on the Global Burden of Diseases highlights that there are nearly 50 million cases of sepsis worldwide every year (Rudd et al., 2020), which affects both sexes and all ages. Sepsis resulted in an estimated 11 million deaths in 2017, equivalent to a standardized mortality of 148 per 100,000 people, representing nearly 20% of global

deaths (Figure 1). Mortality rates of patients with septic shock in intensive care units are ~35% (Machado et al., 2017; Prescott et al., 2020; Rhee et al., 2017). Furthermore, almost 50% of sepsis survivors end up back in the hospital within one year, and around 16% of sepsis survivors do not make it through the first year (Prescott and Angus, 2018; Prescott et al., 2016; Shankar-Hari et al., 2016). Achieving universal sepsis prevention, diagnosis, and treatment remains a significant challenge.

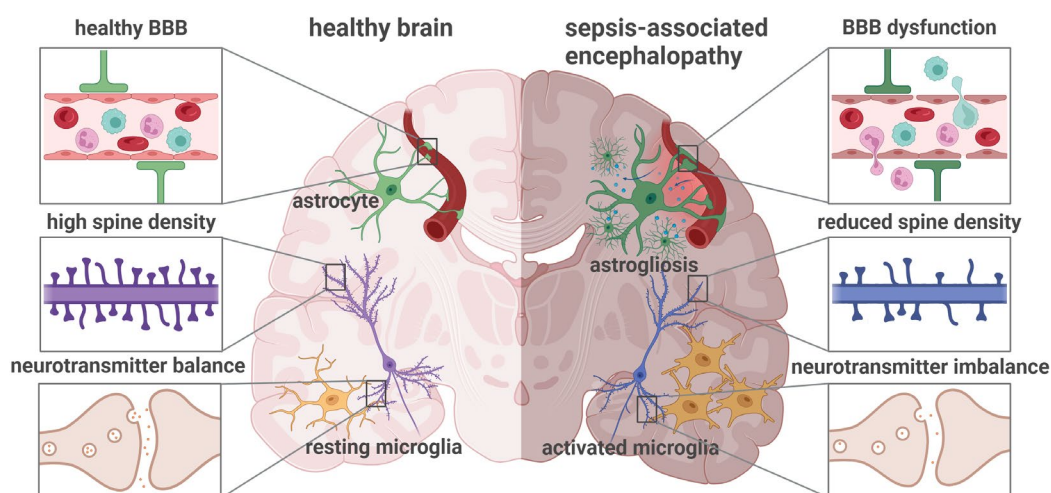


Figure 2. Schematic pathophysiological alterations in sepsis-associated encephalopathy.

SAE results in disrupting BBB integrity, activating astrocyte and microglia to release proinflammatory cytokines, causing neuroinflammation and neural damage in terms of reduced spine density and neurotransmitter imbalance. Based on (Chung et al., 2020).

The brain is considered as one of the critical organs affected by systemic inflammation, leading to the so-called SAE, among all affected organs in sepsis (Michelon et al., 2020; Sankowski et al., 2015; Widmann and Heneka, 2014). As reported, ~70% of critically ill patients with sepsis have any degree of SAE, such as agitation, disorientation, hypersomnolence, and even coma (Andonegui et al., 2018; Goffton and Young, 2012). Moreover, 180-day mortality rate of SAE increased to 55.41% (Sonnevile et al., 2017). However, the mechanism of sepsis-induced cerebral dysfunction has not been fully investigated (Kozlov et al., 2017; Robba et al., 2018; Sonnevile et al., 2013). Interestingly, apparent infection was barely found in the CNS of SAE patients, while neuroinflammation and oxidative stress was commonly observed in the brain (Catalão et al., 2017; Jesus et al., 2020). Uncontrolled neuroinflammation was also regarded as a main process led to brain dysfunctions during sepsis, contributing to BBB damage, altered neural activity, and activation of microglia and astrocyte (Figure 2) (Adam et al., 2013; Hoogland et al., 2015; Mazeraud et al., 2016; Michels et al., 2019; Shulyatnikova and Verkhatsky, 2020; Tian et al., 2019). To understand how systemic inflammation induces the inflammatory response in the brain, previous studies focused on elevated peripheral pro-inflammatory cytokines (such as TNF- α , IL-1 α , IL-1 β , and IL-6) as immune signals to induce neuroinflammation (Dantzer et al., 2008; Hodes et al., 2015). For instance, humoral IL-1 β

and IL-6 can cross the BBB via saturable transport to directly activate astrocytes, microglia, and neurons (Dantzer et al., 2008). Additionally, not only are peripheral cytokines upregulated, but also the production of many metabolic molecules, such as the purine nucleoside adenosine, is increased in systemic inflammation (Chiu and Freund, 2014). However, the roles of those increased metabolic molecules in neuroinflammation are not fully understood.

3.2. Animal model of septic inflammation

Sepsis triggers an intensified neuroinflammatory response, impacting the brainstem, amygdala, and hippocampus, contributing to psychological disorders, cognitive impairment, and potential fatality. Multiple murine models resembling sepsis-associated neuroinflammation have been developed, each with unique strengths and limitations, offering avenues for studying disease mechanisms and testing new interventions (Fink, 2014; Gentile et al., 2014; Kingsley and Bhat, 2016; Lewis et al., 2016; Nemzek et al., 2008; Ozment et al., 2012; Stortz et al., 2017; van der Poll, 2012).

The most prevalent model involves injection with lipopolysaccharide (LPS), a component of Gram-negative bacteria, activating the innate immune system. Peripheral LPS administration induces a cerebral inflammatory response, inducing microglia reactivity, astrocytes reactivity, and BBB disruption, leading to increase the expression of proinflammatory cytokines and the infiltration of immune cell into the CNS (Nava Catorce and Gevorkian, 2016; Qin et al., 2007; Vutukuri et al., 2018). The LPS-mediated activation of the microglial NF- κ B signaling pathway through TLR4 and CD14 (Kingsley and Bhat, 2016). The intensity and duration of the induced inflammatory response can be adjusted by modifying LPS dose, administration route, and injection frequency (Lewis et al., 2016; Meneses et al., 2018; Nava Catorce and Gevorkian, 2016). This model mirrors severe sepsis physiology in humans and induces acute endotoxemia in mice. It is characterized by systemic arterial hypotension, lactic acidosis, impaired myocardial contractility, a transient TNF- α spike, and prolonged IL-6 elevation. Despite mice being less sensitive than humans to LPS toxicity, this animal model remains widely used (Fink, 2014).

3.3. Main features of sepsis-associated encephalopathy

3.3.1. Blood-brain barrier dysfunction in sepsis-associated encephalopathy

The BBB is a dynamic and selective border that separates the brain parenchyma from the blood. It consists of endothelial cells, astrocytic end-feet and pericytes, forming the neurovascular unit (NVU) that controls molecular transport and maintains brain homeostasis (Daneman and Prat, 2015; Profaci et al., 2020). The BBB maintains cerebral microenvironment homeostasis by regulating ions and fluids movements, supplying nutrients, contributing waste removal, and restricting immune cells infiltration as well as inflammation (Abbott et al., 2006) (Figure 3).

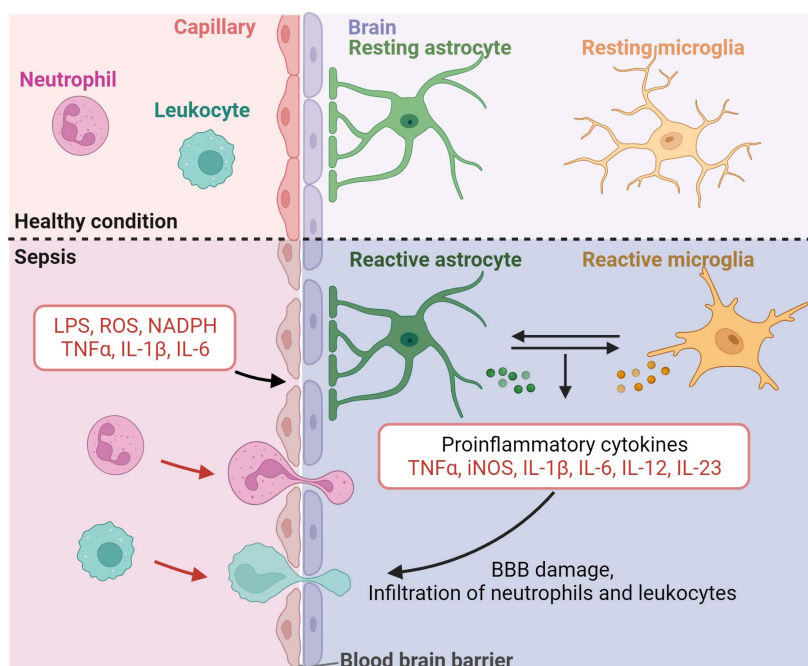


Figure 3. Blood-brain barrier dysfunction in sepsis-associated encephalopathy.

In this pathological process of SAE, the BBB integrity, crucial for CNS separation from peripheral circulation, is disrupted by inflammatory factors released by reactive microglia and astrocytes, leading to immune cells infiltration into the brain parenchyma.

Vascular ECs are the main cellular components of the BBB disrupted by systemic inflammatory factors, through pattern recognition receptors, such as IL-1 β , TNF- α , IL-6 and LPS itself, in SAE (Gosselin and Rivest, 2008; Nagyszosi et al., 2010) (Figure 3). Activation of pattern recognition receptors stimulate NF- κ B enhancing cytokine release and ROS generation which can further increase the expression of matrix metalloproteinases (MMPs) (Masciantonio et al., 2017). Enhanced MMPs expression were reported in sepsis patients as well as animal models, contributing to the degrade tight junction proteins claudin-5, occludin, and zonula occludens-1, resulting in BBB breakdown and peripheral immune cells infiltration (Barichello et al., 2022; Dal-Pizzol et al., 2013; Erikson et al., 2020; Yazdan-Ashoori et al., 2011; Zeng et al., 2016; Zhao et al., 2016). In addition, endothelial cells upregulate the expression of ICAM-1, ICAM-2, VCAM-1, and PECAM on the vascular endothelium. Subsequently, leukocyte ligands adhere to these endothelial cells and migrate towards chemoattractant mediators like CXCL8 and CCL2, eventually infiltrating into the brain (Erikson et al., 2020; Handa et al., 2008; van der Poll et al., 2017). Furthermore, the apoptosis and reduced proliferation of ECs were reported in several septic animal models, contributing to elevate the permeability of BBB (Boitsova et al., 2018; Yamazaki et al., 2019). In addition, other components of the NVU such as astrocytes and pericytes also mediate inflammatory responses, oxidative stress, and cellular responses in SAE (Wu et al., 2020). Recent studies using an LPS (lipopolysaccharide)-induced systemic inflammation mouse model revealed that vascular pericytes behaved as initial sensors of peripheral inflammation in terms of releasing the chemokine CCL2 (Duan et al., 2018).

Taken together, impaired BBB may act as an initiating link of SAE, resulting in the infiltration of various cytokines and immune cells in the brain and causing neuronal dysfunction and a series of neuropsychiatric symptoms with a high mortality.

3.3.2. Astrocyte reactivity in sepsis-associated encephalopathy

Astrocytes are homeostatic cells in the CNS maintaining the BBB integrity, modulating ion and neurotransmitter homeostasis, fluid balance, neurogenesis, synaptic plasticity, and neuroinflammation (Bushong et al., 2002; Halassa et al., 2007; Kirischuk et al., 2012; Oliet et al., 2001; Verkhratsky et al., 2015). Moreover, astrocytes secrete more than 200 molecules, ranging from neuromodulators and growth factors to hormones, that diffuse through the extracellular matrix and influence the activity of other cells in the CNS (Verkhratsky et al., 2016).

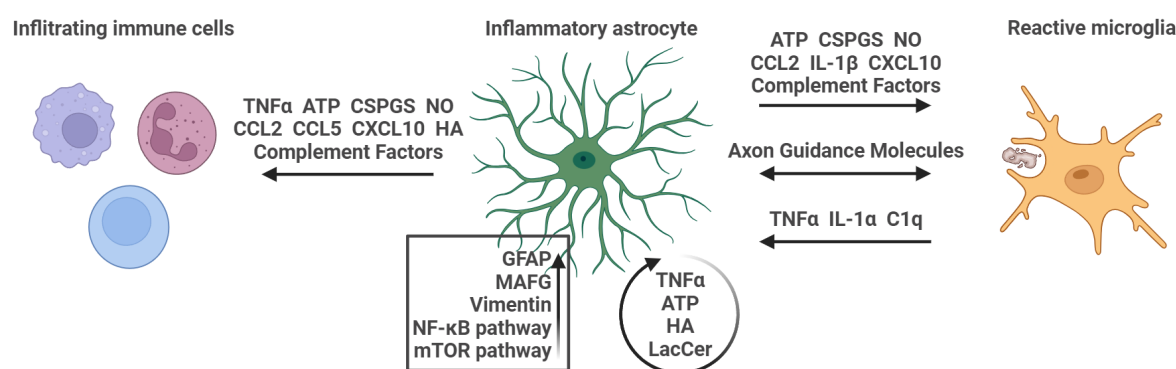


Figure 4. Roles of astrocyte in sepsis-associated encephalopathy

Upregulated markers and pathways in the process of inflammatory astrocyte reactivity, leading to microglia activation and immune cells infiltration.

Astrocytes also play a crucial role in both the initiation and the progression of SAE, as they sense and respond to systemic inflammatory signals and modulate the local brain environment, contributing to maintaining the BBB integrity and neuronal function (Kaplan et al., 2020). Several studies have shown that sepsis impairs the antioxidant capacity of astrocytes by reducing their ability to scavenge extracellular dehydroascorbic acid and intracellular ascorbate, and increasing their production of iNOS, leading to oxidative stress and reduced glutamate uptake, which can exacerbate excitotoxicity and neuronal death (Korcok et al., 2002). Sepsis also induces cytoskeletal and morphological alterations in astrocytes for receiving and transmitting cytokine signals through receptors expressed on their end-feet (Hasegawa-Ishii et al., 2016). Astrocytes then produce and release their own cytokines, such as CCL2, IL1β, TNFα, LacCer, and G-CSF, which modulate microenvironment, and disrupt the synaptic function and plasticity, leading to cognitive impairment in sepsis (Fernandes et al., 2004; Hasegawa-Ishii et al., 2016; Mayo et al., 2014; Parajuli et al., 2015; Villeda et al., 2011) (Figure 4). Astrocytes can also influence the function of microglia, the resident immune cells of the brain, in the context of systemic inflammation. For example, TLR4 stimulation and dopamine receptor D3 co-stimulation in astrocytes can promote the acquisition of proinflammatory ability, such as increased

expression of CCL2, iNOS, TNF- α , CSPGS, CXCL10, and IL1 β , and reduced anti-inflammatory factors levels, such as IL10 and TGF β , enhancing microglial reactivity and neuroinflammation, leading to neuronal damage and behavior deficits (Cekanaviciute et al., 2014; John et al., 2023; Montoya et al., 2019; Shulyatnikova and Verkhatsky, 2020). In addition, recent studies have shown that astrocytes undergo metabolic changes in response to sepsis mediated by the IL-6/AMPK signaling pathway, increasing their mitochondrial biogenesis and ATP production to cope with the high-energy demand and to restore the mitochondrial structure (Chen et al., 2018; Zhao et al., 2017).

Therefore, astrocytes are one of key mediators of SAE, as they regulate the BBB integrity, the brain metabolism, the neuroinflammation and the neuronal function in response to sepsis. Astrocytes can facilitate the course of neuroinflammation and brain dysfunction, leading to encephalopathy and cognitive impairment. Understanding the molecular and cellular mechanisms underlying astrocyte involvement in SAE may provide new therapeutic targets and strategies to prevent and treat this devastating condition.

3.3.3. Microglia reactivity in sepsis-associated encephalopathy

Microglia, the innate immune cell of CNS, plays various roles in brain development, homeostasis, and disease. In the development, microglia participate in the formation and refinement of neural circuits, through pruning excess synapses and regulating synaptic transmissions (Andoh and Koyama, 2021; Castro et al., 2022). Additionally, microglia also act as scavengers and defenders of the CNS by phagocytosing microbes, dead cells, protein aggregates and other harmful substances, as well as producing various chemokines, cytokines and neurotrophic factors, modulating immune responses in the CNS (Colonna and Butovsky, 2017; Schmidt et al., 2021).

Microglia are critically involved in the pathogenesis of SAE, inducing the release of chemokines and inflammatory cytokines, contributes to brain defense and neuronal damage (Hanisch, 2002) (Figure 5). Numerous studies have indicated that microglia undergo morphological and functional changes in response to sepsis. For example, microglia increase their expression of ED-1, a marker of phagocytic activity, and extend their processes around the cerebrovascular system and the parenchyma, indicating a state of activation and surveillance. The degree and duration of microglial activation depend on the severity and timing of sepsis, as well as the brain region involved (Deng et al., 2013; Semmler et al., 2005). Nevertheless, the long-term activation of microglia leads to uncontrolled inflammatory response and even neuronal death. LPS strongly stimulates microglia through TLR4 to produce proinflammatory cytokines (e.g. TNF α , IL-6, IL-1 α , and IL-1 β) during SAE, leading to exacerbate the inflammatory injury and neuronal dysfunction in the brain (Lee et al., 2020; Song et al., 2022).

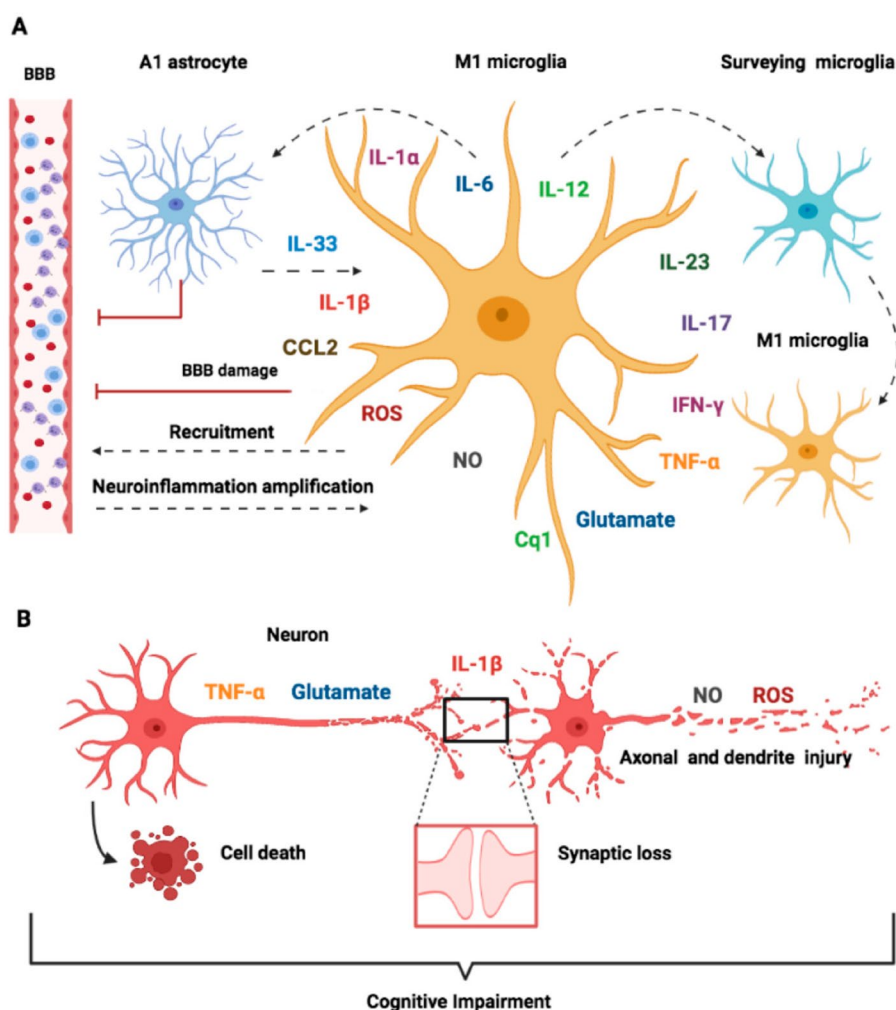


Figure 5. Roles of microglia in sepsis-associated encephalopathy

Microglia plays a critical role in BBB damage, neurotoxic astrocytes reactivity, and neuronal death associated with SAE through various mechanisms, such as the production of pro-inflammatory molecules (e.g. IL-1 β , IL-1 α , IL-6, TNF- α , CCL2, ROS, NO), contributes to cognitive impairments and acute neurological dysfunctions in SAE. Figure taken from Li et al., 2020b.

In addition, microglia can recognize various damage-associated molecular patterns (DAMPs), such as complement components, and cytokines, through different pattern recognition receptors, such as TLR2, TLR4, TLR9 and NLRP3 (Maccioni et al., 2018; Ye et al., 2019). These receptors activate intracellular signaling pathways, such as nuclear factor- κ B (NF- κ B) and p38-MAPK, that regulate the expression of genes involved in inflammation, apoptosis, and neuronal degeneration. For example, IL-1 β and IL-6, which are increased in the serum and cerebrospinal fluid of septic patients and animals, inducing the production of proinflammatory cytokines (e.g. TNF α and IL-17A) via NF- κ B signaling, which can impair the BBB integrity, impact neuronal survival, disturb the memory in septic patients (Danielski et al., 2018; Han et al., 2017; Van Gool et al., 2010). IL-17A and its receptor IL-17R form a positive feedback loop between microglia and other immune cells, such as Th1 and Th17 cells, that amplifies the role of inflammation in the brain and aggravates SAE (Li et al., 2020a; Ye et al., 2019).

Microglia also interacts with other cells of the NVU, such as astrocytes, endothelial cells and neurons, modulating the phenotype and function of microglia through direct contact or paracrine signaling (Montoya et al., 2019; Shimada and Hasegawa-Ishii, 2017). For example, astrocytes can secrete cytokines, such as G-CSF and CCL11, which stimulate microglial growth and migration, leading to oxidative stress and neuronal death (Hasegawa-Ishii et al., 2016). Neurons can also communicate with microglia through chemokines and neurotransmitters, such as CX3CL1, glutamate, and acetylcholine, which bind to receptors on microglia and regulate their functional phenotype and overactivation under inflammatory conditions (Gimenez et al., 2004; Li et al., 2020a; Wang et al., 2015; Wolf et al., 2017).

Therefore, microglia play a critical role in maintaining CNS homeostasis, and defending against pathogens or injury. However, during sepsis, microglia can also facilitate neuroinflammation and brain dysfunction, resulting in encephalopathy and cognitive impairment.

3.4. Adenosine signaling in physiology and pathophysiology

In addition to the role of inflammation itself in sepsis, other signaling such as purinergic signaling, also plays an important role in sepsis which can provide new respect for therapy of sepsis. In sepsis, afferent nerves (such as vagal nerves) triggered by peripheral pathological stimuli induce aberrant neural activities in the CNS, thereby promoting the release of extracellular ATP and adenosine from neural cells (Dantzer et al., 2008; Gourine et al., 2007). A recent *in vivo* study, utilizing a novel genetically modified ATP sensor known as GRAB_{ATP}, has provided compelling evidence of increased ATP release events in the mouse brain following a peripheral LPS challenge. This indicates heightened levels of extracellular ATP and its metabolites in the brain during inflammation. (Wu et al., 2022) (Figure 6). Adenosine, formed from the sequential ATP metabolism, acts as a ubiquitous chemical messenger to modulate the release of various neurotransmitters and, thereby, neuronal excitability and synaptic plasticity via four types of ARs (A1, A2a, A2b, A3) (Benarroch, 2008; Boison, 2008; Boison et al., 2010; Chiu and Freund, 2014; Wei et al., 2011). Transcriptomic results show that A1AR was the most abundantly expressed AR in the brain among four types of ARs. Of note, astrocytes have the highest expressed AR of the NVU, compared to pericytes and endothelial cells (Figure 7).

Under basal conditions, the extracellular adenosine levels are determined by the release of adenosine from cells and the extracellular catabolism of adenine nucleotides (Chiu and Freund, 2014; Wei et al., 2011). In most mammalian cells, adenosine is derived from the dephosphorylation of AMP and the metabolism of methionine, which can be released in the extracellular space via equilibrative nucleoside transporters (ENTs). In the extracellular space, adenosine is generated by a series of catabolism of extracellular ATP. The extracellular ATP is hydrolyzed to ADP and AMP by ectonucleoside triphosphate diphosphohydrolase 1 (ENTPD1, also known as CD39), then rapidly catabolized to adenosine by the ecto-5'-nucleotidase Nt5e (also known as CD73) (Boison, 2008; Welsh and Kucenas, 2018). In healthy tissues, newly generated extracellular adenosine is rapidly taken by cells via ENTs, then metabolized either by adenosine kinase to form AMP or

2014; Wei et al., 2011). Previous studies illustrated that the plasma adenosine concentration increased significantly in human patients and animals with systemic inflammation, modulating the innate and adaptive immune response by triggering various G-protein-coupled ARs in peripheral immune cells (Cekic and Linden, 2016; Chiu and Freund, 2014; Martin et al., 2000; Ramakers et al., 2011). In addition, adenosine can be transported by equilibrative nucleoside transporters (ENTs), or as a small molecule can bypass the tight junctions of endothelial cells (Latini and Pedata, 2001; Mikitsh and Chacko, 2014). Furthermore, adenosine can increase the permeability of BBB through A1 and A2a ARs in endothelial cells, facilitating peripheral immune cells or even bacteria infiltrate into the brain parenchyma (Bynoe et al., 2015b; Carman et al., 2011; Mills et al., 2008; Zhao et al., 2020). The destroyed BBB integrity by systemic inflammation (partially due to the detachment of vascular pericytes, and the elevated plasma adenosine level that increases the permeability of endothelial cell TJs) (Carman et al., 2011; Nishioku et al., 2009) permits even more adenosine entry from circulation to the brain parenchyma. However, in vivo evidence and related molecular mechanism of the impact of such enhanced peripheral adenosine signals on neuroinflammation remains elusive.

4. AIMS OF THE STUDY

Previous research on SAE has primarily focused on the increased levels of proinflammatory cytokines in the blood, such as TNF α , IL-1 α , IL-1 β , and IL-6, which act as immune signals inducing inflammatory responses in the CNS. Additionally, purine metabolites such as adenosine have been observed to be elevated in the blood following a systemic inflammation challenge. However, the role of adenosine signaling in neuroinflammation remains largely undetermined.

Therefore, we aimed to investigate the contribution of adenosine signaling to SAE in a mouse model of peripheral LPS-induced systemic inflammation and to unravel the underlying molecular mechanisms with a particular focus on the astrocytic A1AR signaling.

Specifically, we defined the following aims:

Aim 1. Determine the dynamic extracellular adenosine levels in the blood and brain parenchyma of the mouse after an LPS challenge.

The concentration of extracellular adenosine in the plasma and brain of LPS challenged mice were evaluated by an adenosine assay kit and *in vivo* 2P-LSM imaging of genetically encoded adenosine sensor GRAB_{Ado}, respectively, at 0, 6, 24 hpi. To assess the correlation between peripheral and cerebral adenosine levels, intraperitoneal injections of adenosine were performed during 2P-LSM imaging of GRAB_{Ado}.

Aim 2. Assess the contribution of peripheral adenosine to neuroinflammation.

To achieve this aim, relative gene expressions of inflammatory factors in the brain were evaluated by quantitative PCR (qPCR) upon intraperitoneal administration of adenosine and its analogues. In addition, the effect of pharmacological intervention of A1ARs on neuroinflammation was investigated in LPS-challenged mice by qPCR and immunostaining.

Aim 3. Characterize the role of glial A1ARs in neuroinflammation.

To identify the contribution of glial A1ARs to neuroinflammation, the relative gene expressions of inflammatory factors were evaluated by qPCR in the brain of astrocyte, microglia, and pericyte/OPC-specific A1AR deficient mice upon intraperitoneal administration of A1AR agonists. In particular, the astrocytic, microglial, and neuronal inflammatory responses, as well as the depression-like behavior, were investigated in astrocytic A1AR-deficient mice after a peripheral LPS-challenge by combining immunohistochemistry, genetic RiboTag technology and high-throughput RNA sequencing, cytokine array, qPCR, IMARIS analysis, electrophysiology, and behavioral analysis.

5. MATERIALS AND METHODS

5.1. Materials

5.1.1. Chemicals, reagents, and kits

The chemicals, consumables, and kits used in this study were from various companies, included Abcam (Cambridge, UK), Axon Labortechnik (Kaiserslautern, DE), B. Braun (Melsungen, DE), BD Biosciences (Heidelberg, DE), Bio-Rad (Hercules, USA), Carl Roth (Karlsruhe, DE), Eppendorf (Hamburg, DE), Invitrogen (Karlsruhe, DE), Merck (Darmstadt, DE), Millipore (Burlington, USA), Qiagen (Hilden, Germany), R&D Systems (Minneapolis, USA), Roche (Basel, CH), Sarstedt (Nümbrecht, Germany), Sigma-Aldrich (St. Louis, USA), Tocris (Bristol, UK), Thermo Fisher Scientific (Waltham, USA), VWR International (Radnor, USA).

5.1.2. Devices

Table 1. List of devices

Device	Manufacturer
2Photon LSM	Custom-made (Frank Kirchhoff's lab)
AxioScan.Z1	Zeiss (Oberkochen, DE)
Bead sterilisator	F.S.T. (Heidelberg, DE)
Centrifuges	Eppendorf (Hamburg, DE)
ChemiDoc™ MP Gel Imaging System	Bio-Rad (München, DE)
Consort EV231 Power Supply	Merck (Darmstadt, DE)
DRS-12 Rocking Shaker	neoLab (Heidelberg, DE)
Head holder	Custom-made (Frank Kirchhoff's lab)
HybEZ™ Hybridization System	Advanced Cell Diagnostics (Newark, CA)
Infrared Thermometer (IRF 260-8S)	Voltcraft (Hirschau, DE)
Isoflurane vaporizer	Harvard Apparatus (Holliston, USA),
LSM880	Zeiss (Oberkochen, DE)
Magnetic stirrer C-MAG HS 7	IKA GmbH (Staufen im Breisgau, DE)
Micropipette Puller P-97	Sutter Instruments (Novato, US)
Mini Star Centrifuge	neoLab (Heidelberg, DE)
peqSTAR Thermo Cycler	peqlab Biotechnologie GmbH (Erlangen, DE)
Peristaltic pump LKB P-1	Pharmacia LKB (Uppsala, SE)
Pipettes	Brand (Wertheim, DE)
Preparations- and perfusion instruments	F.S.T. (Heidelberg, DE)
Quantum gel documentation system	peqlab Biotechnologie GmbH (Erlangen, DE)
Robot stereotaxic	Neurostar (Tübingen, DE)
Scales (CPA 8201/CPA 2245)	Sartorius (Göttingen, DE)
Surgical instruments	F.S.T. (Heidelberg, DE)
Vibratome VT1000S/VT1200S	Leica Biosystems (Wetzlar, DE)
Vortex Mixer	VWR International (Darmstadt, DE)
Water bath WNE14	Memmert GmbH (Schwabach, DE)
Water facility Milli-Q	Merck (Darmstadt, DE)

5.1.3. Buffers and aqueous solutions

The buffers or solutions used in this study were made with ultrapure water (ddH₂O) obtained from Milli-Q water purification system (Merck, Germany). The concentrations that were given are the final working ones.

Phosphate buffered saline (PBS, pH 7.4)

NaCl	137	mM
KCl	2.7	mM
Na ₂ HPO ₄	10	mM
KH ₂ PO ₄	1.8	mM

4% Formaldehyde (FA, pH 7.4)

Paraformaldehyde(PFA)	4	%(w/v)
NaH ₂ PO ₄	0.2	M
Na ₂ HPO ₄	0.2	M

Tris-Acetate-EDTA buffer (TAE)

Tris(hydroxymethyl)aminomethane	40	mM
Acetic acid (100%)	20	mM
Ethylendiaminetetraacetic acid	0.4	mM
EDTA, pH 8.0	0.5	M

Agarose gel in TAE buffer (1x)

Agarose Powder	2	%(w/v)
Ethidium Bromide	0.5	µg/ml

DNA extraction solution (pH 9.5)

KCl	0.3	M
EDTA	0	M
Tris-HCl	0.1	M

Neutralization solution in PBS (1x)

Bovine Serum Albumin(BSA)	3	%(w/v)
---------------------------	---	--------

Blocking buffer in PBS (1x)

Horse Serum(HS)	5	%(v/v)
Triton-X-100	0.3	%(v/v)

Cutting solution in ddH₂O (pH 7.4)

NaCl	87	mM
KCl	3	mM
Na ₂ H ₂ PO ₄	1.3	mM
NaHCO ₃	25	mM
Glucose	25	mM
Sucrose	75	mM
MgCl ₂	3	mM
CaCl ₂	0.5	mM
HEPES	5	mM

Incubation solution in ddH₂O (pH 7.4)

NaCl	126	mM
KCl	3	mM
Na ₂ H ₂ PO ₄	1.3	mM
NaHCO ₃	25	mM
Glucose	15	mM
MgCl ₂	1	mM
CaCl ₂	2.5	mM

Perfusion solution in ddH₂O (pH 7.4)

NaCl	126	mM
KCl	3	mM
Na ₂ H ₂ PO ₄	1.3	mM
NaHCO ₃	25	mM
Glucose	15	mM
MgCl ₂	2	mM
CaCl ₂	1	mM

Cortex buffer (pH 7.4)

NaCl	125	mM
KCl	5	mM
Glucose	10	mM
HEPES	10	mM
CaCl ₂	2	mM
MgSO ₄	2	mM

Evans blue solution in PBS (pH 7.4)

Evans blue	4	%(w/v)
------------	---	--------

5.1.4. Enzymes

DreamTaq™ Hot Start Green DNA Polymerase was purchased from Thermo Fisher Scientific (Waltham, USA).

5.1.5. Drugs and Dyes

Table 2. List of drugs

Name	Working concentration	Solvent	Manufacturer
Tamoxifen	10 mg/ml	Miglyol	Caesar & Loretz
Ketamin hydrochlorid	100 mg/ml	Saline	Serumwerk Bernburg AG
Xylazin hydrochlorid	20 mg/ml	Saline	WDT
APCP	220 μ M	H ₂ O	Tocris
NBMPR	100 μ M	DMSO	Sigma
Dipyridamole	40 μ M	DMSO	Sigma
EHNA	100 μ M	H ₂ O	Sigma
Iodotubericidine	10 μ M	DMSO	Sigma
CPA	1 mg/ml	Saline	Abcam
2-Chloro-N6-cyclopentyladenosine	37 mg/ml	DMSO	Tocris
DPCPX	1 mg/ml	DMSO	Abcam
CV1808	1 mg/ml	DMSO	Tocris
Adenosine	2 mg/ml	Saline	Sigma
Tetrodotoxin Citrate (TTX)	1 μ M	H ₂ O	Alomone Labs

5.1.6. Antibodies

5.1.6.1. Primary antibodies

Table 3. List of primary antibodies

Primary antibodies	Manufacturer	Ref.
Goat anti-Sox9 (1:500)	R&D Systems	Cat# AF3075
Rabbit anti-Iba1 (1:1000)	Wako	Cat# 019-19741
Goat anti-Iba1 (1:500)	abcam	Cat# ab5076
Mouse anti-NeuN (1:500)	Millipore	Cat# MAB377
Rat anti-CD31 (1:100)	BD Pharmingen	Cat# 550274
Rat anti-Ly6B (1:500)	Bio Rad	Cat# MCA771GT
Mouse anti-HA (1:500)	Biolegend	Cat# 901513
Goat anti-LCN2 (1:1000)	R&D Systems	Cat# AF1857
Chicken anti-GFP (1:1000)	Thermo Fisher Scientific	Cat# 10524234
Rabbit anti- p65 (1:500)	Cell Signaling Technology	Cat# 8242
Guinea pig anti-cFos (1:4000)	Synaptic Systems	Cat# 226004

5.1.6.2. Secondary antibodies

Table 4. List of secondary antibodies

Secondary antibodies	Manufacturer	Ref.
Donkey anti-rabbit IgG(H+L) Alexa Fluor 488 (1:1000)	Thermo Fisher Scientific	Cat# A-21206
Donkey anti-rabbit IgG(H+L) Alexa Fluor 546 (1:1000)	Thermo Fisher Scientific	Cat# A10040
Donkey anti-rabbit IgG(H+L) Alexa Fluor 647 (1:1000)	Thermo Fisher Scientific	Cat# A-31573
Donkey anti-goat IgG(H+L) Alexa Fluor 488 (1:1000)	Thermo Fisher Scientific	Cat# A-11055
Donkey anti-goat IgG(H+L) Alexa Fluor 546 (1:1000)	Thermo Fisher Scientific	Cat# A-11056
Donkey anti-goat IgG(H+L) Alexa Fluor 647 (1:1000)	Thermo Fisher Scientific	Cat# A-21447
Donkey anti-mouse IgG(H+L) Alexa Fluor 488 (1:1000)	Thermo Fisher Scientific	Cat# A-21202
Donkey anti-mouse IgG(H+L) Alexa Fluor 546 (1:1000)	Thermo Fisher Scientific	Cat# A10036
Donkey anti-mouse IgG(H+L) Alexa Fluor 647 (1:1000)	Thermo Fisher Scientific	Cat# A-31571
Donkey Anti-Guinea Pig IgG(H+L) Alexa Fluor 647 (1:1000)	Jackson ImmunoResearch Labs	Cat# 706-605-148
Donkey anti-chicken IgY(H+L) Alexa Fluor 488 (1:1000)	Thermo Fisher Scientific	Cat# A78948
Donkey Anti-Rat IgG(H+L) Cy5-AffiniPure (1:1000)	Jackson ImmunoResearch Labs	Cat# 712-175-150

5.1.6.3. Primers

Table 5. List of primers

Primer sequences			
Gene	Primer	Sequence (5'-3')	Purpose
<i>Actb</i>	Forward	CTTCCTCCCTGGAGAAGAGC	RT-qPCR
	Reverse	ATGCCACAGGATTCCATACC	
<i>Cxcl1</i>	Forward	AGACCATGGCTGGGATTCAC	RT-qPCR
	Reverse	CTCGCGACCATTCTTGAGTGT	
<i>Cxcl10</i>	Forward	AAGTGCTGCCGTCATTTTCT	RT-qPCR
	Reverse	GTGGCAATGATCTCAACACG	
<i>Ccl2</i>	Forward	GTTGGCTCAGCCAGATGCA	RT-qPCR
	Reverse	AGCCTACTCATTGGGATCATCTTG	
<i>Ccl5</i>	Forward	TGCCACGTCAAGGAGTATTT	RT-qPCR
	Reverse	TCTCTGGGTTGGCACACACTT	
<i>Lcn2</i>	Forward	ATGTCACCTCCATCCTGGTC	RT-qPCR
	Reverse	CACACTCACCACCCATTTCAG	
<i>Tnf</i>	Forward	CCACCACGCTCTTCTGTCTAC	RT-qPCR
	Reverse	AGGGTCTGGGCCATAGAACT	
<i>Il1a</i>	Forward	CGCTTGAGTCGGCAAAGAAAT	RT-qPCR
	Reverse	CTTCCCGTTGCTTGACGTTG	
<i>Il1b</i>	Forward	TGCCACCTTTTGACAGTGATG	RT-qPCR
	Reverse	TGATGTGCTGCTGCGAGATT	
<i>Il6</i>	Forward	GAGTGGCTAAGGACCAAGACC	RT-qPCR
	Reverse	AACGCACTAGGTTTGCCGA	
<i>Gfap</i>	Forward	TGGAGGAGGAGATCCAGTTC	RT-qPCR
	Reverse	AGCTGCTCCCGGAGTTCT	
<i>Pdgfra</i>	Forward	TCCTTCTACCACCTCAGCGAG	RT-qPCR
	Reverse	CCGGATGGTCACTCTTTAGGAAG	
<i>Pdgfrb</i>	Forward	ATGAATCGCTGCTGGGCGCTCTTC	RT-qPCR
	Reverse	TCAAAGGAGCGGATGGAGTGGTCCG	
<i>Itgam</i>	Forward	ATGGACGCTGATGGCAATACC	RT-qPCR
	Reverse	TCCCCATTACGTCTCCCA	
GCaMP3 KI	Forward	CACGTGATGACAAACCTTGG	genotyping PCR
GCaMP3 KI	Reverse	GGCATTAAAGCAGCGTATCC	
GCaMP3 WT	Forward	CTCTGCTGCCTCCTGGCTTCT	genotyping PCR
GCaMP3 WT	Reverse	CGAGGCGGATCACAAGCAATA	
GLAST	Forward	GAGGCACTTGGCTAGGCTCTGAGGA	genotyping PCR
GLAST KI	Reverse	GGTGTACGGTCAGTAAATTGGACAT	
GLAST WT	Reverse	GAGGAGATCCTGACCGATCAGTTGG	genotyping PCR
HA	Forward	GGGAGGCTTGCTGGATATG	
HA	Reverse	TTCCAGACACAGGCTAAGTACAC	genotyping PCR
A1AR	Forward	CTTTGCCCTCAGCTGGCTACCG	
A1AR KI	Reverse	ATCGGAATTCGCTAGCTTCGGC	genotyping PCR
A1AR WT	Reverse	TTCTCGGGGTCAGGAGAGCACC	
CXCT	Forward	TCAGTGTTTTCTCCCGCTTGC	genotyping PCR
CXCT WT	Reverse	GTAGTGGTTGTCTGGGCGAGCAG	
CXCT KI	Reverse	CAGTGATGCTCTTGGGCTTCC	

NGCE	Forward	GGCAAACCCAGAGCCCTGCC	genotyping PCR
NGCE WT	Reverse	GCTGGAGCTGACAGCGGGTG	
NGCE KI	Reverse	GCCCGGACCGACGATGAAGC	

5.2. Methods

5.2.1. Animals

The following animals were used in this study: C57BL/6N (wt); A1AR^{fl/fl} mice (Scammell et al., 2003); Glast-CreERT2 mice (Mori et al., 2006); Cx3cr1-CreERT2 mice (Jung et al., 2000); NG2-CreERT2 mice (Huang et al., 2014); RiboTag mice (Rlp22HA) (Sanz et al., 2009); GCaMP3 reporter mice (Rosa 26-CAG-*Isl*-GCaMP3) (Paukert et al., 2014). To generate cell type-specific A1AR knockout mice, A1AR^{fl/fl} mice were bred with Glast-CreERT2 mice, Cx3cr1-CreERT2 mice, and NG2-CreERT2 mice to selectively delete A1ARs in astrocyte, microglia, and OPC, respectively, after tamoxifen treatment. RiboTag mice (Rlp22HA) were used to isolate ribosome-bound translated mRNA in astrocytes after crossing with A1AR^{fl/fl}xGlastCreERT2 mice. To monitor Ca²⁺ activity in astrocytes, GCaMP3 reporter mice were crossed with A1AR^{fl/fl}xGlastCreERT2 mice.

“Mice of both sexes aged 11-13 weeks were employed for most experiments. All animals were kept at the CIPMM animal facility under controlled temperature-(22°C ± 2°C) and humidity-(45–65%) conditions with 12 h light/dark cycle and free access to food and water. Animal care and procedures were conducted at the CIPMM animal facility, University of Saarland, following European and German guidelines for the welfare of experimental animals. Animal experiments were authorized by the Saarland state’s “Landesamt für Gesundheit und Verbraucherschutz” in Saarbrücken/Germany (animal license number: 65/2013, 12/2014, 34/2016, 36/2016, 03/2021 and 08/2021).” (Guo et al., 2024)

5.2.2. Genotyping

“The animal caretakers at the animal facility of the Center for Integrative Physiology and Molecular Medicine (CIPMM, Homburg, DE) performed mouse sample biopsy and weaned when the pups were between two and three weeks old. The sample was either tail (< 0.5 cm) or ear punch (Ø < 0.5 cm) biopsy and was kept at – 20 °C. The samples were shaken (10 min) with 62.5 µl DNA extraction solution at room temperature (RT). After heating at 95 °C in the water bath for 20 min and then cooling down, 50 µl neutralization solution was added. The DNA sample was stored at 4 °C until used. For genotyping, samples were diluted 1:10 in ddH₂O with DreamTaq™ Hot Start Green DNA Polymerase (Thermo Fisher Scientific, Dreieich, DE) and oligonucleotide primers. The PCR reactions were performed in 96-well PCR plates in peqSTAR Thermo Cycler (peqlab Biotechnologie GmbH, Erlangen, DE).” (Guo et al., 2024). The PCR reactions are detailed in Table 6.

Table 6. PCR reaction protocols

PCR	Hot Start 3 min	Loop(35X)			End	
		Annealing 30 s	Elongation 1 min	Denaturation 30 s	30 s	5 min
A1AR KI	95 °C	60 °C	72 °C	95 C	60 °C	72 °C
GCaMP3		58 °C			58 °C	
GLAST		58 °C			58 °C	
Ribotag		64 °C			64 °C	
CXCT		56 °C			56 °C	
NGCE		60 °C			60 °C	

5.2.3. Tamoxifen and lipopolysaccharide preparation and administration

“Following the previous description (Liu et al., 2023), tamoxifen (CC99648, Carbolution) was dissolved in Miglyol (Caesar & Loretz, Hilden) at 10 mg/ml and intraperitoneally injected to all mice crossed with CreERT2-driver mouse lines (100 mg/kg per body weight) for five consecutive days at 4 weeks old.

For the endotoxin challenge, mice aged 13 weeks were intraperitoneally (i.p.) injected with 5 mg/kg of lipopolysaccharide (LPS, Sigma, DE) or endotoxin-free PBS from 1 p.m. to 3 p.m.(CET) and maintained for up to 72 h after injection (Hasel et al., 2021a).” (Guo et al., 2024)

5.2.4. Plasma adenosine measurement

“To assess plasma adenosine level, 0.4 ml blood was drawn from the right ventricle of deeply anesthetized mice with a syringe containing 0.4 ml ice-cold stop solution (220 μM APCP, 100 μM NBMPR, 40 μM dipyridamole, 13.2 mM Na₂-EDTA, 118 mM NaCl, 5 mM KCl), to prevent adenosine formation and transport. After spinning (1000g, 4°C, 10 min), plasma was kept at -80°C until analysis. The plasma adenosine concentration was determined with an adenosine assay kit (Fluorometric, Abcam), following the protocol. The fluorescence was recorded at excitation/emission = 535/587 nm.” (Guo et al., 2024)

5.2.5. BBB permeability by Evans blue

“EB (4% w/v in saline, 2 mL/kg) was injected into the tail vein 2 hours prior to euthanizing the mice. Then, Mice were perfused through the left ventricle with ice-cold PBS to eliminate intravascular albumin-Evans blue. Next, half of the brains were rapidly taken out, weighed, and homogenized in 1 mL of PBS. After the initial homogenization, 1 mL of 50% trichloroacetic acid was added, followed by vortex for 2 min. After centrifugation (1000g, 4°C, 30 min), the supernatant was transferred to 96 well plate. Fluorescence intensity was recorded at 620 nm on a microplate fluorescence reader and contrasted with a standard curve (serial dilutions of the stock dye solution in the concentration range of 0, 1.25, 2.5, 5, 10, 20 μg/mL). The Evans blue amount was computed and expressed per gram of brain tissue.” (Guo et al., 2024)

5.2.6. Stereotactic injections of adeno-associated viruses

“Adeno-associated viruses (AAV) were stereotactically injected into 10-week-old mice with modifications of previous study (Nagai et al., 2019). In brief, mice were administered 5 mg/kg of carprofen 1 hour before injection (i.p.). Then, under continuous inhalational isoflurane anesthesia (5% for induction and 2% for maintenance with 66% O₂ and 33% N₂O), the mouse head was fitted and secured by blunt ear bars in a stereotactic apparatus (Robot stereotaxic, Neurostar), and the mouse eyes were covered by Bepanthen (Bayer, Leverkusen). After sterile cleaning and skin incision, viruses were injected at a rate of 0.1 $\mu\text{l min}^{-1}$ with a 10 μl Nanofil syringe (34 GA blunt needle, World Precision Instruments) into the striatum (1.1 mm anterior to bregma, ± 1.2 mm from sagittal suture at a depth of 3 mm from the skull surface) or cortex (1.9 mm posterior to bregma, 1.5 mm from sagittal suture at a depth of 0.5 mm from the skull surface). The syringe was kept in the place for 10 min after the injection was completed, to avoid liquid reflux. The skin was closed by simple interrupted sutures (non-absorbable, F.S.T.). Carprofen were administered once per day for three consecutive days and received tramadol hydrochloride in the drinking water (400 mg/L) after surgery for seven days. Mice were used for experiments 3 weeks post virus injection. Viruses used were: AAV2/5 GfaABC1D-GRAB_{Ado} virus (2.3×10^{12} genome copies/ml); AAV2/5 GFAP-hM4Di-mCherry virus (3.04×10^{12} genome copies/ml); AAV2/5 GFAP-tdTomato virus (1.1×10^{13} genome copies/ml), 0.8 μl for striatum, 0.5 μl for cortex, respectively.” (Guo et al., 2024)

5.2.7. Pharmacological analysis of adenosine signaling

“To pharmacologically activate adenosine receptors, adenosine (5 mg/kg per body weight) was intraperitoneally injected every hour until 6 hours after the first injection; NECA (1 mg/kg), CPA (1 mg/kg), and CCPA (0.3 mg/kg) were intraperitoneally injected once at 0 hpi, respectively; DPCPX (1 mg/kg) was intraperitoneally injected 4 hours after LPS (5 mg/kg). To further amplify inflammatory response, CPA (1 mg/kg) was intraperitoneally injected 4 hours after LPS (1 mg/kg). Mice were analyzed at 6 hours post injection.” (Guo et al., 2024)

5.2.8. Cranial window implantation

“Cranial window implantation was performed on GRAB_{ado} virus injected mice as previously described (Cupido et al., 2014; Kislin et al., 2014). The skull of the mice was exposed and underwent a craniotomy followed by removal of the dura in the primary somatosensory cortex (\varnothing 3-4 mm, centered 1.5-2 mm posterior to bregma, 1.5 mm from the sagittal medial axis). The glass coverslip (\varnothing 3 mm, Glaswarenfabrik Karl Hecht GmbH) and a custom-made holder for head restraining with dental cement (3M, DE). Animals received canonical post-surgical care; three-day habituation training and imaging was performed one week after cranial window implantation.” (Guo et al., 2024)

5.2.9. *In vivo* imaging of extracellular adenosine levels

“*In vivo* imaging from GRAB_{ado} virus injected mice was performed using a custom-made two-photon laser-scanning microscope (2P-LSM) setup. Awake mice were maintained head-fixed and placed into a smooth plastic tube to acquire stable recording imaging at

different time points after LPS challenge. In the adenosine & SR-101 administration experiments, 1.5% isoflurane was given to the head-fixed mice via a custom-made nose mask. Solutions of adenosine (0, 5, 10 or 20 mg/kg) and SR101 (20 mg/kg) were prepared in isotonic saline solution and administered after 200 frames of baseline recording (~ 88 s). Squared FOVs (512 x 512 μm) were chosen at a 60-80 μm depth from the surface with 910-nm laser. The laser power under the objective was adjusted from 5 to 30 mW, depending on the focal plane depth. Single focal plane images were acquired with a 2.28 Hz frame rate (1.4 μs pixel dwell time) and a resolution of 512 x 512 pixels.” (Guo et al., 2024)

5.2.10. Reverse transcription-polymerase chain reaction (RT-PCR)

“Deeply anesthetized mice were perfused with ice-cold PBS. Cortex and striatum were dissected in ice cold PBS. Total RNA of cortex and striatum were isolated with the RNeasy mini kit (Qiagen, DE) according to the instructions. cDNA was reversed by using Omniscript RT kit (Qiagen, DE). RT-PCR was performed using EvaGreen (Axon, DE) with CFX96 Real Time System (BioRad). The program was used: 95 °C for 10 min, then 42 cycles at 95 °C for 15 sec, 60 °C for 1 min. Primers (Table 5) were designed to work at approximately + 60°C and the specificity was assessed by melt curve analysis of each reaction indicating a single peak. The expressions of *Gfap*, *Itgam*, *Pdgfra*, *Pdgfrb*, *Cxcl1*, *Cxcl10*, *Ccl2*, *Ccl5*, *Lcn2*, *Il6*, *Il1a*, *Il1b*, *Tnf* were measured and normalized to β -actin.” (Guo et al., 2024)

5.2.11. Immunohistochemistry

“After perfusion with 1x PBS and 4% paraformaldehyde (PFA). the brain was collected and post fixed in 4 % PFA overnight (4°C). Fixed brains were sliced into coronal sections of 35 μm thickness by using a Leica VT1000S vibratom. Sections were incubated for 1 h in blocking buffer (5 % HS, 0.3 % Triton X in 1x PBS) at room temperature and incubated with primary antibodies, diluted in the blocking solution, overnight at 4°C. The next day, sections were washed 3 times in 1x PBS (10 min per times) and incubated for 2 h with secondary antibodies and DAPI diluted in blocking buffer at room temperature in the dark. Subsequently, the sections were washed and mounted on the slide.” (Guo et al., 2024)

5.2.12. Image acquisition and analysis

“Whole brain slices were scanned with the semi-automatic slide scanner AxioScan.Z1 (Zeiss, Oberkochen) as described before (Huang et al., 2020). Cell counting from whole brain slices was manually performed using ZEN software (Zeiss, Jena). cFos intensity within Sox9⁺ and NeuN⁺ areas were automatically measured by using the machine learning function of the ZEN software. For the 3D reconstruction of microglia, confocal images were taken by LSM 710 and LSM780 confocal microscope (Zeiss, Oberkochen) with 1 μm intervals. Reconstruction of the microglial surface was performed using IMARIS (Version 9.6, Oxford Instruments) at the following settings: surface detail 0.700 μm (smooth); thresholding background subtraction (local contrast), diameter of largest sphere: 2.00. Next, the surface reconstruction was used as template for filament reconstruction with the following settings: detect new starting points: largest diameter 7.00 μm , seed

points 0.300 μm ; remove seed points around starting points: diameter of sphere regions: 15 μm . After filament reconstruction, individual data sets of Sholl analysis were exported into separate Excel files for further analysis. Image processing, three-dimensional reconstruction, and data analysis were performed in a blind manner regarding the experimental conditions.” (Guo et al., 2024)

5.2.13. Ribosome immunoprecipitation (IP)

“Cortical regions were isolated from mouse brains after perfusion with ice-cold HBSS and stored at -80°C until further processing. Tissues were lysed in ice-cold buffer containing 50 mM Tris (pH 7.4), 100 mM KCl, 12 mM MgCl_2 , 1% NP-40, 1 mM DTT, 1x protease inhibitor, 200 U/ml RNasin, and 0.1 mg/ml cycloheximide (10% w/v) using a Precellys 24 homogenizer. Lysates were cleared by centrifugation at 10,000 g for 10 min at 4°C and supernatants were collected. The supernatants were incubated with anti-HA antibody (1:100; Covance) for 4 h at 4°C with gentle rotation. Dynabeads Protein G (Thermo Fisher Scientific, US) were washed three times with lysis buffer and added to the antibody-bound supernatants (100 μl per sample). The samples were incubated overnight at 4°C with gentle rotation. The next day, the beads were washed three times with high-salt buffer containing 50 mM Tris, 300 mM KCl, 12 mM MgCl_2 , 1% NP-40, 1 mM DTT, 1x protease inhibitor, 100 U/ml RNasin, and 0.1 mg/ml cycloheximide for 5 min at 4°C . The beads were then resuspended in 350 μl of RLT buffer from the RNeasy Micro Kit (Qiagen, DE) and RNA was extracted according to the manufacturer's protocol.” (Guo et al., 2024)

5.2.14. Next-generation RNA sequencing

“The library was prepared and sequenced by Novogene using the following methods. RNA quality and quantity were assessed using 1% agarose gel electrophoresis and Bioanalyzer 2100 (Agilent Technologies, USA). mRNA was enriched from total RNA using oligo(dT)25 magnetic beads and fragmented randomly. First-strand cDNA was synthesized using random hexamers and reverse transcriptase, followed by second-strand cDNA synthesis using Illumina buffer, dNTPs, RNase H, and E. coli polymerase I. The cDNA products were purified, end-repaired, A-tailed, and ligated with adapters. PCR amplification was performed to enrich the fragments with indexed P5 and P7 primers. The library quality and quantity were verified using Qubit 2.0, real-time PCR, and Bioanalyzer 2100. The libraries were sequenced on the Novaseq6000 platform (Illumina) using the paired-end 150 bp (PE150) strategy.” (Guo et al., 2024)

5.2.15. RNA-seq data processing

“RNA-seq reads were quality-checked using FastQC and aligned to the GRCm38 mouse genome with HISAT2 v2.0.5 (Kim et al., 2019) using default settings. Gene counts were obtained using featureCounts v1.5.0-p3 (Liao et al., 2014). DESeq2 v1.20.0 (Love et al., 2014) was used for downstream analysis in R. Genes with normalized counts below 10 were filtered out. Differentially expressed genes (DEGs) were defined as those with false discovery rate (FDR) below 0.05. Differential expression analysis was performed with the 'DESeq' function using default settings and log fold changes were shrunk. Heatmaps of DEGs with $\text{FDR} < 0.05$ and $\text{log-fold-change} > 1$ at any time point were generated with

heatmap v1.0.12 (Kolde, 2019). Gene ontology (GO) and Kyoto Encyclopedia of Genes and Genomes (KEGG) pathway enrichment analysis of selected gene sets was performed with ClusterProfiler v3.8.1 (Yu et al., 2012). Transcription factors were predicted using Metascape v3.5.20230501 (Han et al., 2018; Zhou et al., 2019) with the DEGs from DEseq2." (Guo et al., 2024)

5.2.16. Cytokine expression analysis

"The cortex and striatum were isolated from 1-mm coronal brain slices after perfusion with ice-cold PBS and stored at -80°C until further analysis. Brain homogenates were prepared in PBS with 1x protease inhibitor cocktail (Roche, CH) and protein concentration was determined using the BCA assay kit (Thermo Fisher Scientific, USA). 200 µg of protein lysate were applied to each membrane of the Proteome Profiler Mouse Cytokine Array Kit (R&D Systems, USA) and Proteome Profiler Mouse XL Cytokine Array (R&D Systems, USA) following the manufacturer's protocol. Membranes were blocked, incubated, and washed as instructed. Four membranes were simultaneously exposed to X-ray film (Fuji) for 15 min. The pixel density of each spot on the membrane was measured using Image J software and adjusted for background and normalized to control." (Guo et al., 2024)

5.2.17. Acute brain slice preparation

"Acute brain slices were prepared from 11- to 13-week-old mice using a previously described method (Zhao et al., 2021a). Briefly, mice were anesthetized with isoflurane (Abbvie, Ludwigshafen, DE) and euthanized them by cervical dislocation followed by decapitation. Brain was swiftly dissected and placed into an ice-cooled, carbogen-saturated (5% CO₂, 95% O₂) cutting solution containing various electrolytes and glucose. 300 µm-thick sections were cutted corresponding to the primary somatosensory cortex (AP -1.6 ± 0.6) with a vibratome VT1200S (Leica Biosystems, Wetzlar, DE) using a 0.12 mm/s cutting speed and a 1.9 mm cutting amplitude. The slices were incubated for 30 min on a custom-made nylon-basket submersed in artificial cerebral spinal fluid (ACSF) containing 126 mM NaCl, 3 mM KCl, 25 mM NaHCO₃, 15 mM glucose, 1.2 mM NaH₂PO₄, 1 mM CaCl₂, and 2 mM MgCl₂ at 32°C. Then the slices were took out from the water bath and placed them to RT with continuous oxygenation before use." (Guo et al., 2024)

5.2.18. Ca²⁺ imaging in hippocampal slices

"The individual acute brain slices were transferred to a self-made imaging chamber under a custom-made 2P-LSM and fixed them by stainless steel rings with 1 mm-spaced nylon fibres (Farmingdale, USA). The imaging chamber was continuously perfused with an oxygenated perfusion solution at a flow rate of 2–5 ml/min by a peristaltic pump LKB P-1 (Pharmacia LKB, SE). Squared field of views (FOVs, 170 x 170 µm) were chosen from the cortical layers II-III of the ctx at a depth ranging from 30 to 100 µm from the slice surface and displaying a uniform astroglial distribution. We performed focal CPA (0.1 mg/ml) and SR101 (0.1 mg/ml) application by borosilicate glass pipettes (Sutter Instrument, US) mounted on 3-axis micromanipulator units (Luigs & Neumann GmbH, DE) controlled by a SM5 Remote Control station (Luigs & Neumann GmbH, DE). Cortical astrocytic Ca²⁺ activity was recorded upon drug application using custom-made detection and MATLAB-

based analysis software (MSparkles v1.8.18) as previously described (Rieder et al., 2022). Fluorescence fluctuations at basal Ca^{2+} concentrations (F_0) were computed along the temporal axes of each individual pixel using a polynomial fitting in a least-squares sense. The range projection of $\Delta F/F_0$ was then used to identify local fluorescence maxima, serving as seed points for simultaneous, correlation-based growing of regions of activity (ROAs).” (Guo et al., 2024)

5.2.19. Electrophysiology of brain slices (LTP)

“LTP recordings from dorsal hippocampus were performed as previously described (Wang et al., 2016; Zhao et al., 2021b). Briefly, acute hippocampal brain slices were prepared as mentioned above. Afterwards, slices were transferred to the recording chamber and continuously perfused with oxygenated ACSF containing (in mM) 1 MgCl_2 and 2.5 CaCl_2 at a flow rate of 2–5 mL/min. Field excitatory postsynaptic potentials (fEPSP) were recorded by a micropipette of 1–3 $\text{M}\Omega$ resistance filled with ACSF in CA1 of hippocampus by stimulating Schaffer collaterals of CA3 using stimulus isolator and a bipolar electrode (WPI). Picrotoxin (50 μM) was perfused in the bath to inhibit ionotropic γ -aminobutyric acid type A receptors (GABAARs). Stimulus duration was 200 μs , current injection was 30–80 μA . To evoke LTP, triple θ -burst stimulation (TBS3) was used. TBS consisted of 10 bursts (4 pulses each burst, 100 Hz) delivered at an interburst interval of 200 ms, and repeated once at 10 s. The stimulation intensity was adjusted to evoke ~30–60% of the maximum response. Waveform analysis was performed by Igor pro v6.3.7.2. The statistical analysis was conducted in Graphpad Prism. All experiments were conducted at RT.” (Guo et al., 2024)

5.2.20. Behavior test

“Depression-like behavior was assessed after LPS challenge with open field and sucrose preference tests, following modified methods from previous studies (Fang et al., 2022; Liu et al., 2018). For the open field test, mice were placed at a random corner of a square open field (50 cm length \times 50 cm width \times 38 cm height) facing the wall and recorded their movement for 10 minutes. The open field tests were performed before and after LPS challenge. The duration in the center area (s), distance moved (cm) and speed (cm/s) were analyzed with EthoVision XT 11.5 (Noldus Technology). For the sucrose preference test, single-housed mice were habituated to two drinking bottles for 2 days. After habituation, mice were presented with 1% sucrose water and tap water in drinking bottles for 2 days. The positions of the bottles were swapped daily. Water and sucrose intake daily were measured by weighing the bottles. Sucrose preference was calculated as the percentage of sucrose intake over total fluid intake and averaged it over the 2 days of testing. The sucrose preference test was performed before and after LPS challenge.” (Guo et al., 2024)

5.2.21. *In vivo* activation of hM4Di

“Three weeks after microinjection of AAV2/5-GFAP-hM4Di-mCherry or AAV2/5-GFAP-tdTomato into the striatum or cortex, CNO (2 mg/kg; dissolved in saline) was intraperitoneally administered two times to mice to activate G_i signaling at 2 hours and 4

hours post LPS challenge, respectively. 6 hours or 24 hours after LPS challenge, animals were used for behavior tests or immunohistochemistry.” (Guo et al., 2024)

5.2.22. Statistics and reproducibility

“The statistical analyses of all data were performed with GraphPad Prism 9.5.1 (GraphPad, San Diego). For all immunostainings, two randomly selected brain slices of each mouse were studied. In addition, For the analysis of Iba1, more than 8 ROIs per mouse was analyzed. For cytokine array, cortex from 2 mice were pooled for each cytokine array membrane. For normally distributed dataset, unpaired t-tests, paired t-test (for studies of behavior), one-way ANOVA and two-way ANOVA were used (indicated in each figure legend), while the Kruskal-Wallis test was used for non-normally distributed datasets. P-values are indicated in the figures and legends. For the *in vivo* experiments, each data point represents the data obtained from a single mouse (except for electrophysiology). The total mouse numbers are indicated in the figure legends. For electrophysiology, each data point refers to a slice and the mouse number is indicated in the figure legends. Normal distributed datasets are shown as mean \pm SEM. else are shown as the median \pm IQR are indicated as thick and thin dashed lines, respectively. *p*-value of ≤ 0.05 was considered statistically significant.” (Guo et al., 2024)

6. RESULTS

6.1. Systemic inflammation augmented adenosine levels in the blood and brain.

Intraperitoneal administration of LPS is widely used for inducing septic systemic inflammation in mice, which can enhance the expression of genes associated with inflammation, astrocyte or microglia reactivity in the brain (Hasel et al., 2021b; Kang et al., 2018). In this study, we i.p. injected LPS (5 mg/kg) into C57BL/6N wild-type mice and analyzed the relative mRNA levels of genes related to inflammation (*Cxcl1*, *Cxcl10*, *Ccl2*, *Ccl5*, *Il1a*, *Il1b*, *Il6*, and *Tnf*), astrocyte reactivity (*Lcn2* and *Gfap*), microglia reactivity (*Itgam*), and pericyte marker (*Pdgfrb*) in the cerebral cortex at 0, 2, 6, and 24 hours post LPS injection (hpi) by quantitative PCR (qPCR) (Figure 8A). We observed that most of these genes were upregulated already at 2 hpi (except *Itgam*), and many of inflammatory genes (*Cxcl1*, *Cxcl10*, *Ccl2*, *Ccl5*, *Il1a*, *Il1b*, *Il6*, and *Tnf*) reached peak between 2-6 hpi. In addition, the expression of *Pdgfrb*, decreased significantly after LPS injection, probably representing dysfunctional changes of the NVU (Figures 8B-8D). These results highlight the rapid neuroinflammatory responses, particularly from astrocytes and pericytes, to systemic inflammation, indicating that brain is highly sensitive to systemic inflammation.

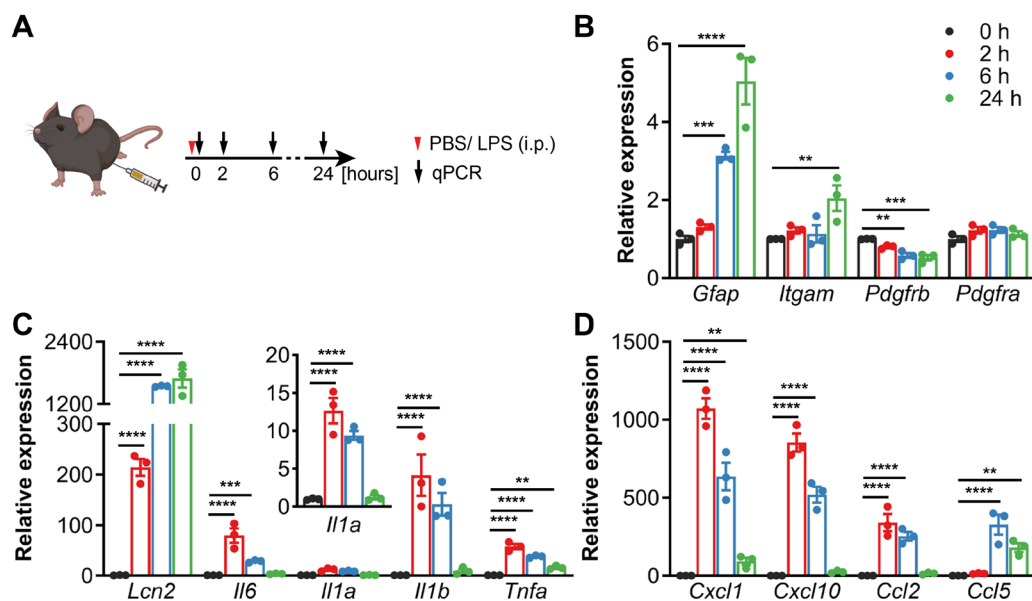


Figure 8. Peripheral LPS challenge altered the gene expression of glial markers as well as chemokines and cytokines.

(A) Schematic experimental illustration. (B-D) Expression levels of glial marker genes (B), proinflammatory cytokine genes (C), and chemokine genes (D) after PBS/LPS injection ($n = 3$ mice per group).

It is known that plasma adenosine levels were elevated in sepsis patients and positively correlated with mortality in sepsis (Martin et al., 2000). In line with previous studies, plasma adenosine levels were rapidly elevated after LPS injection, peaked at 2-6 hpi, and returned to baseline at 24 hpi (Figures 9A and 9B). Studies have shown that systemic inflammation could impair the integrity of BBB (Banks et al., 2015; Haruwaka et al., 2019; Varatharaj and Galea, 2017). Additionally, adenosine has the potential to directly open BBB via endothelial adenosine A1 and A2a receptors (Bynoe et al., 2015a; Carman et al., 2011). Thus, extravasation of Evans blue (EB) dye was used to evaluate the disruption of BBB following LPS challenge. EB was injected intravenously (i.v.) into mice two hours before analysis (Figure 9A). Intriguingly, the disruption of the BBB was detected at 2 hpi, peaked at 6 hpi, and decreased at 12 and 24 hpi (Figure 9C), which was consistent with the changes in plasma adenosine level.

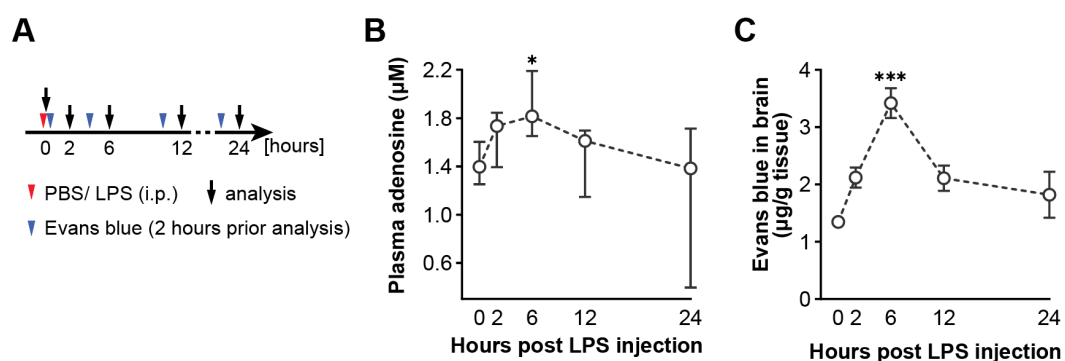


Figure 9. Peripheral LPS challenge increased adenosine levels in the blood.

(A) Schematic illustration of plasma adenosine level experiment and brain EB extravasation experiment. **(B)** Plasma adenosine concentration post peripheral LPS injection ($n = 5$ mice for each time point). **(C)** EB extravasations in the brain post peripheral LPS injection ($n = 3$ mice for each time point).

To investigate whether systemic inflammation could also elicit extracellular adenosine levels in the brain parenchyma, we expressed a newly developed genetically encoded GPCR-Activation-Based adenosine fluorescent sensor (GRAB_{Ado}) in cortical astrocytes and performed 2-photon laser-scanning microscopy (2P-LSM) imaging in awake mice (Figures 10A and 10B) (Peng et al., 2020; Wu et al., 2023). Fluorescence intensities of GRAB_{Ado} increased at 2 hpi, and further increased at 6 and 24 hpi (Figures 10C and 10D), indicating that the extracellular adenosine level was increased in the brain parenchyma in LPS-induced systemic inflammation.

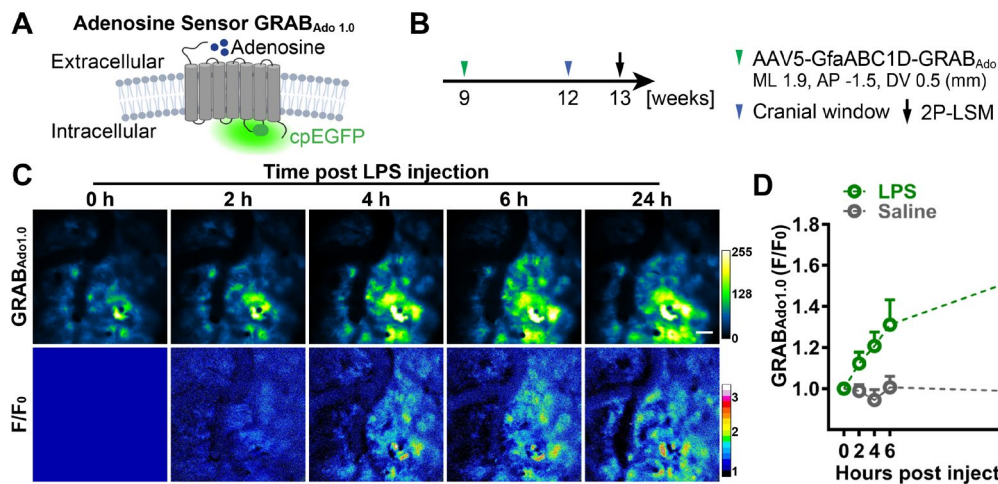


Figure 10. Peripheral LPS challenge increased adenosine levels in the brain.

(A-B) Schematic illustration of the principle of the GRAB_{Ado} sensors (A) and cortical extracellular adenosine level measurement post LPS injection by using GRAB_{Ado} in vivo 2P-LSM live imaging (B). (C) Representative fluorescence images (up) and pseudocolor images (down) of GRAB_{Ado} signals post peripheral LPS injection. Scale bar = 50 μ m. (D) Comparison of relative fluorescence intensities (F.I.) of GRAB_{Ado} acquired in the LPS/Saline injection mice. The recording of 0 h after LPS/Saline injection was used as F₀ (n = 3 mice per group).

We then investigated whether elevated plasma adenosine level could directly affect the homeostasis of extracellular adenosine in the brain. Adenosine (20 mg/kg) and sulforhodamine 101 (SR101, 20 mg/kg) were injected i.p. to GRAB_{Ado}-expressing mice under 2P-LSM live imaging (Figure 11A). Increased GRAB_{Ado} fluorescence intensities were detected in the cortex following adenosine injection, accompanied by an increase in SR101 fluorescence intensities in the cerebral vessels, while injection of saline and SR101 did not result in increased GRAB_{Ado} fluorescence intensities (Figures 11B and 11C). Furthermore, we observed that GRAB_{Ado} fluorescence intensities increased dose-dependently when various doses of adenosine (5 - 20 mg/kg) were applied (Figure 11D), suggesting that elevated plasma adenosine level directly contribute to augmenting brain extracellular adenosine levels.

Altogether our results show that LPS-induced systemic inflammation provoked a rapid increase in adenosine level in the blood resulting in BBB dysfunction, which may contribute to elevating the extracellular adenosine level in the brain at the early phase of systemic inflammation. However, the role of enhanced adenosine signaling in systemic inflammation remains unknown.

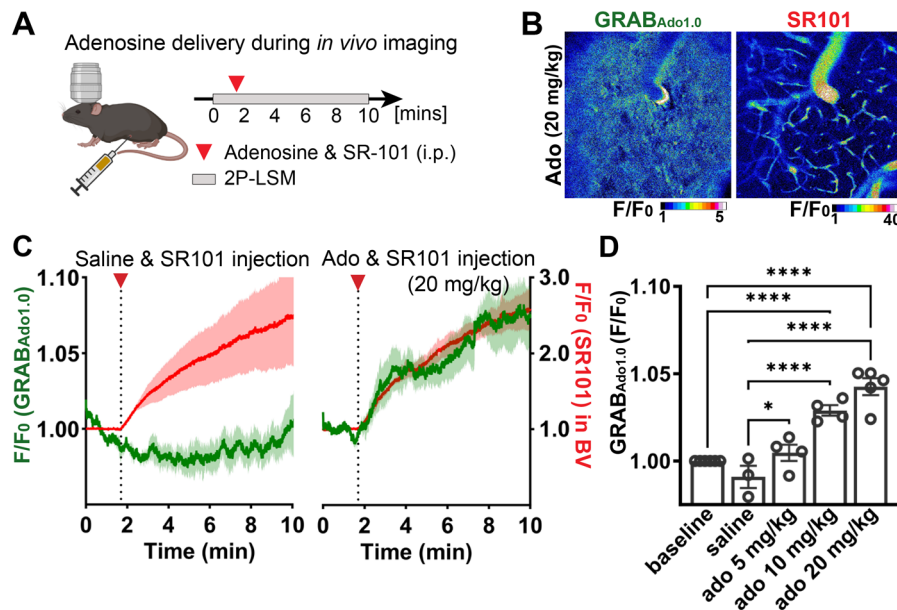


Figure 11. Plasma adenosine contributed to the increase of adenosine levels in the brain.

(A) Schematic illustration of injection of adenosine supplemented with SR101 (i.p.) during the *in vivo* imaging of GRAB_{Ado}. (B) Representative pseudo color images of GRAB_{Ado} signals and SR101 signals after a peripheral adenosine and SR101 injection. Scale bar = 50 μ m. (C) Increase in GRAB_{Ado} signal (green) after the injection of adenosine (20 mg/kg, i.p.) was concomitant with the increase in SR101 signal (red) in blood vessels (BV), while GRAB_{Ado} signal was not altered after saline injection. (D) Relative fluorescence intensities of GRAB_{Ado} upon applications of various dosages of adenosine. The baseline was used as F₀. (baseline n = 6 mice, saline n = 3 mice, ado 5 mg/kg n = 4 mice, ado 10 mg/kg n = 4 mice, ado 20 mg/kg n = 5 mice)

6.2. Peripheral administration of adenosine activated astrocytic A1ARs and induced neuroinflammation.

To determine whether adenosine could evoke cerebral inflammatory response, we intraperitoneally injected adenosine (5 mg/kg) or PBS once per hour to wild-type control (ctl) mice (Figure 12A), due to the short half-life time of adenosine in the blood (~ 1 h) (Chiu et al., 2014). After 6 hours after the first injection, inflammation related gene expression levels in cerebral cortex were quantified by qPCR.

As Figure 12B shown *Lcn2*, expressed by reactive astrocytes (Bi et al., 2013; Kim et al., 2017), was significantly upregulated upon adenosine injection, indicating adenosine administration could induce the astrocyte reactivity. Moreover, the expression levels of several proinflammatory chemokine/cytokine genes such as, *Cxcl1*, *Ccl2*, *Tnf* and *Il1a* were rapidly increased as response to adenosine administration. To confirm this result, NECA, an adenosine analogue with longer half-life (~ 5 h) (Bynoe et al., 2015b), was injected to ctl mice to reduce the impact of multiple injections. Chemokine/cytokine genes expression was analyzed at 6 hpi by qPCR (Figure 12A).

We observed that several inflammatory chemokine/cytokine genes such as *Cxcl1*, *Cxcl10*, *Ccl2*, *Tnf*, *Il6* as well as astrocytic reactive gene *Lcn2* were upregulated in the brain upon

NECA administration (Figure 12C). Taken together, these results suggest that elevated peripheral adenosine directly promotes cerebral proinflammatory factor expression.

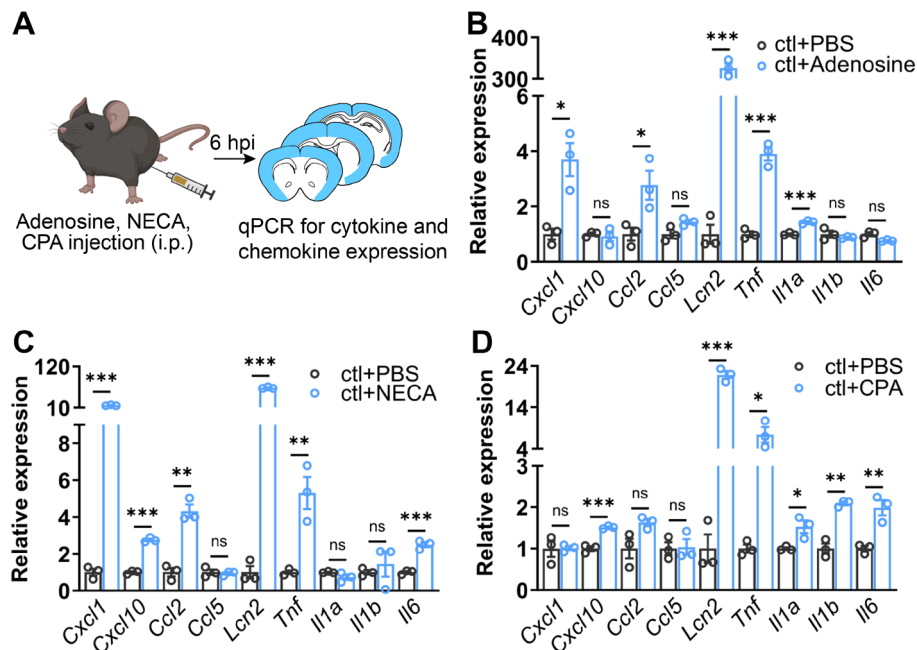


Figure 12. Peripheral adenosine, NECA, CPA administration evoked inflammation-related genes expression in the brain.

(A) Graphic illustration of adenosine, NECA, and CPA administration. (B-D) Expression of inflammatory genes in the mouse cortex upon adenosine, NECA, CPA administration (n = 3 mice per group).

To determine which AR is responsible for provoking cerebral inflammatory gene expression, we injected a selective A1AR agonist CPA (half-life = ~ 0.5 h) to ctl mice as A1ARs are the most abundant AR in the CNS (Elmenhorst et al., 2007; Sebastiao and Ribeiro, 2009). Upregulated gene expressions related to inflammation/astrocyte reactivity were detected at 6 hpi in the cortex (Figure 12D). Furthermore, administration of a low dose of LPS (1 mg/kg, LPS^{low}) combined with CPA significantly augmented the expression of all tested chemokine/cytokine related genes in the cortex compared to LPS^{low} + PBS group (Figure 13A). Moreover, DPCPX, a selective A1AR antagonist, suppressed the expression of inflammation-related genes (e.g., *Cxcl10*, *Ccl2*, *Lcn2*, *Tnf*, and *Il6*) in the cortex of mice exposed to high-dose LPS (5 mg/kg, LPS^{high}) (Figure 13B), as well as reduced glial reactivity and aberrant neuronal activity (Figures 13C and 13D). Taken together, our results indicate that A1AR signaling is directly involved in the induction of neuroinflammation.

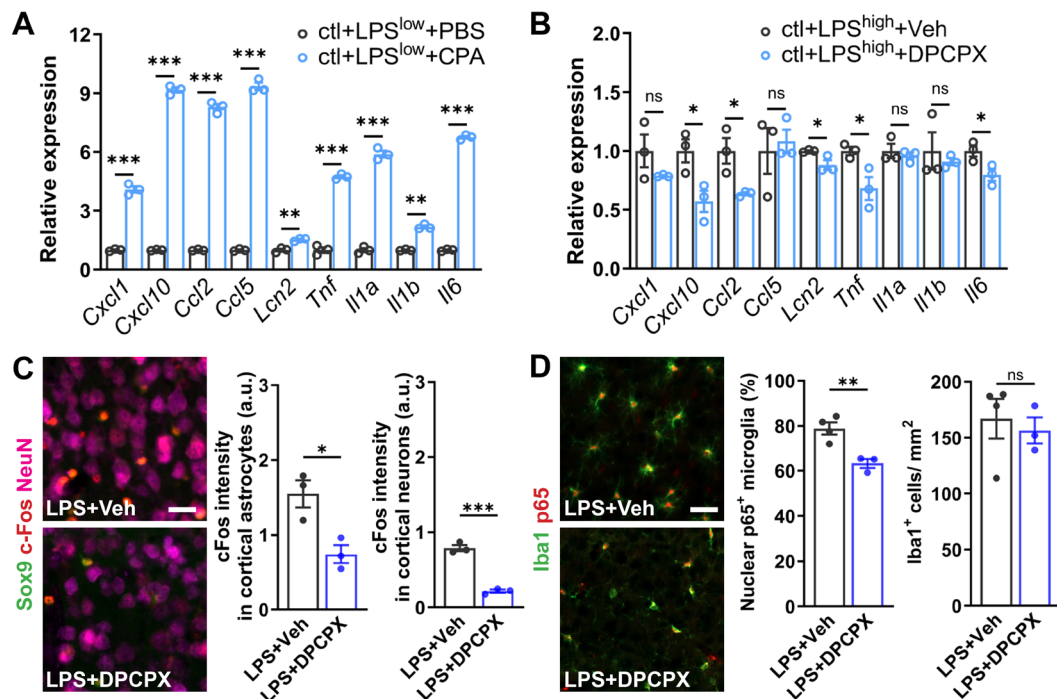


Figure 13. A1AR involved in upregulating inflammation-related genes in the brain.

(A) CPA further upregulated the inflammation-related genes in the cortex induced by a peripheral LPS^{low} (1 mg/kg, i.p.) injection. (n = 3 mice per group). (B) DPCPX administration reduced the inflammation-related genes in the cortex induced by a peripheral LPS^{high} (5mg/kg, i.p.) injection. (n = 3 mice per group). (C) Representative images of immunoreactivity of c-Fos in Sox9⁺ astrocytes and NeuN⁺ neurons in the mouse cortex upon LPS and A1AR antagonist (DPCPX) injection (left). c-Fos expression in astrocytes and neurons was reduced by DPCPX (right) (n = 3 mice per group). (D) Representative images of immunolabeled nuclear p65⁺ microglia upon LPS and DPCPX injection (left). Nuclear p65⁺ microglia were reduced by DPCPX (right) (n = 4 mice in LPS+Veh group, n = 3 mice in LPS+DPCPX group).

To determine the contribution of A1ARs on astrocyte, microglia, pericyte, and oligodendrocyte lineage cell to peripheral adenosine-induced neuroinflammation, we crossed GLAST-CreERT2 mice (Figures 14A and 14B), CX3CR1-CreERT2 mice, and NG2-CreERT2 mice (Huang et al., 2014; Jung et al., 2000; Motori et al., 2013) with floxed A1AR mice (Scammell et al., 2003) to generate inducible astrocytic A1AR conditional knock-out mice (termed GLACx1AR^{fl/fl}, cKO), microglial A1AR conditional knock-out mice (termed CXCTx1AR^{fl/fl}), and pericyte/oligodendrocyte lineage cells conditional knock-out mice (termed NGCEx1AR^{fl/fl}), respectively. In addition, RiboTag reporter (Sanz et al., 2009) was introduced to the breeding to specifically and directly purify mRNAs (mRNA^{RiboTag}) from Cre-expressing cells to avoid the artifacts introduced by cell isolation procedures (Haimon et al., 2018). We were able to show a significant reduction of *Adora1* expression in astrocytes of GLACx1AR^{fl/wt} (het) (by ~40%) and GLACx1AR^{fl/fl} (cKO) (by ~60%) mice compared to ctl mice at six days after Cre activity induction, which was also confirmed by RNA-seq 9 weeks after tamoxifen injection, suggesting successful gene excision of *Adora1* in astrocytes of GLACx1AR^{fl/fl} mice (Fig. 14C and 14D). We also

observed significant reduction of *Adora1* in microglia of CXCTxA1AR^{fl/fl} mice and pericyte/oligodendrocyte lineage cells of NGCExA1AR^{fl/fl} mice (data not shown) with the same strategy.

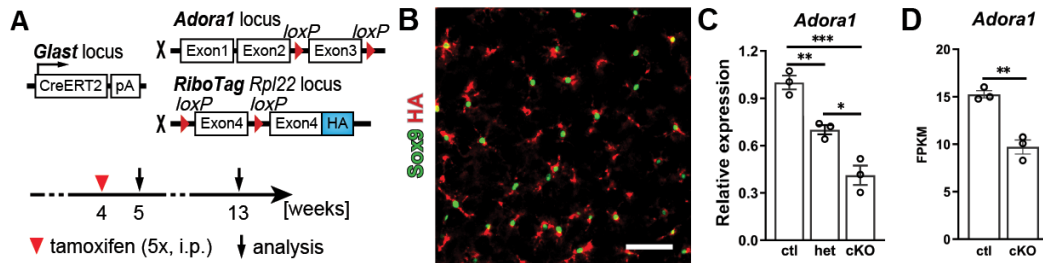


Figure 14. Generation and validation of astrocyte-specific A1AR deficient mice by qPCR and RNA-seq.

(A) Schematic illustration of mouse breeding for astrocyte-specific A1AR deficient mice (GLACxA1AR^{fl/fl}, cKO). **(B)** Representative image of RiboTag expression (indicated by HA-tag) in Sox9⁺ astrocytes. Scale bar = 50 μm. **(C)** *Adora1* expression in astrocytes was reduced in A1AR^{fl/wt} (het) and cKO mice one week after tamoxifen injection by using qPCR (n = 3 mice per group). **(D)** *Adora1* expression in astrocytes was reduced in cKO mice 9 weeks after tamoxifen injection by using RNA-Seq (n = 3 mice per group).

Previous study reported adenosine can evoke rapid onset calcium responses via A1 or A2b receptors (Rittiner et al., 2012), which can be used for monitoring adenosine receptor activation, and adenosine receptor loss function. To confirm the function loss of A1AR in our mutant mice upon tamoxifen administration, a genetically encoded Ca²⁺ reporter (Rosa26-GCaMP3) (Paukert et al., 2014) was introduced to our mutant mice to monitor Ca²⁺ responses. 8 weeks after inducing Cre recombination, *ex vivo* slice recordings of Ca²⁺ response to A1AR selective agonist CPA were performed by 2P-LSM (Figure 15A). Notably, CPA application evoked rapid Ca²⁺ responses in ctl mice which was not observed in cKO mice, indicating A1AR function was lost in cKO mice (Figures 15B-D).

To determine which glial cell contributes more to peripheral adenosine-induced neuroinflammation, we injected CCPA (a more selective A1AR agonist) to GLACxA1AR^{fl/fl} mice, CXCTxA1AR^{fl/fl} mice, NGCExA1AR^{fl/fl} mice and their littermate ctl mice. We observed that the expression of several upregulated cytokines and chemokines (e.g., *Tnf*, *Il1a*, *Ccl2*, *Cxcl10*) was significantly attenuated in GLACxA1AR^{fl/fl} (cKO) mice (Figure 16A), which are not observed in CXCTxA1AR^{fl/fl} mice, NGCExA1AR^{fl/fl} mice (Figure 16B and 16C), indicating astrocytes are the effector of adenosine triggered neuroinflammatory response rather than microglia, OPC, and pericytes.

Taken together, our result strongly suggests that plasma adenosine can evoke neuroinflammation via astrocytic A1AR signaling. However, the underlying mechanism of astrocytic A1AR mediating neuroinflammation remains unclear.

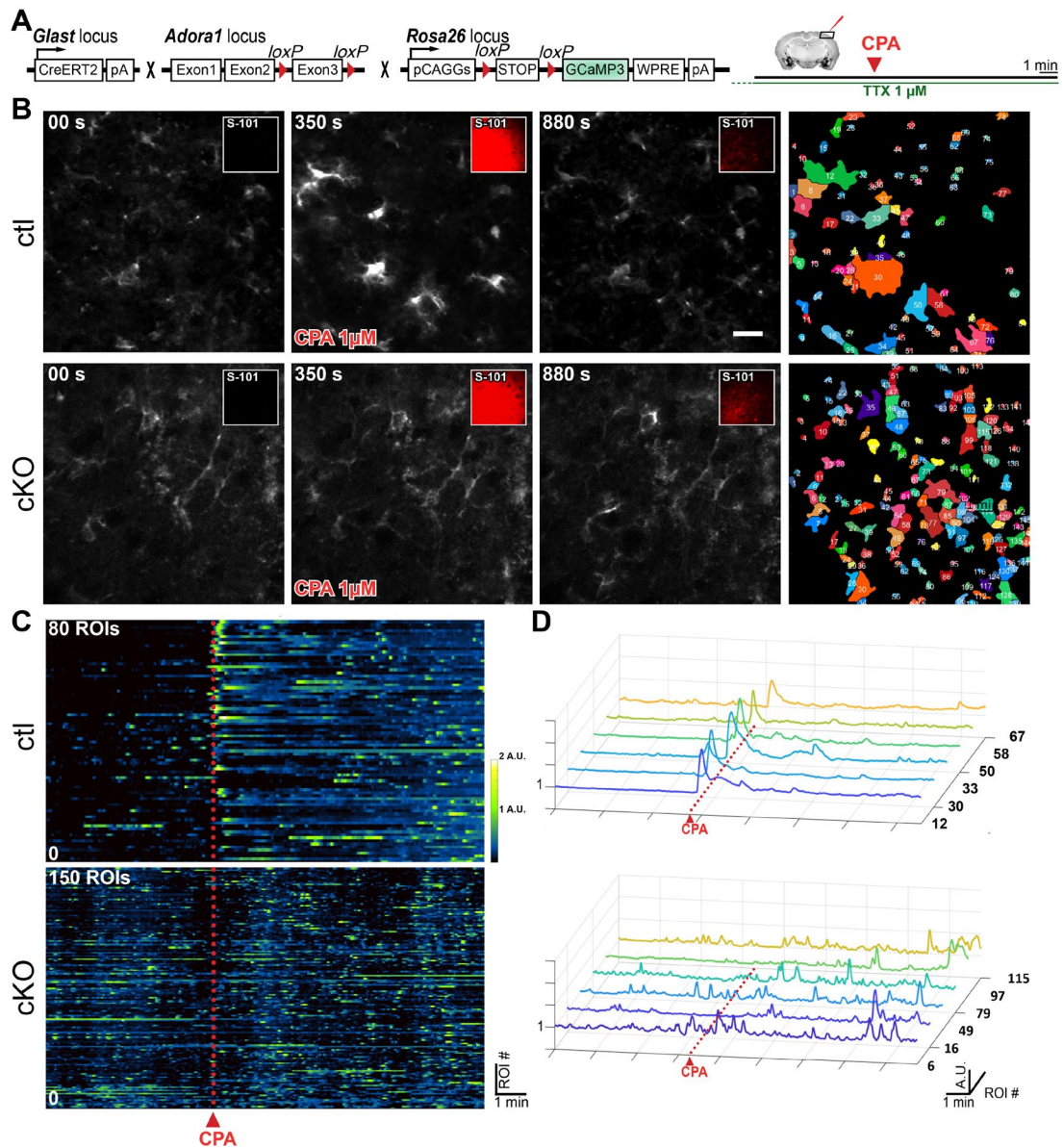


Figure 15. Validation of astrocyte-specific A1AR deficient mice by Ca^{2+} imaging.

(A) Schematic illustration of mouse breeding for Ca^{2+} imaging and experiment plan. **(B)** Images showing the change of Ca^{2+} activity during the recording in ctl and GLACx1A1R^{fl/fl} (cKO) mice. The rightmost images show automatically detected regions of interests (ROIs) with dynamic Ca^{2+} activities by a custom-made tool MSparkles. **(C)** Heatmap plot showing amplitude and duration of spontaneous Ca^{2+} events detected from all ROIs. **(D)** Six ROIs were selected to show the characteristics of Ca^{2+} events.

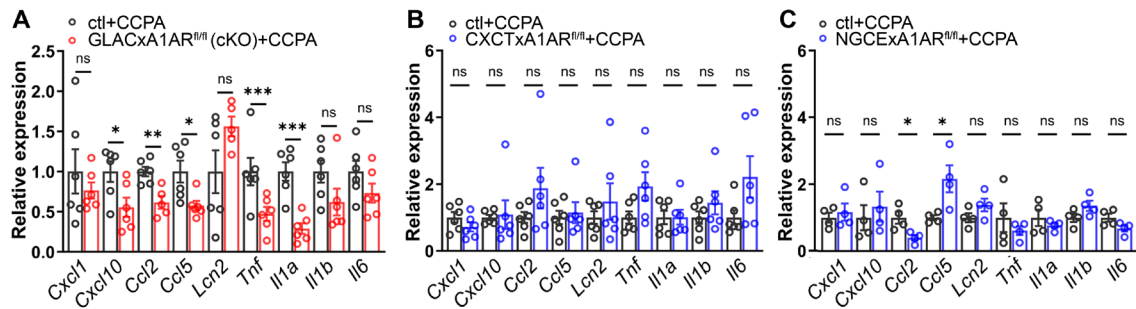


Figure 16. Astrocytic A1AR promoted inflammation-related gene expression.
(A-C) Inflammation-related genes expression in GLACx1A1AR^{fl/fl} mice **(A)**, CXCTx1A1AR^{fl/fl} mice **(B)**, NGCEx1A1AR^{fl/fl} mice **(C)**, and ctl mice upon CCPA injection.

6.3. A1AR signaling promoted the inflammatory reactivity of astrocytes in the early phase of systemic inflammation.

To assess the function of astrocytic A1AR signaling in the early phase of LPS induced systemic inflammation, we first performed the immunostaining marker for reactive astrocytes. Although Glial fibrillary acidic protein (GFAP) is the most widely used marker for reactive astrocytes (Eng et al., 1971), it is difficult to detect significant changes in cortex during the early phase of LPS-induced systemic inflammation by immunostaining (Norden et al., 2016). Indeed, the immediate early gene *Fos* family is frequently used to indicate rapid reactivity of astrocytes and neurons (Ceccatelli et al., 1989; Cruz-Mendoza et al., 2022; He et al., 2019). Therefore, we investigated the time course of astrocyte reactivity after LPS (5 mg/kg) injection by immunostaining of c-Fos along with astrocyte marker Sox9 on mouse brain slices (Figure 17A). We observed that the expressions of c-Fos were not unaltered in the astrocytes of both groups at 0, 2, and 24 hpi. However, the expression of c-Fos in cortical and striatal astrocytes of ctl mice was significantly upregulated at 6 hpi, which was attenuated by the deficiency of astrocytic A1ARs (Figures 17B-17D), suggesting astrocytic A1AR signaling plays a critical role in the early phase of systemic inflammation.

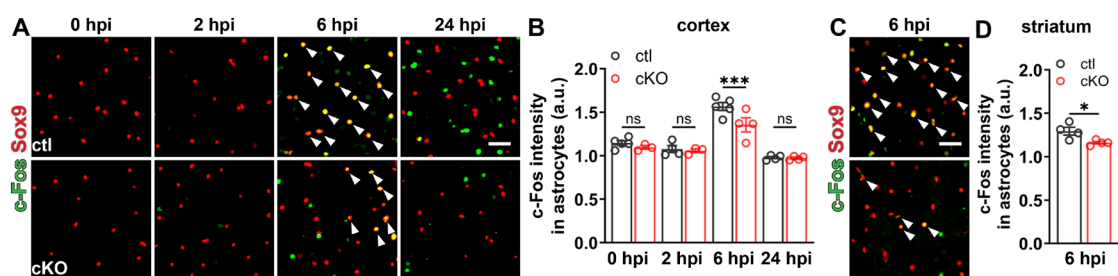


Figure 17. A1AR-deficient astrocytes were less reactive to the peripheral LPS challenge.

(A, C) Representative images of c-Fos expression in Sox9⁺ astrocytes (arrowheads) of cortex and striatum post LPS injection. Scale bar = 20 μ m. **(B, D)** Astrocytic c-Fos immunofluorescence intensity (arbitrary unit, a.u.) was enhanced at 6 hpi in the cortex and striatum of ctl which was inhibited in cKO mice.

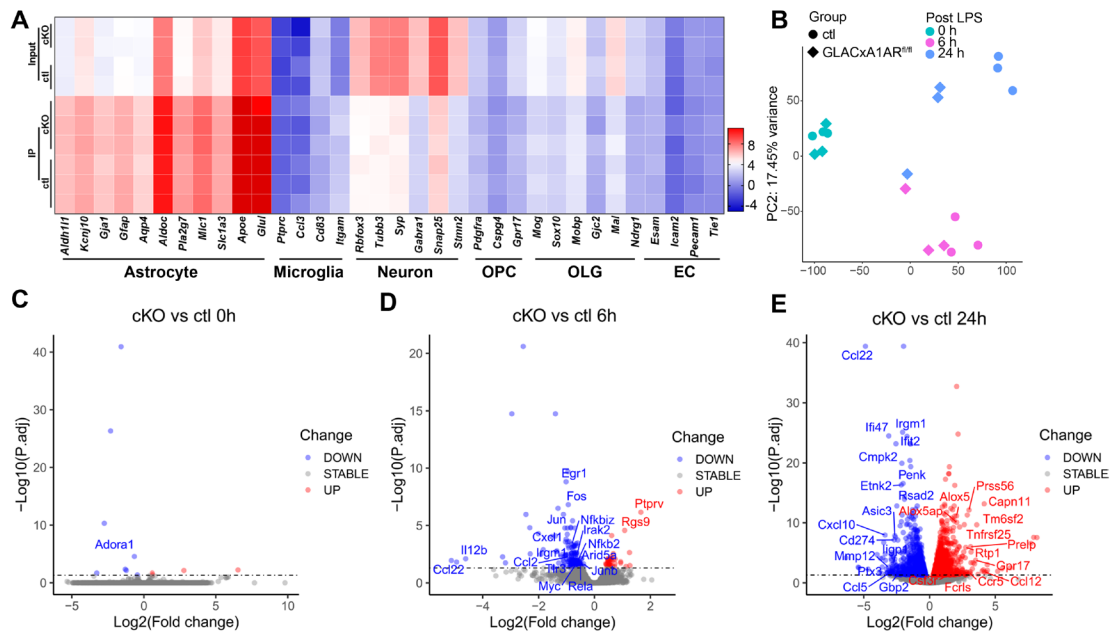


Figure 18. Transcriptional profile of astrocyte after systemic LPS challenge.

(A) Heatmap of cell type-specific marker gene expression showed immunoprecipitation (IP) of RiboTag enriched astrocyte-specific genes. OPC: oligodendrocyte precursor cell, OL: oligodendrocyte, EC: endothelial cell (B) PCA (principal component analysis) of the RNA-seq dataset ($n = 3$ mice per group). (C-E) Volcano plots showed gene expression changes in cKO group compared to ctl group at 0 hpi (C), 6 hpi (D), 24 hpi (E).

To understand the molecular changes of A1AR-mediated astrocyte reactivity, we purified mRNA from cortical astrocytes by RiboTag strategy and cortical homogenates, then performed high-throughput RNA-sequencing (RNA-seq). To confirm the cell type enrichment, marker genes of astrocyte, microglia, neuron, OPC, oligodendrocyte, and endothelial cell were shown in heatmap (Figure 18A). mRNA of astrocyte marker genes was strongly enriched in immunoprecipitated ctl and cKO groups (IP) compared to mRNA from cortical homogenates (input). Next, we compared the differences of gene expression between the ctl astrocytes and A1AR-deficient astrocytes at 0, 6, 24 hpi. Principal component analysis (PCA) separated the ctl astrocytes and A1AR-deficient astrocytes at 6 and 24 hpi, but not at 0 hpi (Figure 18B). In A1AR-deficient astrocytes, we identified 12 (4 up, 8 down), 185 (38 up, 147 down), 2643 (1465 up, 1178 down) differentially expressed genes (DEGs) at 0, 6, 24 hpi, respectively, compared to ctl astrocytes (Figures 18C-18E). Among the downregulated genes in A1AR-deficient astrocytes at 6, 24 hpi, many are key regulators related to inflammatory responses, such as *Fos*, *Jun*, *Junb*, *Nfkb2*, *Nfkbiz*, *Rela*, *Ccl2*, *Cxcl1*, *Cxcl10*, *Mmp12*, which are significantly increased in ctl astrocyte after LPS challenge.

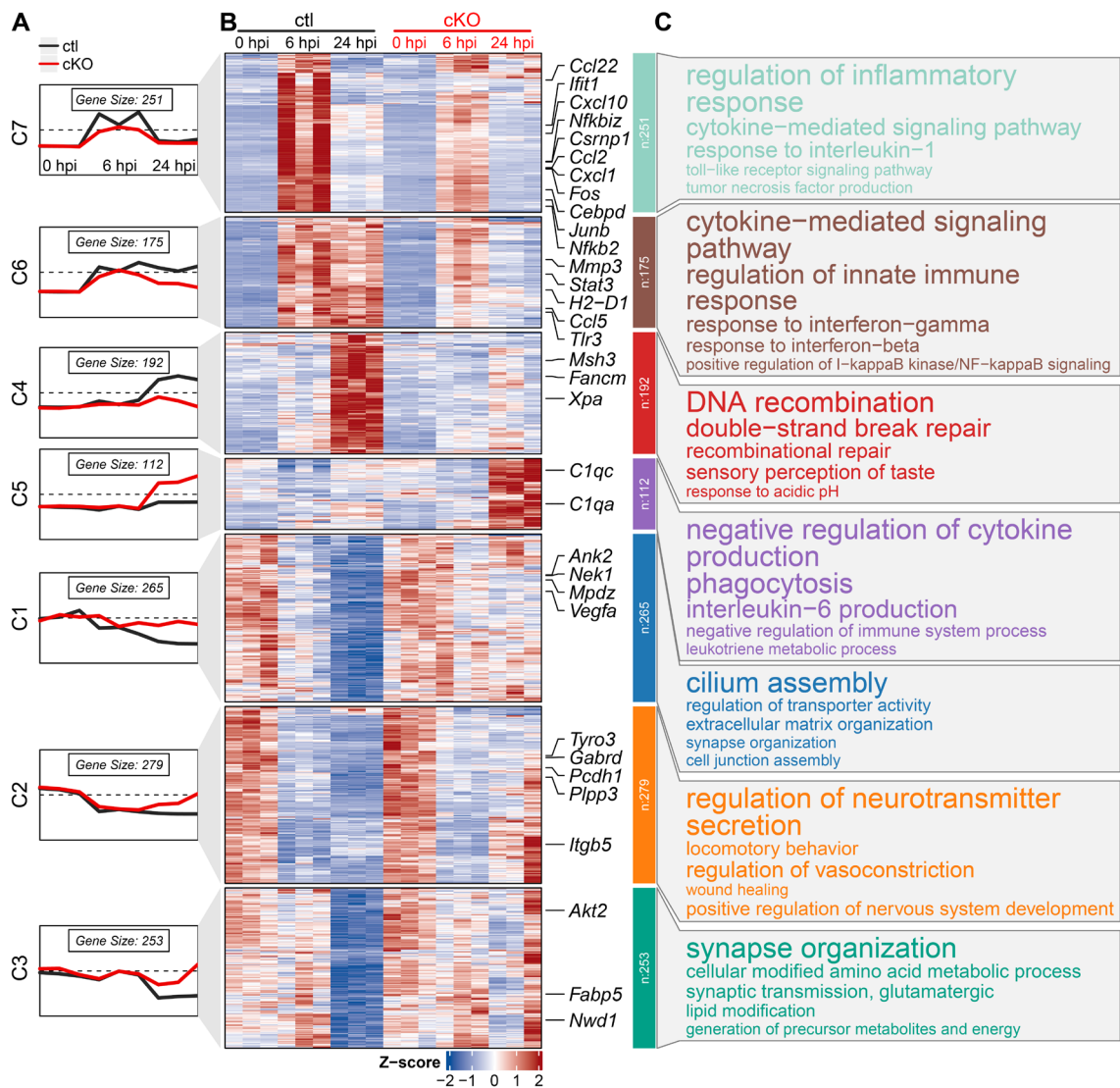


Figure 19. A1AR activation shaped the astrocytic transcriptional profile after systemic LPS challenge.

(A) Profile representation of the temporal gene expression pattern for each cluster at 0, 6, 24 hpi. **(B)** Heatmap of altered gene expression (Padj < 0.05) from astrocytic mRNA^{RiboTag} of male cKO and ctl mice in any of the three time points (n = 3 mice per group). Clustering was done with 7 K-means. **(C)** GO term of each cluster.

Further analysis utilizing Hierarchical Clustering analysis combined with K-means classified DEGs at 0, 6, 24 hpi into 7 distinct clusters (Figures 19A and 19B). At the early phase of systemic inflammation (6 hpi), 426 genes within clusters 6 and 7 exhibited rapid upregulation in ctl mice, which were mainly related to inflammatory chemokines and cytokines (e.g., *Ccl2*, *Ccl5*, *Ccl22*, *Cxcl1*, *Cxcl10*, *Mmp3*, and *Il1a*), inflammatory transcription factors (e.g., *Nfkbiz*, *Nfkb2*, *Cebpd*, *Stat3*, etc.), early responding markers of reactive astrocytes (e.g., *Ifit1*, 2, 3), and antigen presentation (e.g., *Tlr3*, *H2-D1*, *H2-K1*) (Dozio and Sanchez, 2018; Hasel et al., 2021b). Interestingly, the expression of proinflammatory genes was inhibited in A1AR-deficient astrocytes of cKO mice. Notably, many immediate early genes and their transcription factor, presented in cluster 7 (e.g., *Fos*, *Egr1*, *Jun*, and *Junb*), were rapidly upregulated in ctl astrocytes at 6 hpi and subsequently

down-regulated to baseline at 24 hpi as previous studies reported (Dozio and Sanchez, 2018; Hasel et al., 2021b; Kodali et al., 2021), which were also inhibited in A1AR-deficient astrocytes of cKO mice at 6 hpi, consistent with c-Fos immunohistochemistry results. Compared to genes in cluster 7, genes in cluster 6 (e.g., *Ccl5*, *Cxcl10*, *Mmp3*, *Stat3*) maintained high expression level in the ctl astrocytes at 24 hpi but were also inhibited in A1AR-deficient astrocytes. In addition, these genes in clusters 6 and 7 were primarily annotated to inflammation-related Gene Ontology Biological Process terms (GO-BP), indicating LPS induced inflammatory responses were inhibited in A1AR-deficient astrocytes (Figure 19C).

In clusters 1, 2, 3, and 4, 989 genes exhibited slight dysregulation in both ctl and A1AR-deficient astrocytes at 0, 6 hpi but were upregulated in cluster 4 and downregulated in clusters 1, 2, and 3 in ctl astrocytes at 24 hpi. However, these genes in A1AR-deficient astrocytes at 24 hpi were only slightly altered. Furthermore, GO-BP analysis revealed genes in these clusters contributes to 'double-strand break repair' (e.g., *Msh3*, *Fancm*, *Xpa*, etc. in cluster 4), 'positive regulation of nervous system development' (e.g., *Ank2*, *Mpdz*, *Gabrd*, etc. in clusters 1, 2), and 'regulation of neurotransmitter secretion' (e.g., *Pcdh1*, *Plpp3*, etc. in clusters 1, 2), suggesting LPS-induced DNA damage and neurotransmitter deficiency were attenuated in A1AR-deficient astrocytes at 24 hpi which may be considered as the consequence of attenuated inflammatory response in A1AR-deficient astrocytes at 6 hpi.

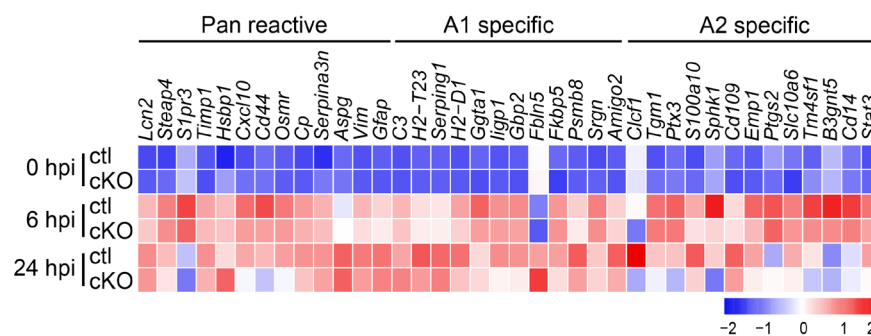


Figure 20. Expression changes of A1/A2 astrocyte marker gene expression in A1AR-deficient astrocytes post LPS injection.

Comparison of the mean expression of pan-reactive, A1-neurotoxic, and A2-neuroprotective marker genes in cortical astrocyte by heatmap.

Regarding of reactive astrocytes, previous studies classified reactive astrocytes into two subtypes, neurotoxic (A1) and neuroprotective (A2) astrocytes, based on the specific upregulated gene expression sets (Clarke et al., 2018; Liddelow et al., 2017a). In our model, we observed most marker genes of A1/A2 astrocyte (except *Fbln5*, *Clcf1*) were upregulated in ctl astrocytes at 6 hpi (Figure 20). Furthermore, all A1 astrocyte marker genes expression remained at high level at 24 hpi, while many of A2 astrocyte marker genes expression was decreased at 24 hpi (e.g., *Tgm1*, *Ptx3*, *Sphk1*, *Emp1*, *Ptgs2*, *Slc10a6*, *Tm4sf1*, *B3gnt5*, *Cd14*, *Stat3*). Many of A1 astrocyte marker genes (e.g., *H2-T23*, *H2-D1*, *Gbp2*, *Iigp1*, *Psmb8*), A2 astrocyte marker genes (e.g., *Clcf1*, *Tgm1*, *Ptx3*), and

reactive astrocytes pan marker genes (e.g., *Lcn2*, *Steap4*, *S1pr3*, *Timp1*, *Cxcl10*, *Cd44*, *Osmr*, *Cp*, *Vim*) were also decreased in A1AR-deficient astrocytes at both 6 hpi and 24 hpi, indicating A1AR-deficient astrocytes were less reactive to systemic LPS challenge.

To investigate the involved signaling pathways, a GSEA-based KEGG pathway analysis (GSEA-KEGG) was performed (Figures 21A and 21B). We observed the suppression of pathways related to the inflammatory response in A1AR-deficient astrocytes of mutant mice at 6 hpi (e.g., 'NF-kappa B signaling pathway', 'JAK-STAT signaling pathway', 'IL-17 signaling pathway', 'NOD-like receptor signaling pathway', 'TNF signaling pathway', etc.) (Han et al., 2021; Sofroniew, 2020). Concurrently, GSEA-GO-BP analysis highlighted the suppression of genes associated with inflammation-related GO terms (e.g., 'interleukin-1 production', 'toll-like receptor signaling pathway', 'receptor signaling via JAK-STAT', 'I-kappaB/NF-kappaB signaling', 'inflammatory response, cytokine response', 'interferon-gamma production', etc.) in A1AR-deficient astrocytes at 6 hpi (Figures 21C and 21E). Furthermore, Metascape analysis revealed that the suppressed genes in A1AR-deficient astrocytes at 6 hpi were under the control of transcription factors (e.g., *Cebpb*, *Fos*, *Jun*, *Nfkb1*, *Stat3*, etc.) known to regulate downstream proinflammatory pathways of reactive astrocytes (Figure 21D) (Han et al., 2021).

Taken together, our results demonstrated that adenosine triggered the inflammatory response of reactive astrocytes via A1ARs during the early phase following a peripheral LPS challenge, potentially influencing the subsequent progression of neuropathology.

6.4. Astrocyte reactivity in the early phase of systemic inflammation boosted the inflammatory response of microglia as well as global neuroinflammation.

Astrocyte as well as microglia are the key mediators of neuroinflammation. Previous studies suggested that interaction between astrocyte and microglia contributes to the modulation of neuroinflammation (Bhusal et al., 2023; Han et al., 2021; Kwon and Koh, 2020; Linnerbauer et al., 2020). However, pioneering studies predominantly delved into the late phase of this model. Here, our findings strongly suggest an adenosine-mediated rapid response of astrocytes (2-6 hpi) regulates the expression of inflammation-related genes (e.g., *Ccl2*, *Ccl5*, *Cxcl1*, *Cxcl10*, *Il1a*, and *Il1b*), which can trigger reactive microglia (Jha et al., 2019). Therefore, we hypothesized that astrocytes could modulate microglia reactivation in the early phase of systemic inflammation rather than just be the effector of reactive microglia.

We first investigated the reactivity of microglia in LPS-induced neuroinflammation model by detecting nuclear translocation of p65, a co-factor of NF- κ B which serves as a pivotal mediator of microglial inflammatory responses (Borst et al., 2021; Liu et al., 2017) (Figure 22A). In the cortex of ctl mice, the percentage of nuclear p65⁺ microglia rose from approximately 13% at 2 hpi to nearly 90% at 6 hpi, then reduced to 30% at 24 hpi. Conversely, this percentage fell to around 9% at 2 hpi, 50% at 6 hpi, and 13% at 24 hpi, respectively, in the cortex of cKO mice (Figure 22B). A similar reduction in nuclear p65⁺ microglia was also observed in the hippocampus and striatum of cKO mice at 6 hpi

(Figures 22C and 22D). However, the microglial densities in both ctl and cKO mice were similar at 0 hpi, 2 hpi, 6 hpi, and 24 hpi (data not shown).

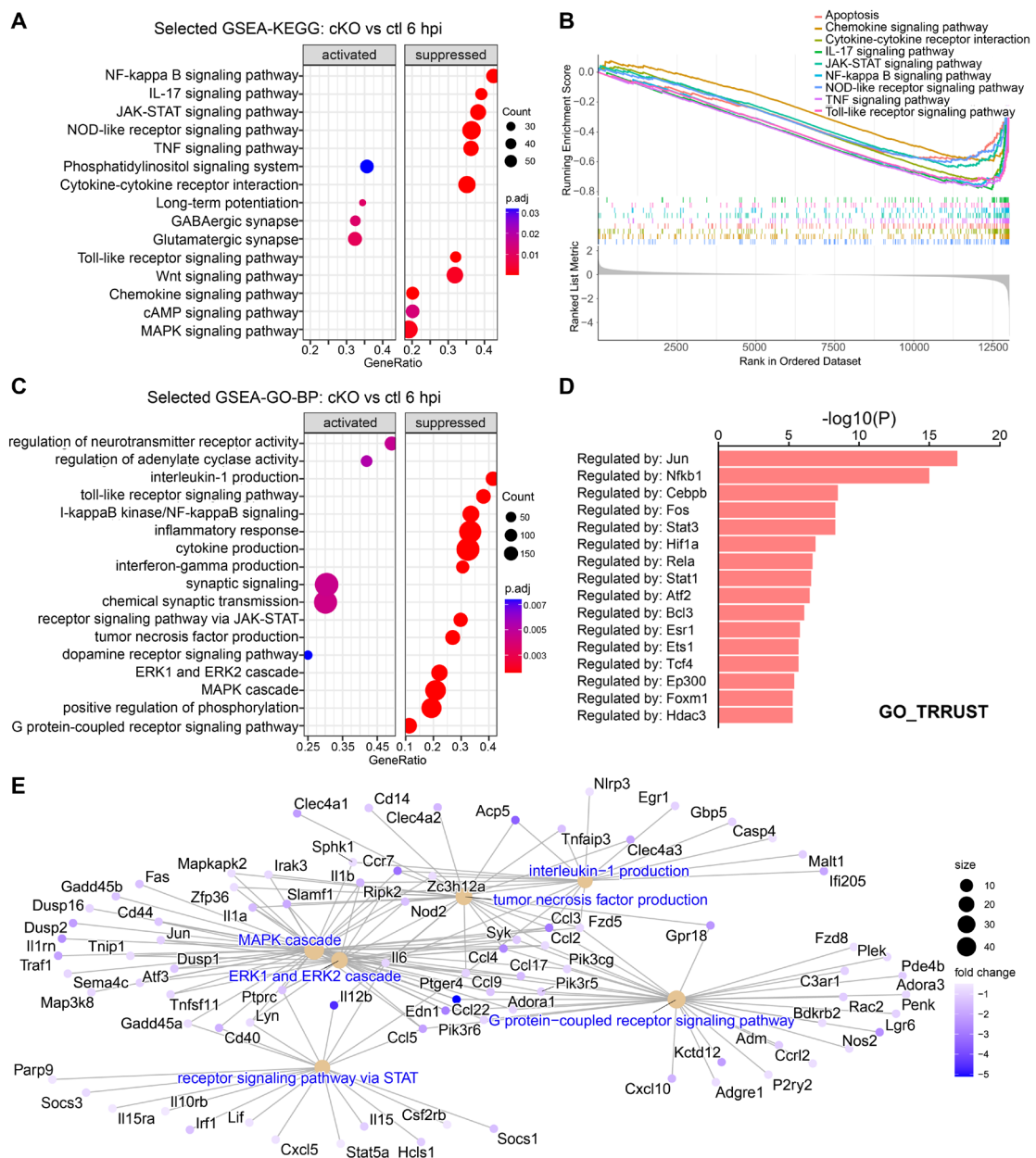


Figure 21. Pathway analysis of RNA-seq data obtained from cortical astrocytes of A1AR-deficient and ctl mice post LPS injection.

(A) Selected GSEA-KEGG pathway analysis of the astrocytic RNA-seq dataset between the cKO and ctl groups at 6 hpi. (B) Selected GSEA plot of the enriched KEGG pathways related to inflammation between the cKO and ctl groups at 6 hpi. (C) Selected GSEA-GO pathway analysis of the astrocytic RNA-seq dataset between the cKO and ctl groups at 6 hpi. (D) Prediction of transcription regulators following expression pattern of sub-clusters (cluster 6 and 7 in Figure 17D) by Metascape analysis (Han et al., 2018; Zhou et al., 2019). (E) Category net plot of selected enriched GO pathways relative to G protein-coupled receptor signaling pathway. The color gradient indicates the fold changes between the cKO and ctl groups.

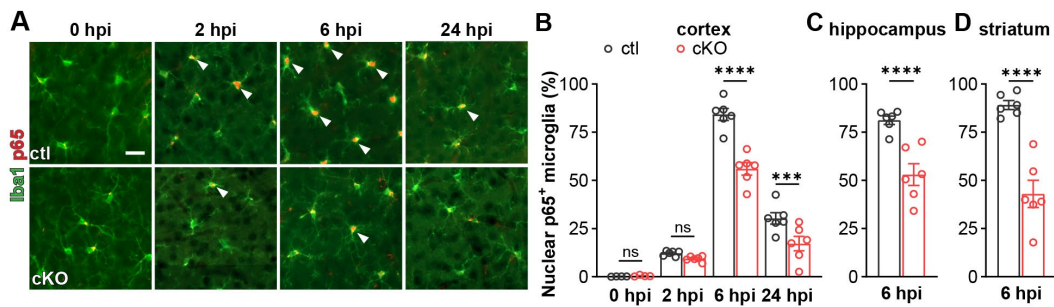


Figure 22. Astrocytic A1AR deficiency inhibited microglial p65 expression after LPS challenge.

(A) Representative images of p65 immunoreactivity in Iba1⁺ microglia post LPS injection. Arrowheads indicated Iba1⁺ microglia with nuclear p65. Scale bar = 20 μ m. (B-D) Proportions of nuclear p65⁺ microglia were reduced in the cortex, hippocampus, and striatum of cKO mice post LPS injection compared to ctl mice (n = 4 mice in ctl/ cKO at 0 hpi, n = 6 mice in ctl/cKO at 2 hpi, 6 hpi, and 24 hpi).

To investigate the functional changes of microglia, e.g. phagocytic ability, in our cKO mice after LPS challenge, the cumulation of CD68⁺ lysosome volume in microglia was calculated by microglial 3D reconstruction (Figure 23A). In line with the p65⁺ results, reduced CD68⁺ lysosome volume was observed in our cKO mice at 6 hpi and 24 hpi compared to ctl mice, which was not observed at 0 hpi (Figure 23B). Altogether, our results revealed that a systemic LPS challenge initiates astrocyte activation in the early phase via A1AR to augment microglial reactivation.

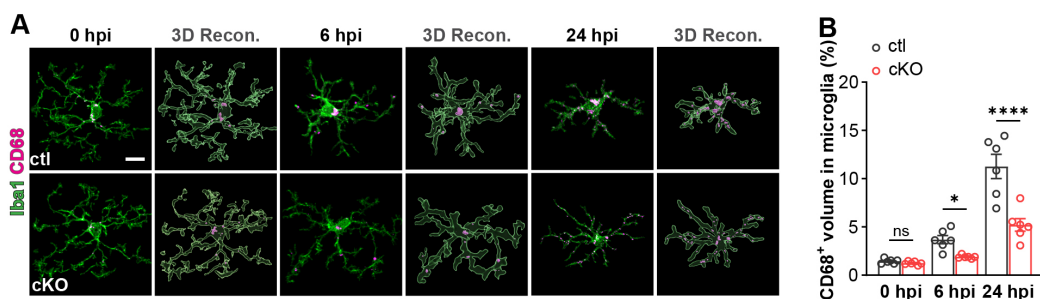


Figure 23. Astrocytic A1AR deficiency reduced microglial lysosomes after LPS challenge.

(A) Representative images and 3D reconstructions of CD68⁺ and Iba1⁺ volume post the LPS injection by IMARIS. Scale bar = 10 μ m. (B) Percentage of CD68⁺ volume in microglia in the cortex of cKO mice were reduced post LPS injection compared to ctl mice (n = 6 in ctl and cKO at 0 hpi, 6 hpi, and 24 hpi).

Previous studies show activation of microglia normally reduces the ramified morphology and *P2ry12* gene expression, which is used for evaluating microglia activation and inflammation in the brain (Adrian et al., 2023; Vidal-Itriago et al., 2022). Therefore, the morphology change of microglia was analyzed in both ctl and cKO mice (Figure 24A). In healthy conditions (0 hpi), microglia exhibited comparable ramified morphology in ctl and cKO mice. After LPS challenge, the microglia in ctl mice demonstrated increased

intersections in the Sholl analysis, reduced total process length, decreased occupied area, and declined segment number, while the change of microglial morphology was ameliorated in cKO mice (Figures 24B and 24C). In addition, *P2ry12* gene expression was rapidly reduced in both ctl and cKO mice at 6 hpi. It was recovered to baseline in cKO mice at 24 hpi, but not in ctl mice (Figure 24D). Taken together, our data suggests that activation of microglia was decreased in the absence of astrocytic A1AR signaling.

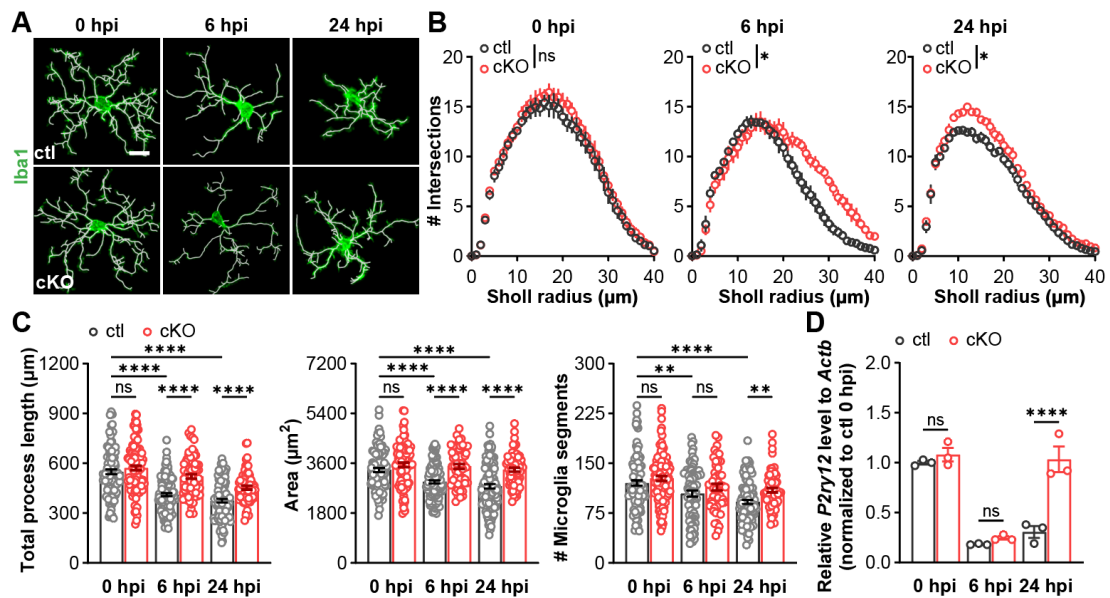


Figure 24. Astrocytic A1AR deficiency inhibited microglial activation and global neuroinflammation upon peripheral LPS challenge.

(A) Morphology of Iba1⁺ microglia post the LPS injection. 3D reconstruction was obtained using IMARIS. Scale bar = 10 μm. **(B)** Sholl analysis of Iba1⁺ microglia at 0 hpi, 6 hpi, 24 hpi (n = 3 mice per group). **(C)** Total process length of Iba1⁺ microglia in cKO and ctl mice post LPS injection (n = 3 mice per group). **(D)** Relative expression of *P2ry12* was elevated in the cortex of cKO mice at 24 hpi (n = 3 mice per group).

Since reactive astrocyte and microglia can release multiple proinflammatory factors as response to systemic inflammation (Giovannoni and Quintana, 2020; Hanisch, 2002), we then investigated the cytokine expression in the brain at the early phase of LPS-induced systemic inflammation (6 hpi) (Figures 25A and 25B). Under healthy conditions, the expression level of all detected cytokines showed a similar pattern in the cortex and striatum of ctl and cKO mice. However, the expression level of many proinflammatory cytokines and chemokines released by reactive astrocyte (e.g., CXCL1, CXCL10, CXCL12, ICAM-1, LCN-2, MMP3) and many other cytokines and chemokines released by reactive astrocyte and microglia (e.g., CCL2, CCL5, CCL12, IL-1 α , CXCL2, etc) were significantly increased in the cortex of ctl mice at 6 hpi, which was alleviated in cKO mice (Figure 25A). Consistently, ctl mice also showed enhanced cytokine and chemokines expression in the striatum at 6 hpi, while cKO mice exhibited a similarly reduced pattern of inflammatory response (Figure 25B).

Taken together, adenosine signaling via A1ARs triggers astrocytic rapid response at the early phase of systemic inflammation, enhancing microglial activation and exacerbating global neuroinflammation.

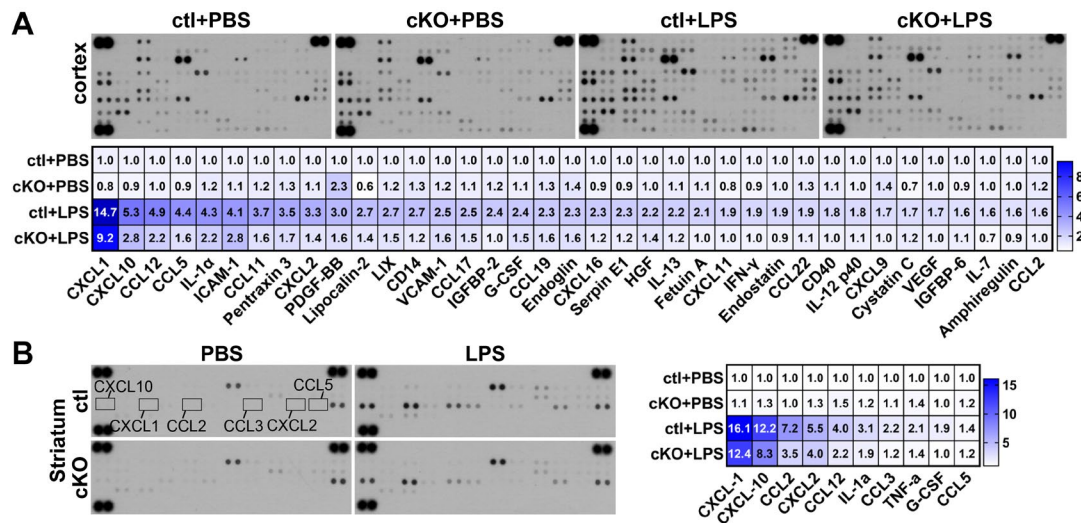


Figure 25. Astrocytic A1AR deficiency inhibited global neuroinflammation at 6 hpi upon peripheral LPS challenge.

(A) Cytokine expression in the cortex of ctl and cKO mice was measured by a proteomic profiling assay at 6 hpi (samples from 3 mice were pooled for each group). Color bar range is between 0.5 and 9.5, out range value was labelled with dark blue. (B) cytokine expression in the striatum of ctl and cKO mice was measured by a proteomic profiling assay at 6 hpi (samples from 3 mice were pooled for each group).

6.5. Astrocytic A1AR signaling activation impaired BBB integrity in systemic inflammation.

Adenosine signaling itself or proinflammatory cytokines and chemokines could mediate BBB integrity via multiple pathways. A recent study shows the microglia could migrate to blood vessels and impair BBB integrity via the CCL5-CCR5 axis in systemic inflammation (Haruwaka et al., 2019). In line with the previous study, we also found that the migration of microglia to blood vessels rose from ~35% at 0 hpi to ~50% at 6 hpi and 24 hpi, which only slightly increased from ~35% at 0 hpi to ~43% at 6 hpi and ~43% at 24 hpi (Figures 26A-26C), which may be due to less CCL5 expression in cKO mice, suggesting BBB dysfunction was reduced in cKO mice. To evaluate the integrity of the BBB, EB was intravenously injected after LPS injection. After 24 hours of circulation, EB leakage was lower in the brain parenchyma of cKO mice (~10 µg/g tissue), compared to ctl mice (~22 µg/g tissue) (Figure 26D). These results suggested the absence of astrocytic A1ARs reduced systemic inflammation-induced BBB disruption. Systemic inflammation induces neutrophil infiltration into the brain parenchyma, related to disrupted BBB and upregulated chemokine (e.g., CXCL1) and extracellular matrix protein (e.g., ICAM-1) (Huang et al., 2023; Rummel et al., 2010). Ly6B immunostaining confirmed reduced infiltration of Ly6B⁺ cells into the brain parenchyma at 24 hpi in cKO mice compared to ctl (Figures 26E and 26F). In summary, astrocytic A1AR deficiency alleviates systemic inflammation-induced BBB impairment.

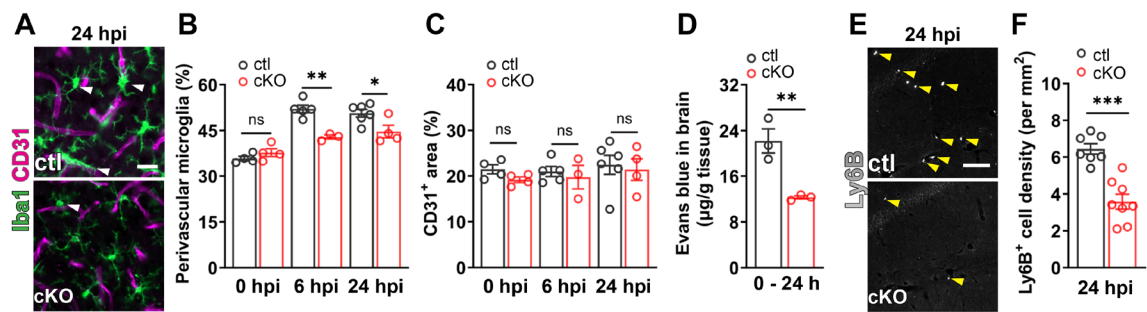


Figure 26. Astrocytic A1AR deficiency reduced BBB disruption and neutrophil infiltration post peripheral LPS injection.

(A) Representative images of immunolabeled Iba1⁺ microglia and CD31⁺ blood vessels at 24 hpi. Perivascular microglia were indicated by arrowheads. Scale bar = 20 µm. (B) Proportion of perivascular microglia was reduced in cKO mice compared to ctl mice (n = 4 mice in ctl/ cKO at 0 hpi, n = 5 mice in ctl at 6 hpi, n = 3 mice in cKO at 6 hpi, n = 6 mice in ctl at 24 hpi, n = 4 mice in cKO at 24 hpi). (C) CD31⁺ area was not altered in cKO and ctl mice at 0 hpi, 6 hpi, 24 hpi. (D) EB extravasation was reduced in the brains of cKO mice compared to ctl mice which were injected with EB at 0 hpi and analyzed at 24 hpi (n = 3 mice per group). (E) Representative images of immunolabeled Ly6B⁺ neutrophils in brain parenchyma at 24 hpi. Scale bars = 200 µm. (F) The density of Ly6B⁺ cells were reduced in the brain of cKO mice compared to ctl mice at 24 hpi (n = 7 ctl mice and 8 cKO mice).

6.6. A1AR-mediated astrocyte activation promoted aberrant neuronal functions and depression-like behavior in systemic inflammation.

A common symptom of SAE is aberrant neuronal functions mediated by proinflammatory factors, such as CCL2, CCL3, LCN-2 (Vachharajani et al., 2005; Xin et al., 2023) (Duan et al., 2018). To define the role of astrocytic A1ARs in LPS-induced aberrant neuronal hyperactivity, co-immunostaining of NeuN (a pan marker for neuron) and c-Fos were analyzed (Figure 27A). The c-Fos immunostaining intensity gradually increased in the cortical neurons of ctl mice at 6 hpi and 24 hpi, which was lower in the cKO mice (Figure 27B). Similarly, a decreased intensity of c-Fos in NeuN⁺ neurons was observed in the striatum of cKO mice at 24 hpi, compared to ctl mice (Figures 27C and 27D), indicating the activation of astrocytic A1AR contributed to aberrant neuronal activity in systemic inflammation.

Systemic inflammation was reported to transiently impair the response of hippocampal neurons to repeated synapse stimulation, in terms of long-term potentiation (LTP) (Izumi et al., 2021; Shemer et al., 2020; Wu et al., 2021). To probe the impact of astrocytic A1AR on neuronal fitness, we performed extracellular electrophysiological recordings on acute slices from the dorsal hippocampi of ctl and cKO mice at 0 hpi, 6 hpi, and 24 hpi (Figure 28A). Neurons of ctl and cKO mice displayed comparable LTP after PBS injection (Figures 28B and 28C). However, cKO mice displayed a greater preserved LTP than ctl mice at 6 hpi (Figures 28B and 28C). Moreover, cKO mice displayed a better recovery of LTP at 24 hpi, compared to ctl mice (Figures 28B and 28C). These findings suggest that

hyperactivation of astrocytes via A1ARs in systemic inflammation causes impairment of neuronal function in the hippocampus.

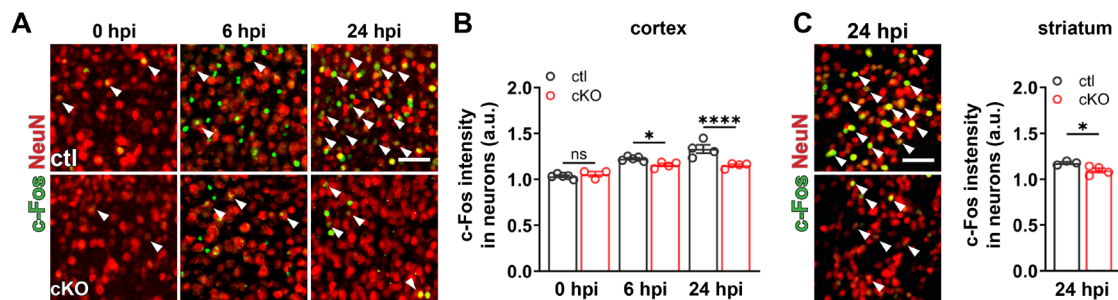


Figure 27. Astrocytic A1AR deficiency prevented aberrant neuronal hyperactivation after LPS treatment.

(A) Representative images of c-Fos immunoreactivity in cortical NeuN⁺ neurons after LPS injection. Scale bar = 20 μ m. (B, C) c-Fos immunofluorescence intensities (a.u.) in NeuN⁺ neurons in cortex and striatum of cKO mice were reduced compared to ctl mice at 6 and 24 hpi (n = 4 mice in ctl/ cKO at 0 hpi, n = 5 mice in ctl at 6 hpi, n = 3 mice in cKO at 6 hpi, n = 6 mice in ctl at 24 hpi, n = 4 mice in cKO at 24 hpi in B; n = 4 mice per group in C).

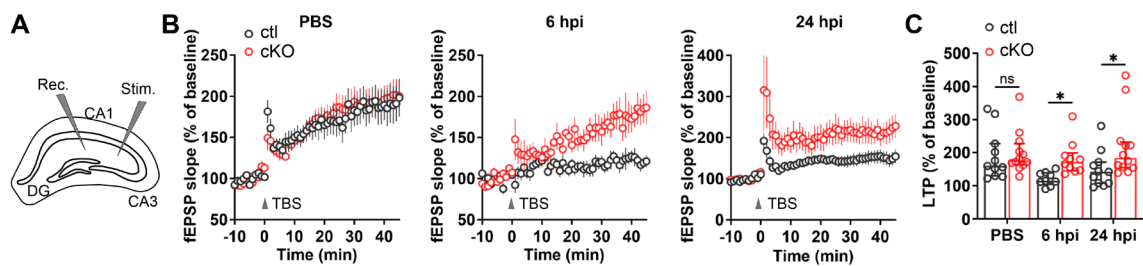


Figure 28. Astrocytic A1AR deficiency protected LTP of the mice after LPS treatment.

(A) Graphical description of LTP measurement protocol. (B) Scatter plots showing LTP induced by stimulation of Schaffer collateral (SC) — cornu ammonis (CA) 1 synapses with TBS in acute hippocampal slices from ctl and cKO at 0 hpi, 6 hpi, 24 hpi. Averaged fEPSP are plotted versus time (n = 11 slices in ctl at 0 hpi, n = 12 slices in cKO at 0 hpi, n = 9 slices in ctl at 6 hpi, n = 10 slices in cKO at 6 hpi, n = 11 slices in ctl at 24 hpi, n = 12 slices in cKO at 24 hpi). (C) LTP evoked in hippocampi of cKO and ctl mice.

Peripheral administration of LPS induces an onset of sickness behavior in mice, characterized by hunched posture and reduced food and water intake, peaking between 2-6 hpi. Subsequently, depression-like behavior emerges, such as decreased locomotion in the open-field test and loss of preference for sweetened water, peaking at 24 hpi (Dantzer et al., 2008; Kang et al., 2018). To assess depression-like behavior induced by systemic inflammation, we performed the open-field test and sucrose preference test at 24 hpi (Figure 29A). Both ctl and cKO mice exhibited reduced locomotion after LPS injection, whereas cKO mice demonstrated increased total traveled distances compared to ctl mice (Figures 29B and 29C). Of note, PBS injected ctl and cKO mice showed similar performance of locomotion. In addition, sucrose preference test showed that while

peripheral LPS challenge substantially reduced sucrose preference in ctl mice from 24-48 hpi (~45%), with partial recovery to ~60% from 48-72 hpi, cKO mice displayed only partial impairment (~65%) from 24-48 hpi, nearly fully recovering to a healthy level (~80%) from 48-72 hpi (Figure 29D). Taken together, our findings indicate the role of astrocytic A1AR activation in contributing to depression-like behavior triggered by systemic inflammation.

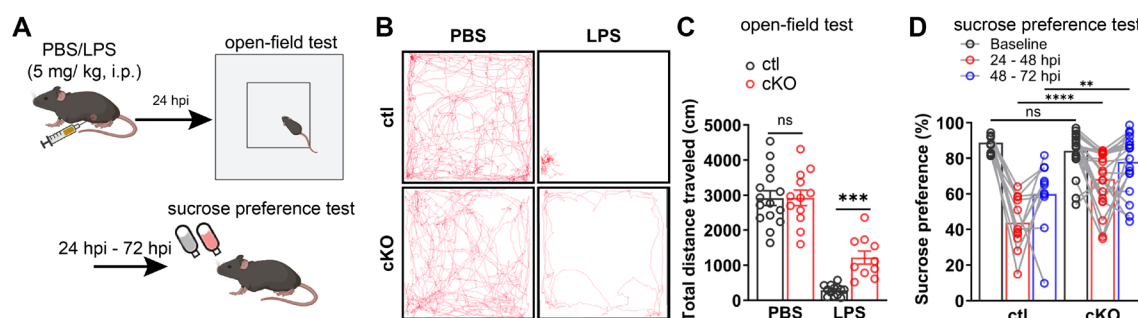


Figure 29. Astrocytic A1AR deficiency ameliorated depression-like behavior of the mice after LPS treatment.

(A) Schematic illustration of open-field test and sucrose preference test post PBS/LPS injection. **(B)** Representative trajectory analysis of ctl and cKO mice in 10 min in the open-field test at 24 hpi. **(C)** cKO mice displayed protected locomotion compared to ctl mice at 24 hpi ($n = 15$ mice in ctl PBS group, $n = 12$ mice in cKO PBS group, $n = 12$ mice in ctl LPS group, $n = 10$ mice in cKO LPS group). **(D)** cKO mice displayed less LPS-induced decreased in sucrose preference than ctl after LPS injection ($n = 11$ mice in ctl group, $n = 20$ mice in cKO group).

6.7. Enhancing G_i signaling in A1AR-deficient astrocytes restored neuroinflammation upon peripheral LPS challenge.

A1ARs are known as $G_{i/o}$ protein-coupled receptors, suggesting G_i signaling response was also compromised in the astrocyte of cKO mice. In addition, accumulating evidence suggests striatum is the core brain region, contributing to the development of severe depression-like behaviors in LPS-induced systemic inflammation (Klawonn et al., 2021). Hence, to rescue the phenotype we observed in astrocytic A1AR cKO mice, we expressed Designer Receptors Exclusively Activated by Designer Drugs (DREADDs) GFAP-hM4Di-mCherry in the striatum of ctl and cKO mice by using AAV to artificially stimulate G_i signaling upon clozapine N-oxide (CNO) administration (Figure 30A). 4 weeks after AAV injected, we observed ~97% of Sox9⁺ striatal astrocyte was labeled with mCherry, while only ~1% of NeuN⁺ neuron was labeled with mCherry (Figures 30B and 30C). To explore whether A1AR- G_i signaling is crucial to induce the activation of astrocytes, we injected CNO into GFAP-hM4Di expressed and GFAP-tdTomato expressed cKO mice at 2 hpi and 4 hpi to specifically stimulate G_i signaling in A1AR-deficient astrocytes (Figure 30D). We observed increased c-Fos expression, in terms of c-Fos intensity, in the striatal hM4Di-expressed astrocytes, compared to tdTomato-expressed astrocytes (Figure 30E), indicating that G_i signaling could reactive A1AR-deficient astrocytes in systemic inflammation. As activation of astrocyte contributed to microglia reactivity, we did double immunostaining of Iba1 and p65 to access the microglia reactivity (Figure 30F).

Consistently, we observed increased nuclear p65⁺ microglia in the striatum of GFAP-hM4Di expressed cKO mice, rather than GFAP-tdTomato expressed cKO mice (Figure 30E), suggesting that stimulation of astrocytic Gi signaling could enhance microglia response at the early phase of systemic inflammation.

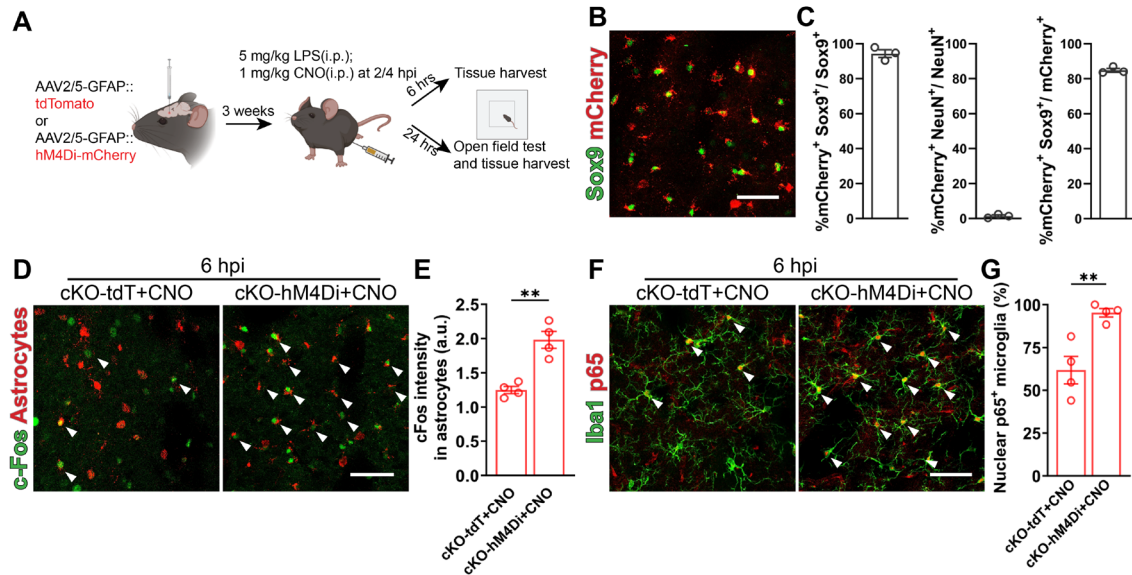


Figure 30. Activation of Gi signaling in A1AR-deficient astrocytes restored the astrocytic and microglial response to peripheral LPS challenge.

(A) Schematic illustration of activation of Gi signaling in A1AR deficient astrocytes experiment employing DREADD hM4Di and experimental plan. (B) Representative image of hM4Di expression indicated by mCherry in the Sox9⁺ astrocytes. Scale bar = 50 μ m. (C) hM4Di was expressed in 94% of striatal astrocytes, with > 84% specificity (n = 3 mice). (D) Representative images of immunolabeled reactive A1AR-deficient astrocytes by c-Fos immunostaining after LPS and CNO injection. Scale bar = 50 μ m. (E) Activation of hM4Di increased c-Fos expression in hM4Di-mCherry⁺ A1AR-deficient astrocytes after LPS injection (n = 4 mice per group). (F) Representative images of immunoreactivity of p65 in Iba1⁺ microglia in cKO mice with astrocytic tdT or hM4Di expression after LPS and CNO injection. Scale bars = 50 μ m. Arrowheads indicates Iba1⁺ microglia with nuclear p65 expression. (G) Nuclear p65⁺ microglia was increased in hM4Di-expressing cKO mice after LPS and CNO injection compared to ctl mice (n = 4 mice per group).

Furthermore, to explore the consequence of activating Gi signaling in A1AR-deficient astrocytes, we used cytokine array to explore the expression of proinflammatory factors in AAV-infected brain regions at 24 hpi. In line with previous results, we observed reduced cytokine expression in tdT-expressed cKO mice, compared to tdT-expressed ctl mice. However, we observed comparable expression levels in hM4Di-expressed ctl and cKO mice (Figures 31A and 31B). We also observed similar expression pattern in hM4Di-expressed cortex (Figures 31C and 31D). These results indicate a uniform and extensive impact of Gi signaling in astrocytes throughout various brain regions, which contributes to the advancement of neuroinflammation indicating activation of astrocytic Gi signaling at early phase of systemic inflammation promotes proinflammatory cytokine expression.

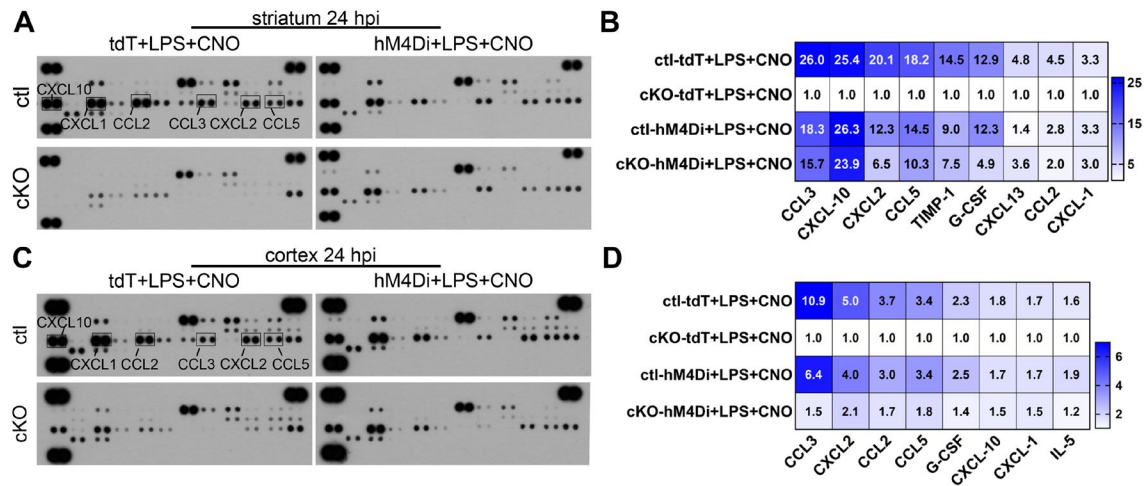


Figure 31. Activation of Gi signaling in A1AR-deficient astrocytes restored global inflammation to peripheral LPS challenge.

(A, C) The expression of 40 cytokines in the striatum and cortex of AAV-infected ctl and cKO mice was measured by a proteomic profiling assay after LPS and CNO injection. (B, D) Enhancing Gi signaling in cKO mice increased cytokine expression after LPS and CNO injection (samples from 3 mice were pooled for each group).

Additionally, we conducted the open-field test and observed that the alleviated LPS-induced depression-like behavior, in terms of total distance moved, in cKO mice could be exacerbated to the level of control mice upon enhance of astrocytic Gi signaling (Figures 31A-31C). In conclusion, our data indicates that systemic inflammation induced early reactivity of astrocyte via A1AR signaling plays a pivotal role in promoting neuroinflammation and driving the pathogenesis of SAE.

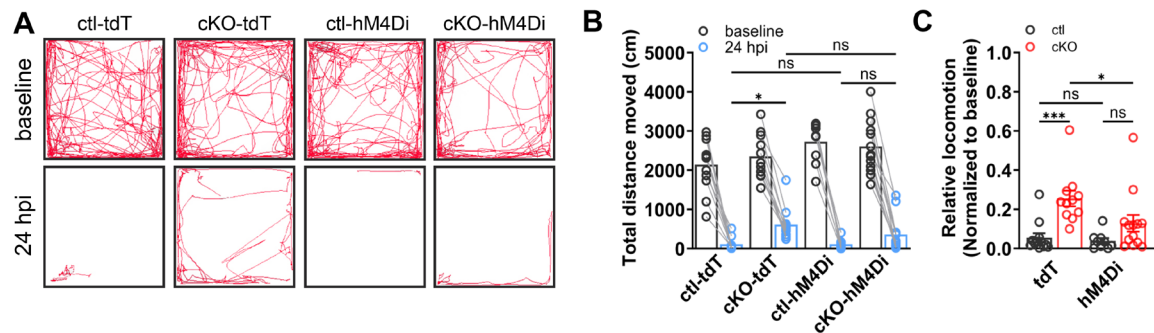


Figure 32. Activation of Gi signaling in A1AR-deficient astrocytes restored the depression-like behavior of mice to peripheral LPS challenge.

(A) Representative trajectory analysis digitally tracked movement of ctl and cKO mice injected with LPS and CNO in the open-field test at 24 hpi. (B, C) Enhancing Gi signaling in A1AR-deficient astrocyte reduced locomotion in the open-field test (n = 12 mice in ctl-tdT+CNO group, n = 11 mice in cKO-tdT+CNO group, n = 9 mice in ctl-hM4Di+CNO group, n = 13 mice in cKO-hM4Di+CNO group).

7. DISCUSSION

Systemic injection of LPS induced rapid and dramatic immune responses both in peripheral organs and CNS. Since the penetration of LPS across the BBB is minimal, it is still unclear which signals stimulate the CNS immune system (Banks and Robinson, 2010). Some studies suggested pro-inflammatory cytokines produced by peripheral immune systems can pass through BBB and induce neuroinflammation (Banks, 2005; Licinio and Wong, 1997; Pan and Kastin, 2002). In our study, we identified adenosine serves as an immune signaling, leading to early astrocyte reactivity, provoking microglial responses, and inducing neuronal dysfunction.

7.1. Extracellular adenosine level is increased in the blood and brain in systemic inflammation.

In accordance with earlier research, elevated levels of adenosine were found in the plasma of patients suffering from septic shock or volunteers who received an LPS injection (Martin et al., 2000; Ramakers et al., 2011). Similarly, we observed a rise in extracellular adenosine levels in the blood of rodents during the initial phase of systemic inflammation, peaking between 2-6 hours and returning to baseline levels at 12 and 24 hours post LPS injection. However, it's challenging to measure the cerebral extracellular molecular levels without causing injury or implantation. Recent studies directly demonstrated that peripheral LPS challenge increased extracellular ATP levels in the mouse brain Using a novel genetically modified ATP sensor (GRAB_{ATP1.0}), overcoming the technical challenges in separating intracellular and extracellular ATP *in vivo* (Wu et al., 2022). Of note, the extracellular adenosine level is highly determined by a close balance of production, transport, and degradation. Thus, it is plausible that elevated extracellular ATP in the brain also leads to adenosine accumulation. Here, we utilized an innovative genetically modified adenosine sensor called GRAB_{Ado} (with an EC₅₀ of approximately 60nM) to examine the levels of extracellular adenosine. Our findings indicate that there was a rapid increase in cerebral extracellular adenosine levels at 2 hpi, reaching a peak at 6 hpi, and remaining elevated for at least 24 hours. These results are consistent with previous findings in the context of inflammation or hypoxia (Benarroch, 2008; Chiu and Freund, 2014). However, the origin of extracellular adenosine in the brain is still elusive.

Additionally, adenosine can be transported by equilibrative nucleoside transporters (ENTs) or directly bypass the tight junctions (TJs) of endothelial cells due to its small size (Latini and Pedata, 2001). Moreover, adenosine can enhance the permeability of the BBB through A1 and A2a ARs in endothelial cells (Carman et al., 2011). Our 2P-LSM results strongly suggest that elevated adenosine level in the blood could increase the extracellular adenosine level in the brain, although the origin of central extracellular adenosine is still unclear.

7.2. Adenosine signaling provokes neuroinflammation via astrocytic A1ARs.

Adenosine signaling is widely acknowledged as a protective molecule that performs defensive roles in the CNS (Borea et al., 2016). Adenosine receptors are widely expressed in all the cells in the CNS. In our study, we observed enhanced proinflammatory cytokines

and chemokines in the brain upon peripheral adenosine, adenosine analogue, and A1AR agonist administration, which can be at least partially inhibited by intercepting astrocytic A1ARs. Increasing evidence indicates that adenosine can participate in immune modulation of the CNS mainly through A1 and A2a ARs, although recent studies suggest A2b and A3 ARs are also involved in immune modulation (Coppi et al., 2020; Farr et al., 2020; Martí Navia et al., 2020; Pedata et al., 2014). For example, the administration of A2a AR antagonist SCH-58261 induces regional-specific microglia activation in response to quinolinic acid injection (Minghetti et al., 2007), which also can reduce M1 markers and prevent the recruitment of activated microglia in other studies (Colella et al., 2018; Rebola et al., 2011). The reduced microglia activation is also observed by the application of an A3AR agonist, IB-MECA (Terayama et al., 2018). The selective A3AR agonist 2-Cl-IB-MECA was effective in controlling microglial reactivity induced by elevated hydrostatic pressure, with potentially positive implications in glaucoma (Ferreira-Silva et al., 2020). Additionally, a recent study shows activation of A2bAR promotes IL-6 production and proliferation in primary microglia culture (Merighi et al., 2017). Moreover, stimulation of A1AR inhibits microglial activation induced by ATP, and both A1AR agonists and A2aAR antagonists prevent inflammatory effects in microglia, showing a synergistic effect when combined (Luongo et al., 2014; Marucci et al., 2021). However, our data shows stimulation of A1AR provokes proinflammatory cytokine and chemokine expression, exacerbating microglia activation and neuroinflammation. Indeed, this pro-inflammatory effect is inhibited by knock-out astrocytic A1AR, suggesting A1AR has multiple functions in different glial cells, highlighting a complex interplay between peripheral and central adenosine signaling. Thus, adenosine, much like its precursor ATP, can function as a damage-associated molecular pattern (DAMP) molecule in neuroinflammation, with its effects varying depending on the context.

7.3. Loss of astrocytic A1ARs attenuate LPS-induced neuroinflammation.

7.3.1. A1AR activation was involved in triggering astrocyte reactivity at the early phase of neuroinflammation.

Astrocytes are the most abundant glia in the CNS, providing metabolites and growth factors to neurons, facilitating synapse plasticity, and regulating the balance of ions, fluid, and neurotransmitters in the extracellular environment (Lee et al., 2022; Pekny and Nilsson, 2005). In neuroinflammation, astrocytes, as immune-competent cells, can recognize danger signals, respond by secreting cytokines and chemokines, and activate adaptive immune defense (Cordiglieri and Farina, 2010). GFAP is most used to identify astrocyte activation, which is also a hallmark of CNS pathologies (Sofroniew, 2009). However, GFAP is not a proper marker to investigate the fast reactivity of astrocytes, due to its unaltered expression levels at the early stage of neuroinflammation. In our study, we find c-Fos expression is rapidly upregulated in cortical astrocytes, reaching ~100% at 6 hours post LPS injection, which could be a reliable marker for fast astrocytic activation. Indeed, our astrocytic RNA^{RiboTag} sequencing shows massive changes in the transcriptional profile of proinflammatory cytokine and chemokine 6 hours after LPS injection. In line with previous study (Hasel et al., 2021), many of these altered cytokines or chemokines (e.g., CXCL1, CXCL10, CXCL12, ICAM-1, LCN-2, MMP3) are released by reactive astrocytes,

contributing to the expression level of cytokines and chemokines in the brain. Of note, the specific molecules that initiate or enhance such rapid astrocyte reactivity to systemic inflammation remain unidentified (Patani et al., 2023). Our data shows removing astrocytic A1AR can significantly ameliorate this rapid astrocytic response and reduce the expression of cytokines and chemokines in the brain. Furthermore, deletion of astrocytic A1AR can also reduce the proinflammatory gene expression provoked by adenosine and its analogue. Our data provide solid evidence that humoral or extracellular small molecules, e.g., adenosine, can contribute to the reactivity of astrocytes at the early stages of LPS-induced systemic inflammation. In this context, adenosine could be a new member of DAMP molecules that mediate neuroinflammation by triggering the early response of astrocyte via A1AR signaling.

7.3.2. Astrocyte-microglia interaction in neuroinflammation.

Astrocytes and microglia can rapidly respond to systemic inflammation in terms of a robust change of transcriptomic profile (Hasel et al., 2021a; Kodali et al., 2021; Shemer et al., 2020). However, astrocytes were usually considered as the follower of microglia activation. In particular, a previous study shows microglial released IL-1 α , TNF- α , and C1q induce the A1 subtype of reactive astrocyte, which drives the apoptosis of neurons and oligodendrocytes (Liddel et al., 2017). Another study shows microglia TGF- β signaling inhibits astrocyte reactivation and reduces neuroinflammation after stroke (Cekanaviciute et al., 2014). Our RNA sequencing results show a series of proinflammatory genes rapidly upregulate in astrocytes 6 hours after LPS injection, which has been reported to promote microglial NF- κ B expression, microglial phagocytosis, and global neuroinflammation. The removal of A1AR signaling in astrocytes can partially inhibit the elevation of proinflammatory genes in astrocytes, further reducing microglia NF- κ B expression, microglial phagocytosis and overall neuroinflammation. Stimulation of astrocytic Gi signaling, downstream of A1AR, restores the microglia activation and global neuroinflammation in astrocytic A1AR-deficient mice at the early stages of systemic inflammation. Our findings suggest that adenosine acts as an immune signal in systemic inflammation, which triggers astrocyte via A1AR enhancing microglia activation at the early phase of systemic inflammation. Consequently, reactive microglia could also influence astrocyte reactivity, leading to a temporal change in the transcriptomic profiles to induce the neurotoxic A1 astrocyte at 24 hours post LPS challenge, suggesting that astrocytes are not only the targets of reactive microglia but also drive microglia activation in neuroinflammation.

7.3.3. Astrocyte mediates peripheral immune cell infiltration in neuroinflammation.

All four types of adenosine receptors existed in all immune cells, regulating the reactions of immune cells. For example, A1ARs promote neutrophil phagocytosis and chemotaxis, whereas A2a and A2b ARs inhibit neutrophil activation (Corriden et al., 2013; Riff et al., 2021; Wang and Chen, 2018). Moreover, adenosine has the ability to increase BBB permeability via A1 and A2a ARs, facilitating peripheral immune cell infiltration (Bynoe et al., 2015; Haskó et al., 2005; Kim and Bynoe, 2015). Furthermore, the microglia could migrate to blood vessels and impair BBB integrity via the CCL5-CCR5 axis in systemic

inflammation (Haruwaka et al., 2019). Our data shows increased adenosine levels in the blood at 2-6 hours post LPS injection, suggesting peripheral immune cells are activated at the early stages of systemic inflammation. Indeed, our data show elevated extracellular adenosine levels at 2-24 hours post LPS injection and an increased number of perivascular microglia, which increases the BBB permeability and promotes neutrophil infiltration. Due to each astrocyte extending its end-feet to envelop at least one blood vessel (Hösli et al., 2022), neutrophil infiltration and BBB dysfunction are prevented by the deletion of astrocytic A1AR. Our study provides new evidence that astrocytic A1AR mediates BBB function and peripheral immune cell infiltration.

7.3.4. Astrocyte-neuron interaction in neuroinflammation.

Astrocytes are essential for maintaining neuronal homeostasis in the central nervous system (CNS). They perform various functions such as providing metabolic and bioenergetic support, clearing neurotransmitters from synaptic clefts, buffering extracellular potassium, scavenging reactive oxygen species (ROS), regulating cerebral blood flow, and supporting axonal guidance and synaptogenesis. Disruptions in any of these functions can lead to significant neuronal dysfunction, as seen in various neurodegenerative diseases, such as AD, PD, and ALS. Astrocyte activation, or reactive astrocytosis, is a common response in almost all neurodegenerative diseases and is characterized by morphological changes and altered gene expression. This process is typically triggered by various stimuli, including PAMPs and DAMPs. Upon activation, astrocytes can produce a wide range of chemokines and inflammatory mediators that contribute to neuroinflammation. Our study provides new evidence that adenosine acts as a type of DAMP to modulate astrocytic proinflammatory response in LPS-induced neuroinflammation, leading to neuronal aberrant activation, LTP impairment, and sickness/depressive-like behavior. However, further investigation is needed to determine which astrocytic signaling pathways modulate microglia activation, neuronal dysfunction, and sickness/depressive behavior to gain new insights into the progression of neuroinflammation in sepsis.

8. CONCLUSION

In conclusion, we present compelling evidence that adenosine, a ubiquitous signaling molecule, serves as an immune mediator exacerbating neuroinflammation by initiating early astrocyte reactivity through A1 adenosine receptors (A1ARs). This process contributes to the pathogenesis of sepsis-associated encephalopathy (SAE). To the best of our knowledge, this is the first report of adenosine as a small molecule that induces such early astrocyte reactivity via A1AR signaling. Furthermore, our findings provide novel insights into the role of early reactive astrocytes, suggesting they act as drivers of neuroinflammation rather than simply being secondary responders to reactive microglia. Given that A1ARs are the most prevalent adenosine receptors in the brain and are also expressed in other cell types, including pericytes, microglia, and oligodendrocyte precursor cells, understanding their contribution to neuroinflammation could significantly advance our knowledge of adenosine signaling in inflammation-related CNS diseases. This understanding may lay the groundwork for future therapeutic strategies.

9. APPENDIX

Table S1. Detailed information for experiments and statistics

Figure	Panel	Data	Group	Number of samples	Statistical test	P value	Significance
9	B	Plasma adenosine (μM)	0 h	5 mice (3 male, 2 female)	Kruskal-Wallis test	0.1691 (0 h vs 2 h)	ns
			2 h	5 mice			
			6 h	(3 male, 2 female)			
			12 h	5 mice			
			24 h	(4 male, 1 female)			
				(4 male, 1 female)			
9	C	Evans blue in brain ($\mu\text{g/g}$)	0 h	(3 male, 2 female)	One-way ANOVA followed by Tukey's multiple comparisons test	0.7984 (0 h vs 2 h)	ns
			2 h	3 mice			
			6 h	(2 male, 1 female)			
			12 h	3 mice			
			24 h	(2 male, 1 female)			
				3 mice			
				(2 male, 1 female)			
				3 mice			
				(2 male, 1 female)			
				3 mice			
	(2 male, 1 female)						
10	D	GRAB _{Ado} intensity post LPS/saline injection	0 h	(2 male, 1 female)	Two-way ANOVA followed by Tukey's multiple comparisons test	>0.9999 (0 hpi LPS vs Saline)	ns
			2 h	3mice (3 male)			
			6 h				
			12 h				
			24 h				
11	D	GRAB _{Ado} intensity post adenosine/saline injection	baseline	6 mice (4 male, 2 female)	One-way ANOVA followed by Uncorrected Fisher's LSD	0.2270 (2 hpi LPS vs Saline)	ns
			saline	3 mice (2 male, 1 female)			

12	B	qPCR of adenosine injection	ado 5mg/kg	4 mice (2 male, 2 female)	0.3750 (5mg vs baseline); 0.0381	ns
			ado 10mg/kg	4 mice (2 male, 2 female)	(5mg vs saline); <0.0001 (10mg vs baseline); <0.0001	****
			ado 20mg/kg	5 mice (3 male, 2 female)	(10mg vs saline); <0.0001 (20mg vs baseline); <0.0001	****
			<i>Cxcl1</i>	PBS: 3 mice (2 male, 1 female); Adenosine: 3 mice (2 male, 1 female);	Unpaired Student's t-test	*
			<i>Cxcl10</i>		Unpaired Student's t-test	ns
			<i>Ccl2</i>		Unpaired Student's t-test	*
			<i>Ccl5</i>		Unpaired Student's t-test	ns
			<i>Lcn2</i>		Unpaired Student's t-test	****
			<i>Tnf</i>		Unpaired Student's t-test	***
			<i>Il1a</i>		Unpaired Student's t-test	***
			<i>Il1b</i>		Unpaired Student's t-test	ns
			<i>Il6</i>		Unpaired Student's t-test	ns
12	C	qPCR of NECA injection	<i>Cxcl1</i>	PBS: 3 mice (3 male) NECA: 3 mice (3 male)	<0.0001	****
			<i>Cxcl10</i>		<0.0001	****
			<i>Ccl2</i>		0.0015	**
			<i>Ccl5</i>		0.7522	ns
			<i>Lcn2</i>		<0.0001	****
			<i>Tnf</i>		0.008	**
			<i>Il1a</i>		0.1376	ns
			<i>Il1b</i>		0.5576	ns
			<i>Il6</i>		0.0005	***
			<i>Cxcl1</i>	PBS: 3 mice (3 male) CPA: 3 mice (3 male)	0.9379	ns
			<i>Cxcl10</i>		0.001	***
			<i>Ccl2</i>		0.0646	ns

13	A	qPCR of LPS+CPA injection	<i>Ccl5</i>	Unpaired Student's t-test	0.888	ns
			<i>Lcn2</i>	Unpaired Student's t-test	<0.0001	****
			<i>Tnf</i>	Unpaired Student's t-test	0.0259	*
			<i>Il1a</i>	Unpaired Student's t-test	0.0265	*
			<i>Il1b</i>	Unpaired Student's t-test	0.0011	**
			<i>Il6</i>	Unpaired Student's t-test	0.0071	**
			<i>Cxcl1</i>	LPS+PBS: 3 mice (3 male)	<0.0001	****
			<i>Cxcl10</i>	LPS+CPA: 3 mice (3 male)	<0.0001	****
			<i>Ccl2</i>	Unpaired Student's t-test	<0.0001	****
			<i>Ccl5</i>	Unpaired Student's t-test	<0.0001	****
			<i>Lcn2</i>	Unpaired Student's t-test	0.0025	**
			<i>Tnf</i>	Unpaired Student's t-test	<0.0001	****
			<i>Il1a</i>	Unpaired Student's t-test	<0.0001	****
			<i>Il1b</i>	Unpaired Student's t-test	<0.0001	****
			<i>Il6</i>	Unpaired Student's t-test	<0.0001	****
			13	B	qPCR of LPS+DPCPX injection	<i>Cxcl1</i>
<i>Cxcl10</i>	Unpaired Student's t-test	0.05381				ns
<i>Ccl2</i>	Unpaired Student's t-test	0.028765				*
<i>Ccl5</i>	Unpaired Student's t-test	0.730331				ns
<i>Lcn2</i>	Unpaired Student's t-test	0.041818				*
<i>Tnf</i>	Unpaired Student's t-test	0.037035				*
<i>Il1a</i>	Unpaired Student's t-test	0.579465				ns
<i>Il1b</i>	Unpaired Student's t-test	0.597726				ns
<i>Il6</i>	Unpaired Student's t-test	0.042695				*
<i>LPS+Veh</i>	3 mice (2 male, 1 female)	0.0206				*
<i>LPS+DPCPX</i>	3 mice (2 male, 1 female)					
<i>LPS+Veh</i>	3 mice (2 male, 1 female)					
<i>LPS+Veh</i>	3 mice (2 male, 1 female)					
<i>LPS+DPCPX</i>	3 mice (2 male, 1 female)					
<i>LPS+DPCPX</i>	3 mice (2 male, 1 female)					
13	C	cFos in neurons upon LPS and DPCPX injection				Unpaired Student's t-test

13	D	Nuclear p65 ⁺ microglia upon LPS and DPCPX injection	LPS+Veh	Unpaired Student's t-test	0.0074	**	
			LPS+DPCPX				
		Perivascular microglia upon LPS and DPCPX injection	LPS+Veh	Unpaired Student's t-test	0.0111	*	
			LPS+DPCPX				
14	C	Confirmation of Adora1 deletion by qPCR ^{ribotag}	ctl	One-way ANOVA followed by Tukey's multiple comparisons test	0.0097 (ctl vs. het)	**	
			het		0.0003 (ctl vs cKO)	***	
			cKO		0.0114 (het vs cKO)	*	
14	D	Confirmation of Adora1 deletion by RNA-seq	ctl		Unpaired Student's t-test	0.0012	**
			cKO				
16	A	qPCR of GLACx1AR ^{fl/fl} +CCPA injection	Cxcl1	Unpaired Student's t-test	0.439713	ns	
			Cxcl10	Unpaired Student's t-test	0.029192	*	
			Ccl2	Unpaired Student's t-test	0.003266	**	
			Ccl5	Unpaired Student's t-test	0.017025	*	
			Lcn2	Unpaired Student's t-test	0.106363	ns	
			Tnf	Unpaired Student's t-test	0.020531	*	
			Il1a	Unpaired Student's t-test	0.000335	***	
			Il1b	Unpaired Student's t-test	0.110556	ns	
			Il6	Unpaired Student's t-test	0.161959	ns	
16	B	qPCR of CXCTx1AR ^{fl/fl} +CCPA injection	Cxcl1	Unpaired Student's t-test	0.207236	ns	
			Cxcl10	Unpaired Student's t-test	0.846928	ns	
			Ccl2	Unpaired Student's t-test	0.192607	ns	
			Ccl5	Unpaired Student's t-test	0.706776	ns	
			Lcn2	Unpaired Student's t-test	0.424211	ns	
			Tnf	Unpaired Student's t-test	0.070882	ns	

16	C	qPCR of NGCEXA1AR ^{fl/fl} +CCPA injection	<i>I11a</i>	Unpaired Student's t-test	0.982785	ns
			<i>I11b</i>	Unpaired Student's t-test	0.283633	ns
			<i>I16</i>	Unpaired Student's t-test	0.094169	ns
			<i>Cxcl1</i>	Unpaired Student's t-test	0.603734	ns
			<i>Cxcl10</i>	ctl+CCPA: 4 mice (2 male, 2 female); NGCEXA1AR ^{fl/fl} +CCPA: 4 mice (2 male, 2 female);	0.588284	ns
			<i>Ccl2</i>	Unpaired Student's t-test	0.021384	*
			<i>Ccl5</i>	Unpaired Student's t-test	0.030104	*
			<i>Lcn2</i>	Unpaired Student's t-test	0.155522	ns
			<i>Tnf</i>	Unpaired Student's t-test	0.426998	ns
			<i>I11a</i>	Unpaired Student's t-test	0.406665	ns
			<i>I11b</i>	Unpaired Student's t-test	0.117039	ns
			<i>I16</i>	Unpaired Student's t-test	0.077284	ns
			17	B	cFos intensity in cortex	ctl_0 hpi
cKO_0 hpi						
ctl_2 hpi		0.7674 (2 hpi ctl vs cKO)				ns
cKO_2 hpi						
ctl_6 hpi		0.0008 (6 hpi ctl vs cKO)				***
cKO_6 hpi						
ctl_24 hpi		0.9082 (24 hpi ctl vs cKO)				ns
cKO_24 hpi						
ctl	Unpaired Student's t-test	0.0304				*
cKO						
22	B	Nuclear P65 ⁺ Microglia in cortex	ctl_0 hpi	Two-way ANOVA followed by Tukey's multiple comparisons test	0.9710 (0 hpi ctl vs cKO)	ns
			cKO_0 hpi			
			ctl_2 hpi		0.3172	ns

									(2 hpi ctl vs cKO)	
									<0.0001 (6 hpi ctl vs cKO)	****
22	B	Microglia density in cortex	ctl_0 hpi	4 mice (3 male, 1 female)					0.8677 (0 hpi ctl vs cKO)	ns
			ctl_6 hpi	4 mice						
			cKO_6 hpi	3 mice (1 male, 2 female)						
			ctl_0 hpi	4 mice						
			cKO_0 hpi	(2 male, 2 female) 4 mice						
			ctl_2 hpi	(2 male, 2 female) 3 mice (3 male)					0.3562 (2 hpi ctl vs cKO)	ns
			cKO_2 hpi	4 mice						
			ctl_6 hpi	(3 male, 1 female) 4 mice					0.6886 (6 hpi ctl vs cKO)	ns
			cKO_6 hpi	(2 male, 2 female) 3 mice						
22	C	Nuclear P65+ Microglia in striatum 6 hpi	ctl	(1 male, 2 female) 4 mice					0.0067	**
			cKO	(2 male, 2 female) 4 mice						
22	C	Microglia density in striatum 6 hpi	ctl	(2 male, 2 female) 4 mice					0.0867	ns
			cKO	(2 male, 2 female) 4 mice						
22	E	Sholl analysis	ctl_0 hpi	(2 male, 2 female) 3 mice (3 female)					0.5259	ns
			cKO_0 hpi	3 mice (3 female)						
			ctl_6 hpi	3 mice					0.0408	*
			cKO_6 hpi	(2 male, 2 female) 3 mice						
			ctl_24 hpi	(2 male, 2 female) 3 mice					0.0146	*
			cKO_24 hpi	(1 male, 2 female) 3 mice (3 female)						
22	F	Total process length	ctl_0 hpi	Same as Fig 21E					0.1658	ns
			cKO_0 hpi							
			ctl_6 hpi						<0.0001	*
			cKO_6 hpi							
			ctl_24 hpi						<0.0001	**

22	F	Microglia Area	cKO_24 hpi ctl_0 hpi cKO_0 hpi ctl_6 hpi cKO_6 hpi ctl_24 hpi cKO_24 hpi ctl_0 hpi cKO_0 hpi ctl_6 hpi cKO_6 hpi ctl_24 hpi cKO_24 hpi ctl_0 hpi cKO_0 hpi ctl_6 hpi cKO_6 hpi ctl_24 hpi cKO_24 hpi	Same as Fig 21E	Two-way ANOVA followed by Tukey's multiple comparisons test	0.0668 (0 hpi ctl vs cKO) <0.0001 (6 hpi ctl vs cKO) <0.0001 (24 hpi ctl vs cKO) <0.0001 (ctl 0 hpi vs 6 hpi) <0.0001 (ctl 0 hpi vs 24 hpi)	ns **** **** **** **** ****
22	F	# Microglia segments	ctl_0 hpi cKO_0 hpi ctl_6 hpi cKO_6 hpi ctl_24 hpi cKO_24 hpi	Same as Fig 21E	Two-way ANOVA followed by Tukey's multiple comparisons test	0.1702 (0 hpi ctl vs cKO) 0.1359 (6 hpi ctl vs cKO) 0.0021 (24 hpi ctl vs cKO) 0.0118 (ctl 0 hpi vs 6 hpi) <0.0001 (ctl 0 hpi vs 24 hpi)	ns ns ** * ****
22	F	Soma area	ctl_0 hpi cKO_0 hpi ctl_6 hpi cKO_6 hpi ctl_24 hpi cKO_24 hpi	Same as Fig 21E	Two-way ANOVA followed by Tukey's multiple comparisons test	0.2192 (0 hpi ctl vs cKO) 0.4711 (6 hpi ctl vs cKO) 0.8470 (24 hpi ctl vs cKO) 0.1029 (ctl 0 hpi vs 6 hpi) <0.0001 (ctl 0 hpi vs 24 hpi)	ns ns ns ns ****
24	B	Perivascular microglia	ctl_0 hpi cKO_0 hpi ctl_6 hpi cKO_6 hpi	4 mice (4 female) 4 mice (1 male, 3 female) 5 mice (3 male, 2 female) 3 mice (1 male, 2 female)	Two-way ANOVA followed by uncorrected Fisher's LSD	0.3337 0.0002	ns ***

24	C	CD31 ⁺ area	ctl_24 hpi cKO_24 hpi ctl_0 hpi cKO_0 hpi ctl_6 hpi cKO_6 hpi ctl_24 hpi cKO_24 hpi	6 mice (6 male) 4 mice (4 male) Same as Fig 23B	0.0034	*
24	D	Evans blue in brain (µg/g)	ctl cKO	3 mice (3 male) 3 mice (3 male)	0.0094	**
24	F	Ly6B ⁺ cells	ctl cKO	7 mice (6 male, 1 female) 8 mice (7 male, 1 female)	<0.0001	****
25	B	cFos intensity in cortical Neuron	ctl_0 hpi cKO_0 hpi ctl_6 hpi cKO_6 hpi ctl_24 hpi cKO_24 hpi	5 mice (4 male, 1 female) 3 mice (3 female) 5 mice (5 male) 4 mice (2 male, 2 female) 4 mice (4 female) 4 mice (1 male, 3 female)	0.4867 (0 hpi ctl vs cKO) 0.0365 (6 hpi ctl vs cKO) <0.0001 (24 hpi ctl vs cKO)	ns * ****
25	C	cFos intensity in striatum Neuron	ctl_24 hpi cKO_24 hpi	4 mice (2 male, 2 female) 4 mice	0.0441	*
26	B	EPSP slope (% of baseline)	ctl_0 hpi cKO_0 hpi ctl_6 hpi cKO_6 hpi	(2 male, 2 female) 11 slices from 4 mice (2 male, 2 female) 12 slices from 5 mice (2 male, 3 female) 9 slices from 4 mice (2 male, 2 female) 10 slices from 4 mice (1 male, 3 female)	0.43 <0.0001	ns ****

		ctl_24 hpi	11 slices from 4 mice (1 male, 3 female) 12 slices from 5 mice	Two-way ANOVA Multiple comparisons	<0.0001	****
		cKO_24 hpi				
26	C	LTP (% of baseline)	ctl_0 hpi cKO_0 hpi ctl_6 hpi cKO_6 hpi ctl_24 hpi cKO_24 hpi	Two-way ANOVA Multiple comparisons	0.7515	ns
			(1 male, 4 female) Same as Fig 25B		0.0464	*
					0.0154	*
27	C	Open field test 24 h post injection	ctl_PBS cKO_PBS ctl_LPS cKO_LPS	Two-way ANOVA Multiple comparisons	0.9731	ns
			15 mice (15 male) 12 mice (12 male) 12 mice (12 male) 10 mice (10 male)		0.0012	**
27	D	Sucrose preference test	ctl_baseline cKO_baseline e ctl_24-48 hpi cKO_24-48 hpi ctl_48-72 hpi cKO_48-72 hpi	Two-way ANOVA Multiple comparisons	0.408 (ctl_baseline vs cKO_baseline) <0.0001 (ctl_24-48 hpi vs cKO_24-48 hpi) 0.0019 (ctl_48-72 hpi vs cKO_48-72 hpi) 0.0016	ns **** **
			ctl 11 mice (5 male, 6 female) cKO 20 mice (8 male, 12 female)			
28	E	cFos intensity in astrocyte (LPS+Di_6 hplPS)	cKO-tdT cKO-h4MDI	Unpaired Student's t-test		**
			4 mice (2 male, 2 female) 4 mice (2 male, 2 female)		0.0072	**
28	G	Nuclear P65 ⁺ Microglia (LPS+Di_6 hplPS)	cKO-tdT cKO-h4MDI	Unpaired Student's t-test		**
			4 mice (2 male, 2 female) 4 mice (2 male, 2 female)			
30	B	Open field test (LPS+Di_24 hplPS)	ctl-tdT cKO-tdT	Mixed-effects model(REML) followed by uncorrected Fisher's LSD	0.0166	*
			12 mice (10 male, 2 female) 11 mice (8 male, 3 female)			

30	C	Relative locomotion (LPS+Di_24 hpLPS)	ctl-h4MDi	9 mice (7 male, 2 female)	0.2086	ns		
			cKO-h4MDi	13 mice (10 male, 3 female) Same as Fig 29B				
			ctl-tdT	Two-way ANOVA followed by Tukey's multiple comparisons test			0.0008	***
			cKO-tdT				0.2836	ns
							(ctl h4MDi vs cKO h4MDi)	
							0.0475	*
	(cKO tdT vs cKO h4MDi)							

10. REFERENCES

- Abbott, N.J., Rönnebeck, L., and Hansson, E. (2006). Astrocyte–endothelial interactions at the blood–brain barrier. *Nat Rev Neurosci* 7, 41-53.
- Adam, N., Kandelman, S., Mantz, J., Chrétien, F., and Sharshar, T. (2013). Sepsis-induced brain dysfunction. Expert review of anti-infective therapy 11, 211-221.
- Adrian, M., Weber, M., Tsai, M.-C., Glock, C., Kahn, O.I., Phu, L., Cheung, T.K., Meilandt, W.J., Rose, C.M., and Hoogenraad, C.C. (2023). Polarized microtubule remodeling transforms the morphology of reactive microglia and drives cytokine release. *Nature Communications* 14, 6322.
- Agapito Fonseca, J., Gameiro, J., Marques, F., and Lopes, J.A. (2020). Timing of initiation of renal replacement therapy in sepsis-associated acute kidney injury. *Journal of Clinical Medicine* 9, 1413.
- Allard, B., Allard, D., Buisseret, L., and Stagg, J. (2020). The adenosine pathway in immunoncology. *Nat Rev Clin Oncol* 17, 611-629.
- Andoh, M., and Koyama, R. (2021). Microglia regulate synaptic development and plasticity. *Dev Neurobiol* 81, 568-590.
- Andonegui, G., Zelinski, E.L., Schubert, C.L., Knight, D., Craig, L.A., Winston, B.W., Spanswick, S.C., Petri, B., Jenne, C.N., and Sutherland, J.C. (2018). Targeting inflammatory monocytes in sepsis-associated encephalopathy and long-term cognitive impairment. *JCI insight* 3.
- Banks, W.A. (2005). Blood-brain barrier transport of cytokines: a mechanism for neuropathology. *Current pharmaceutical design* 11, 973-984.
- Banks, W.A., Gray, A.M., Erickson, M.A., Salameh, T.S., Damodarasamy, M., Sheibani, N., Meabon, J.S., Wing, E.E., Morofuji, Y., and Cook, D.G. (2015). Lipopolysaccharide-induced blood-brain barrier disruption: roles of cyclooxygenase, oxidative stress, neuroinflammation, and elements of the neurovascular unit. *Journal of neuroinflammation* 12, 1-15.
- Banks, W.A., and Robinson, S.M. (2010). Minimal penetration of lipopolysaccharide across the murine blood–brain barrier. *Brain, behavior, and immunity* 24, 102-109.
- Barichello, T., Generoso, J.S., Domingui, D., Córneo, E., Giridharan, V.V., Sahrapour, T.A., Simões, L.R., da Rosa, M.I., Petronilho, F., and Ritter, C. (2022). Postmortem evidence of brain inflammatory markers and injury in septic patients: a systematic review. *Crit Care Med* 50, e241-e252.
- Benarroch, E. (2008). Adenosine and its receptors - Multiple modulatory functions and potential therapeutic targets for neurologic disease. *Neurology* 70, 231-236.
- Bhusal, A., Afridi, R., Lee, W.-H., and Suk, K. (2023). Bidirectional communication between microglia and astrocytes in neuroinflammation. *Current neuropharmacology* 21, 2020-2029.
- Bi, F., Huang, C., Tong, J., Qiu, G., Huang, B., Wu, Q., Li, F., Xu, Z., Bowser, R., and Xia, X.-G. (2013). Reactive astrocytes secrete Icn2 to promote neuron death. *Proceedings of the National Academy of Sciences* 110, 4069-4074.
- Boison, D. (2008). Adenosine as a neuromodulator in neurological diseases. *Current Opinion in Pharmacology* 8, 2-7.
- Boison, D., Chen, J., and Fredholm, B. (2010). Adenosine signaling and function in glial cells. *Cell Death and Differentiation* 17, 1071-1082.

- Boitsova, E., Morgun, A., Osipova, E., Pozhilenkova, E., Martinova, G., Frolova, O., Olovannikova, R., Tohidpour, A., Gorina, Y., and Panina, Y. (2018). The inhibitory effect of LPS on the expression of GPR81 lactate receptor in blood-brain barrier model in vitro. *J Neuroinflammat* 15 (1): 196.
- Borea, P.A., Gessi, S., Merighi, S., and Varani, K. (2016). Adenosine as a Multi-Signalling Guardian Angel in Human Diseases: When, Where and How Does it Exert its Protective Effects? *Trends Pharmacol Sci* 37, 419-434.
- Borea, P.A., Gessi, S., Merighi, S., Vincenzi, F., and Varani, K. (2017). Pathological overproduction: the bad side of adenosine. *Br J Pharmacol* 174, 1945-1960.
- Borst, K., Dumas, A.A., and Prinz, M. (2021). Microglia: Immune and non-immune functions. *Immunity* 54, 2194-2208.
- Bushong, E.A., Martone, M.E., Jones, Y.Z., and Ellisman, M.H. (2002). Protoplasmic astrocytes in CA1 stratum radiatum occupy separate anatomical domains. *J Neurosci* 22, 183-192.
- Bynoe, M.S., Viret, C., Yan, A., and Kim, D.G. (2015). Adenosine receptor signaling: a key to opening the blood-brain door. *Fluids Barriers CNS* 12, 20.
- Carman, A.J., Mills, J.H., Krenz, A., Kim, D.G., and Bynoe, M.S. (2011). Adenosine receptor signaling modulates permeability of the blood-brain barrier. *J Neurosci* 31, 13272-13280.
- Castro, L.V.G., Gonçalves-de-Albuquerque, C.F., and Silva, A.R. (2022). Polarization of microglia and its therapeutic potential in sepsis. *International Journal of Molecular Sciences* 23, 4925.
- Catalão, C.H.R., Santos-Júnior, N.N., da Costa, L.H.A., Souza, A.O., Alberici, L.C., and Rocha, M.J.A. (2017). Brain oxidative stress during experimental sepsis is attenuated by simvastatin administration. *Molecular neurobiology* 54, 7008-7018.
- Ceccatelli, S., Villar, M.J., Goldstein, M., and Hökfelt, T. (1989). Expression of c-Fos immunoreactivity in transmitter-characterized neurons after stress. *Proceedings of the National Academy of Sciences* 86, 9569-9573.
- Cekanaviciute, E., Dietrich, H.K., Axtell, R.C., Williams, A.M., Egusquiza, R., Wai, K.M., Koshy, A.A., and Buckwalter, M.S. (2014). Astrocytic TGF- β signaling limits inflammation and reduces neuronal damage during central nervous system *Toxoplasma* infection. *The Journal of Immunology* 193, 139-149.
- Cekic, C., and Linden, J. (2016). Purinergic regulation of the immune system. *Nat Rev Immunol* 16, 177-192.
- Chen, X.-L., Wang, Y., Peng, W.-W., Zheng, Y.-J., Zhang, T.-N., Wang, P.-J., Huang, J.-D., and Zeng, Q.-Y. (2018). Effects of interleukin-6 and IL-6/AMPK signaling pathway on mitochondrial biogenesis and astrocytes viability under experimental septic condition. *Int Immunopharmacol* 59, 287-294.
- Chiu, G., and Freund, G. (2014). Modulation of neuroimmunity by adenosine and its receptors: Metabolism to mental illness. *Metabolism-Clinical and Experimental* 63, 1491-1498.
- Chiu, G.S., Darmody, P.T., Walsh, J.P., Moon, M.L., Kwakwa, K.A., Bray, J.K., McCusker, R.H., and Freund, G.G. (2014). Adenosine through the A2A adenosine receptor increases IL-1 β in the brain contributing to anxiety. *Brain Behav Immun* 41, 218-231.
- Chung, H.-Y., Wickel, J., Brunkhorst, F.M., and Geis, C. (2020). Sepsis-Associated Encephalopathy: From Delirium to Dementia? *Journal of Clinical Medicine* 9, 703.

- Clarke, L.E., Liddelow, S.A., Chakraborty, C., Münch, A.E., Heiman, M., and Barres, B.A. (2018). Normal aging induces A1-like astrocyte reactivity. *Proceedings of the National Academy of Sciences* 115, E1896-E1905.
- Colella, M., Zinni, M., Pansiot, J., Cassanello, M., Mairesse, J., Ramenghi, L., and Baud, O. (2018). Modulation of microglial activation by adenosine A2a receptor in animal models of perinatal brain injury. *Frontiers in Neurology* 9, 605.
- Colonna, M., and Butovsky, O. (2017). Microglia function in the central nervous system during health and neurodegeneration. *Annual review of immunology* 35, 441-468.
- Coppi, E., Dettori, I., Cherchi, F., Bulli, I., Venturini, M., Lana, D., Giovannini, M.G., Pedata, F., and Pugliese, A.M. (2020). A2B adenosine receptors: when outsiders may become an attractive target to treat brain ischemia or demyelination. *International Journal of Molecular Sciences* 21, 9697.
- Cordiglieri, C., and Farina, C. (2010). Astrocytes exert and control immune responses in the brain. *Current Immunology Reviews* 6, 150-159.
- Corriden, R., Self, T., Akong - Moore, K., Nizet, V., Kellam, B., Briddon, S.J., and Hill, S.J. (2013). Adenosine - A3 receptors in neutrophil microdomains promote the formation of bacteria - tethering cytonemes. *EMBO reports* 14, 726-732.
- Cruz-Mendoza, F., Jauregui-Huerta, F., Aguilar-Delgadillo, A., García-Estrada, J., and Luquin, S. (2022). Immediate early gene c-fos in the brain: focus on glial cells. *Brain Sciences* 12, 687.
- Cupido, A., Catalin, B., Steffens, H., and Kirchhoff, F. (2014). Surgical procedures to study microglial motility in the brain and in the spinal cord by in vivo two-photon laser-scanning microscopy. *Laser scanning microscopy and quantitative image analysis of neuronal tissue*, 37-50.
- Dal-Pizzol, F., Rojas, H.A., Dos Santos, E.M., Vuolo, F., Constantino, L., Feier, G., Pasquali, M., Comim, C.M., Petronilho, F., and Gelain, D.P. (2013). Matrix metalloproteinase-2 and metalloproteinase-9 activities are associated with blood-brain barrier dysfunction in an animal model of severe sepsis. *Molecular neurobiology* 48, 62-70.
- Daneman, R., and Prat, A. (2015). The blood-brain barrier. *Cold Spring Harbor perspectives in biology* 7, a020412.
- Danielski, L.G., Giustina, A.D., Badawy, M., Barichello, T., Quevedo, J., Dal-Pizzol, F., and Petronilho, F. (2018). Brain barrier breakdown as a cause and consequence of neuroinflammation in sepsis. *Molecular Neurobiology* 55, 1045-1053.
- Dantzer, R., O'Connor, J.C., Freund, G.G., Johnson, R.W., and Kelley, K.W. (2008). From inflammation to sickness and depression: when the immune system subjugates the brain. *Nat Rev Neurosci* 9, 46-56.
- Deng, Y., Fang, M., Zhu, G., Zhou, Y., and Zeng, H. (2013). Role of microglia in the pathogenesis of sepsis-associated encephalopathy. *CNS & Neurological Disorders-Drug Targets (Formerly Current Drug Targets-CNS & Neurological Disorders)* 12, 720-725.
- Dozio, V., and Sanchez, J.-C. (2018). Profiling the proteomic inflammatory state of human astrocytes using DIA mass spectrometry. *Journal of Neuroinflammation* 15, 331.
- Duan, L., Zhang, X.D., Miao, W.Y., Sun, Y.J., Xiong, G., Wu, Q., Li, G., Yang, P., Yu, H., Li, H., et al. (2018). PDGFR β Cells Rapidly Relay Inflammatory Signal from the Circulatory System to Neurons via Chemokine CCL2. *Neuron* 100, 183-200.e188.

- Elmenhorst, D., Meyer, P.T., Winz, O.H., Matusch, A., Ermert, J., Coenen, H.H., Basheer, R., Haas, H.L., Zilles, K., and Bauer, A. (2007). Sleep deprivation increases A1 adenosine receptor binding in the human brain: a positron emission tomography study. *J Neurosci* 27, 2410-2415.
- Eng, L.F., Vanderhaeghen, J., Bignami, A., and Gerstl, B. (1971). An acidic protein isolated from fibrous astrocytes. *Brain research* 28, 351-354.
- Erikson, K., Tuominen, H., Vakkala, M., Liisanantti, J.H., Karttunen, T., Syrjälä, H., and Ala-Kokko, T.I. (2020). Brain tight junction protein expression in sepsis in an autopsy series. *Critical Care* 24, 1-7.
- Farr, S.A., Cuzzocrea, S., Esposito, E., Campolo, M., Niehoff, M.L., Doyle, T.M., and Salvemini, D. (2020). Adenosine A₃ receptor as a novel therapeutic target to reduce secondary events and improve neurocognitive functions following traumatic brain injury. *Journal of Neuroinflammation* 17, 1-14.
- Fang, L.-P., Zhao, N., Caudal, L.C., Chang, H.-F., Zhao, R., Lin, C.-H., Hainz, N., Meier, C., Bettler, B., and Huang, W. (2022). Impaired bidirectional communication between interneurons and oligodendrocyte precursor cells affects social cognitive behavior. *Nature Communications* 13, 1394.
- Fernandes, A., Silva, R.F., Falcao, A.S., Brito, M.A., and Brites, D. (2004). Cytokine production, glutamate release and cell death in rat cultured astrocytes treated with unconjugated bilirubin and LPS. *Journal of neuroimmunology* 153, 64-75.
- Ferreira-Silva, J., Aires, I.D., Boia, R., Ambrósio, A.F., and Santiago, A.R. (2020). Activation of adenosine A₃ receptor inhibits microglia reactivity elicited by elevated pressure. *International Journal of Molecular Sciences* 21, 7218.
- Fink, M.P. (2014). Animal models of sepsis. *Virulence* 5, 143-153.
- Fritz, M., Klawonn, A.M., Nilsson, A., Singh, A.K., Zajdel, J., Wilhelms, D.B., Lazarus, M., Löfberg, A., Jaarola, M., Kugelberg, U., et al. (2016). Prostaglandin-dependent modulation of dopaminergic neurotransmission elicits inflammation-induced aversion in mice. *J Clin Invest* 126, 695-705.
- Gentile, L.F., Nacionales, D.C., Lopez, M.C., Vanzant, E., Cuenca, A., Szpila, B.E., Cuenca, A.G., Joseph, A., Moore, F.A., and Leeuwenburgh, C. (2014). Host responses to sepsis vary in different low-lethality murine models. *Plos One* 9, e94404.
- Gimenez, M.A.T., Sim, J.E., and Russell, J.H. (2004). TNFR1-dependent VCAM-1 expression by astrocytes exposes the CNS to destructive inflammation. *Journal of neuroimmunology* 151, 116-125.
- Giovannoni, F., and Quintana, F.J. (2020). The role of astrocytes in CNS inflammation. *Trends in immunology* 41, 805-819.
- Gofton, T.E., and Young, G.B. (2012). Sepsis-associated encephalopathy. *Nature Reviews Neurology* 8, 557-566.
- Gosselin, D., and Rivest, S. (2008). MyD88 signaling in brain endothelial cells is essential for the neuronal activity and glucocorticoid release during systemic inflammation. *Molecular psychiatry* 13, 480-497.
- Gourine, A.V., Dale, N., Llaudet, E., Poputnikov, D.M., Spyer, K.M., and Gourine, V.N. (2007). Release of ATP in the central nervous system during systemic inflammation: real-time measurement in the hypothalamus of conscious rabbits. *J Physiol* 585, 305-316.

- Guo Q, Gobbo D, Zhao N, Zhang H, Awuku NO, Liu Q, Fang LP, Gampfer TM, Meyer MR, Zhao R, Bai X, Bian S, Scheller A, Kirchhoff F, Huang W (2024). Adenosine triggers early astrocyte reactivity that provokes microglial responses and drives the pathogenesis of sepsis-associated encephalopathy in mice. *Nat Commun* 15(1):6340.
- Haimon, Z., Volaski, A., Orthgiess, J., Boura-Halfon, S., Varol, D., Shemer, A., Yona, S., Zuckerman, B., David, E., Chappell-Maor, L., et al. (2018). Re-evaluating microglia expression profiles using RiboTag and cell isolation strategies. *Nature Immunology* 19, 636-644.
- Halassa, M.M., Fellin, T., Takano, H., Dong, J.-H., and Haydon, P.G. (2007). Synaptic islands defined by the territory of a single astrocyte. *J Neurosci* 27, 6473-6477.
- Han, H., Cho, J.W., Lee, S., Yun, A., Kim, H., Bae, D., Yang, S., Kim, C.Y., Lee, M., Kim, E., et al. (2018). TRRUST v2: an expanded reference database of human and mouse transcriptional regulatory interactions. *Nucleic Acids Res* 46, D380-d386.
- Han, Q., Lin, Q., Huang, P., Chen, M., Hu, X., Fu, H., He, S., Shen, F., Zeng, H., and Deng, Y. (2017). Microglia-derived IL-1 β contributes to axon development disorders and synaptic deficit through p38-MAPK signal pathway in septic neonatal rats. *Journal of neuroinflammation* 14, 1-18.
- Han, R.T., Kim, R.D., Molofsky, A.V., and Liddelow, S.A. (2021). Astrocyte-immune cell interactions in physiology and pathology. *Immunity* 54, 211-224.
- Handa, O., Stephen, J., and Cepinskas, G. (2008). Role of endothelial nitric oxide synthase-derived nitric oxide in activation and dysfunction of cerebrovascular endothelial cells during early onsets of sepsis. *American Journal of Physiology-Heart and Circulatory Physiology* 295, H1712-H1719.
- Hanisch, U.K. (2002). Microglia as a source and target of cytokines. *Glia* 40, 140-155.
- Haruwaka, K., Ikegami, A., Tachibana, Y., Ohno, N., Konishi, H., Hashimoto, A., Matsumoto, M., Kato, D., Ono, R., Kiyama, H., et al. (2019). Dual microglia effects on blood brain barrier permeability induced by systemic inflammation. *Nat Commun* 10, 5816.
- Hasegawa-Ishii, S., Inaba, M., Umegaki, H., Unno, K., Wakabayashi, K., and Shimada, A. (2016). Endotoxemia-induced cytokine-mediated responses of hippocampal astrocytes transmitted by cells of the brain-immune interface. *Scientific reports* 6, 25457.
- Hasel, P., Rose, I.V., Sadick, J.S., Kim, R.D., and Liddelow, S.A. (2021). Neuroinflammatory astrocyte subtypes in the mouse brain. *Nat Neurosci* 24, 1475-1487.
- Haskó, G., Pacher, P., Vizi, E.S., and Illes, P. (2005). Adenosine receptor signaling in the brain immune system. *Trends in pharmacological sciences* 26, 511-516.
- He, Q., Wang, J., and Hu, H. (2019). Illuminating the Activated Brain: Emerging Activity-Dependent Tools to Capture and Control Functional Neural Circuits. *Neurosci Bull* 35, 369-377.
- Hodes, G.E., Kana, V., Menard, C., Merad, M., and Russo, S.J. (2015). Neuroimmune mechanisms of depression. *Nat Neurosci* 18, 1386-1393.
- Hoogland, I., Houbolt, C., van Westerloo, D.J., van Gool, W.A., and van de Beek, D. (2015). Systemic inflammation and microglial activation: systematic review of animal experiments. *Journal of neuroinflammation* 12, 1-13.
- Hösl, L., Zuend, M., Bredell, G., Zanker, H.S., Porto de Oliveira, C.E., Saab, A.S., and Weber, B. (2022). Direct vascular contact is a hallmark of cerebral astrocytes. *Cell Rep* 39, 110599.

- Hotchkiss, R.S., and Karl, I.E. (2003). The pathophysiology and treatment of sepsis. *New England journal of medicine* 348, 138-150.
- Huang, W., Bai, X., Meyer, E., and Scheller, A. (2020). Acute brain injuries trigger microglia as an additional source of the proteoglycan NG2. *Acta Neuropathol Commun* 8, 146.
- Huang, W., Zhao, N., Bai, X., Karram, K., Trotter, J., Goebbels, S., Scheller, A., and Kirchhoff, F. (2014). Novel NG2-CreERT2 knock-in mice demonstrate heterogeneous differentiation potential of NG2 glia during development. *Glia* 62, 896-913.
- Huang, X., Guo, M., Zhang, Y., Xie, J., Huang, R., Zuo, Z., Saw, P.E., and Cao, M. (2023). Microglial IL-1RA ameliorates brain injury after ischemic stroke by inhibiting astrocytic CXCL1-mediated neutrophil recruitment and microvessel occlusion. *Glia* 71, 1607-1625.
- Izumi, Y., Cashikar, A.G., Krishnan, K., Paul, S.M., Covey, D.F., Mennerick, S.J., and Zorumski, C.F. (2021). A Proinflammatory Stimulus Disrupts Hippocampal Plasticity and Learning via Microglial Activation and 25-Hydroxycholesterol. *J Neurosci* 41, 10054-10064.
- Jesus, A.A., Passaglia, P., Santos, B.M., Rodrigues-Santos, I., Flores, R.A., Batalhao, M.E., Stabile, A.M., and Carnio, E.C. (2020). Chronic molecular hydrogen inhalation mitigates short and long-term memory loss in polymicrobial sepsis. *Brain research* 1739, 146857.
- Jha, M.K., Jo, M., Kim, J.-H., and Suk, K. (2019). Microglia-astrocyte crosstalk: an intimate molecular conversation. *The Neuroscientist* 25, 227-240.
- John, U., Patro, N., and Patro, I.K. (2023). Astroglialosis and associated CSPG upregulation adversely affect dendritogenesis, spinogenesis and synaptic activity in the cerebellum of a double-hit rat model of protein malnutrition (PMN) and lipopolysaccharide (LPS) induced bacterial infection. *J Chem Neuroanat* 131, 102286.
- Jung, S., Aliberti, J., Graemmel, P., Sunshine, M.J., Kreutzberg, G.W., Sher, A., and Littman, D.R. (2000). Analysis of fractalkine receptor CX(3)CR1 function by targeted deletion and green fluorescent protein reporter gene insertion. *Mol Cell Biol* 20, 4106-4114.
- Kang, S.S., Ren, Y., Liu, C.C., Kurti, A., Baker, K.E., Bu, G., Asmann, Y., and Fryer, J.D. (2018). Lipocalin-2 protects the brain during inflammatory conditions. *Mol Psychiatry* 23, 344-350.
- Kaplan, L., Chow, B.W., and Gu, C. (2020). Neuronal regulation of the blood–brain barrier and neurovascular coupling. *Nat Rev Neurosci* 21, 416-432.
- Kim, D., Paggi, J.M., Park, C., Bennett, C., and Salzberg, S.L. (2019). Graph-based genome alignment and genotyping with HISAT2 and HISAT-genotype. *Nat Biotechnol* 37, 907-+.
- Kim, D.-G., and Bynoe, M.S. (2015). A2A adenosine receptor regulates the human blood-brain barrier permeability. *Molecular neurobiology* 52, 664-678.
- Kim, J.H., Ko, P.W., Lee, H.W., Jeong, J.Y., Lee, M.G., Kim, J.H., Lee, W.H., Yu, R., Oh, W.J., and Suk, K. (2017). Astrocyte-derived lipocalin-2 mediates hippocampal damage and cognitive deficits in experimental models of vascular dementia. *Glia* 65, 1471-1490.
- Kingsley, S.M.K., and Bhat, B.V. (2016). Differential paradigms in animal models of sepsis. *Current infectious disease reports* 18, 1-11.
- Kirschuk, S., Parpura, V., and Verkhratsky, A. (2012). Sodium dynamics: another key to astroglial excitability? *Trends in neurosciences* 35, 497-506.

- Kislin, M., Mugantseva, E., Molotkov, D., Kuleskaya, N., Khirug, S., Kirilkin, I., Pryazhnikov, E., Kolikova, J., Toptunov, D., and Yuryev, M. (2014). Flat-floored air-lifted platform: a new method for combining behavior with microscopy or electrophysiology on awake freely moving rodents. *JoVE (Journal of Visualized Experiments)*, e51869.
- Klawonn, A.M., Fritz, M., Castany, S., Pignatelli, M., Canal, C., Similä, F., Tejada, H.A., Levinsson, J., Jaarola, M., Jakobsson, J., et al. (2021). Microglial activation elicits a negative affective state through prostaglandin-mediated modulation of striatal neurons. *Immunity* 54, 225-234.e226.
- Kodali, M.C., Chen, H., and Liao, F.F. (2021). Temporal unsnarling of brain's acute neuroinflammatory transcriptional profiles reveals panendothelitis as the earliest event preceding microgliosis. *Mol Psychiatry* 26, 3905-3919.
- Kolde, R. (2019). Pheatmap: Pretty Heatmaps, R Package Version 1.0. 12. 2019.
- Korcok, J., Wu, F., Tyml, K., Hammond, R.R., and Wilson, J.X. (2002). Sepsis inhibits reduction of dehydroascorbic acid and accumulation of ascorbate in astroglial cultures: intracellular ascorbate depletion increases nitric oxide synthase induction and glutamate uptake inhibition. *J Neurochem* 81, 185-193.
- Kozlov, A.V., Bahrami, S., Redl, H., and Szabo, C. (2017). Alterations in nitric oxide homeostasis during traumatic brain injury. *Biochimica et Biophysica Acta (BBA)-Molecular Basis of Disease* 1863, 2627-2632.
- Kwon, H.S., and Koh, S.-H. (2020). Neuroinflammation in neurodegenerative disorders: the roles of microglia and astrocytes. *Translational neurodegeneration* 9, 1-12.
- Latini, S., and Pedata, F. (2001). Adenosine in the central nervous system: release mechanisms and extracellular concentrations. *J Neurochem* 79, 463-484.
- Lee, H.-G., Wheeler, M.A., and Quintana, F.J. (2022). Function and therapeutic value of astrocytes in neurological diseases. *Nat Rev Drug Discov* 21, 339-358.
- Lee, J.-S., Jeon, Y.-J., Kang, J.-Y., Lee, S.-K., Lee, H.-D., and Son, C.-G. (2020). Aquilariae lignum methylene chloride fraction attenuates IL-1 β -driven neuroinflammation in BV2 microglial cells. *International journal of molecular sciences* 21, 5465.
- Lewis, A.J., Seymour, C.W., and Rosengart, M.R. (2016). Current murine models of sepsis. *Surgical infections* 17, 385-393.
- Li, Y., Yin, L., Fan, Z., Su, B., Chen, Y., Ma, Y., Zhong, Y., Hou, W., Fang, Z., and Zhang, X. (2020). Microglia: a potential therapeutic target for sepsis-associated encephalopathy and sepsis-associated chronic pain. *Frontiers in Pharmacology* 11, 600421.
- Liao, Y., Smyth, G.K., and Shi, W. (2014). featureCounts: an efficient general purpose program for assigning sequence reads to genomic features. *Bioinformatics* 30, 923-930.
- Licinio, J., and Wong, M.-L. (1997). Pathways and mechanisms for cytokine signaling of the central nervous system. *The Journal of clinical investigation* 100, 2941-2947.
- Liddelow, S.A., Guttenplan, K.A., Clarke, L.E., Bennett, F.C., Bohlen, C.J., Schirmer, L., Bennett, M.L., Münch, A.E., Chung, W.S., Peterson, T.C., et al. (2017). Neurotoxic reactive astrocytes are induced by activated microglia. *Nature* 541, 481-487.
- Linnerbauer, M., Wheeler, M.A., and Quintana, F.J. (2020). Astrocyte Crosstalk in CNS Inflammation. *Neuron* 108, 608-622.

- Liu, M.Y., Yin, C.Y., Zhu, L.J., Zhu, X.H., Xu, C., Luo, C.X., Chen, H.S., Zhu, D.Y., and Zhou, Q.G. (2018). Sucrose preference test for measurement of stress-induced anhedonia in mice. *Nat Protoc* 13, 1686-1698.
- Liu, Q., Guo, Q., Fang, L.P., Yao, H., Scheller, A., Kirchhoff, F., and Huang, W. (2023). Specific detection and deletion of the sigma-1 receptor widely expressed in neurons and glial cells in vivo. *J Neurochem* 164, 764-785.
- Liu, T., Zhang, L., Joo, D., and Sun, S.-C. (2017). NF- κ B signaling in inflammation. *Signal Transduction and Targeted Therapy* 2, 17023.
- Love, M.I., Huber, W., and Anders, S. (2014). Moderated estimation of fold change and dispersion for RNA-seq data with DESeq2. *Genome Biol* 15.
- Luongo, L., Guida, F., Imperatore, R., Napolitano, F., Gatta, L., Cristino, L., Giordano, C., Siniscalco, D., Di Marzo, V., and Bellini, G. (2014). The A1 adenosine receptor as a new player in microglia physiology. *Glia* 62, 122-132.
- Maccioni, R.B., González, A., Andrade, V., Cortés, N., Tapia, J.P., and Guzmán-Martínez, L. (2018). Alzheimer's Disease in the Perspective of Neuroimmunology. *The open neurology journal* 12, 50.
- Machado, F.R., Cavalcanti, A.B., Bozza, F.A., Ferreira, E.M., Carrara, F.S.A., Sousa, J.L., Caixeta, N., Salomao, R., Angus, D.C., and Azevedo, L.C.P. (2017). The epidemiology of sepsis in Brazilian intensive care units (the Sepsis PREvalence Assessment Database, SPREAD): an observational study. *The Lancet Infectious Diseases* 17, 1180-1189.
- Martin, C., Leone, M., Viviand, X., Ayem, M.-L., and Guieu, R. (2000). High adenosine plasma concentration as a prognostic index for outcome in patients with septic shock. *Crit Care Med* 28, 3198-3202.
- Martí Navia, A., Dal Ben, D., Lambertucci, C., Spinaci, A., Volpini, R., Marques-Morgado, I., Coelho, J.E., Lopes, L.V., Marucci, G., and Buccioni, M. (2020). Adenosine receptors as neuroinflammation modulators: role of A1 agonists and A2A antagonists. *Cells* 9, 1739.
- Marucci, G., Ben, D.D., Lambertucci, C., Navia, A.M., Spinaci, A., Volpini, R., and Buccioni, M. (2021). Combined therapy of A1AR agonists and A2AAR antagonists in neuroinflammation. *Molecules* 26, 1188.
- Masciantonio, M.G., Lee, C.K., Arpino, V., Mehta, S., and Gill, S.E. (2017). The balance between metalloproteinases and TIMPs: critical regulator of microvascular endothelial cell function in health and disease. *Progress in molecular biology and translational science* 147, 101-131.
- Mayo, L., Trauger, S.A., Blain, M., Nadeau, M., Patel, B., Alvarez, J.I., Mascanfroni, I.D., Yeste, A., Kivisäkk, P., Kallas, K., et al. (2014). Regulation of astrocyte activation by glycolipids drives chronic CNS inflammation. *Nat Med* 20, 1147-1156.
- Mazeraud, A., Pascal, Q., Verdonk, F., Heming, N., Chrétien, F., and Sharshar, T. (2016). Neuroanatomy and physiology of brain dysfunction in sepsis. *Clinics in chest medicine* 37, 333-345.
- Meneses, G., Rosetti, M., Espinosa, A., Florentino, A., Bautista, M., Diaz, G., Olvera, G., Barcena, B., Fleury, A., and Adalid-Peralta, L. (2018). Recovery from an acute systemic and central LPS-inflammation challenge is affected by mouse sex and genetic background. *Plos One* 13, e0201375.
- Meng, F., Guo, Z., Hu, Y., Mai, W., Zhang, Z., Zhang, B., Ge, Q., Lou, H., Guo, F., Chen, J., et al. (2019). CD73-derived adenosine controls inflammation and neurodegeneration by modulating dopamine signalling. *Brain* 142, 700-718.

- Merighi, S., Bencivenni, S., Vincenzi, F., Varani, K., Borea, P.A., and Gessi, S. (2017). A2B adenosine receptors stimulate IL-6 production in primary murine microglia through p38 MAPK kinase pathway. *Pharmacological Research* 117, 9-19.
- Michelon, C., Michels, M., Abatti, M., Vieira, A., Borges, H., Dominguni, D., Barichello, T., and Dal-Pizzol, F. (2020). The role of secretase pathway in long-term brain inflammation and cognitive impairment in an animal model of severe sepsis. *Molecular Neurobiology* 57, 1159-1169.
- Michels, M., Ávila, P., Pescador, B., Vieira, A., Abatti, M., Cucker, L., Borges, H., Goulart, A.I., Junior, C.C., and Barichello, T. (2019). Microglial cells depletion increases inflammation and modifies microglial phenotypes in an animal model of severe sepsis. *Molecular Neurobiology* 56, 7296-7304.
- Mikitsh, J.L., and Chacko, A.M. (2014). Pathways for small molecule delivery to the central nervous system across the blood-brain barrier. *Perspect Medicin Chem* 6, 11-24.
- Mills, J.H., Thompson, L.F., Mueller, C., Waickman, A.T., Jalkanen, S., Niemela, J., Airas, L., and Bynoe, M.S. (2008). CD73 is required for efficient entry of lymphocytes into the central nervous system during experimental autoimmune encephalomyelitis. *Proc Natl Acad Sci U S A* 105, 9325-9330.
- Minghetti, L., Greco, A., Potenza, R.L., Pezzola, A., Blum, D., Bantubungi, K., and Popoli, P. (2007). Effects of the adenosine A2A receptor antagonist SCH 58621 on cyclooxygenase-2 expression, glial activation, and brain-derived neurotrophic factor availability in a rat model of striatal neurodegeneration. *Journal of neuropathology and experimental neurology* 66, 363-371.
- Montoya, A., Elgueta, D., Campos, J., Chovar, O., Falcón, P., Matus, S., Alfaro, I., Bono, M.R., and Pacheco, R. (2019). Dopamine receptor D3 signalling in astrocytes promotes neuroinflammation. *Journal of Neuroinflammation* 16, 1-19.
- Mori, T., Tanaka, K., Buffo, A., Wurst, W., Kuhn, R., and Gotz, M. (2006). Inducible gene deletion in astroglia and radial glia - A valuable tool for functional and lineage analysis. *Glia* 54, 21-34.
- Motori, E., Puyal, J., Toni, N., Ghanem, A., Angeloni, C., Malaguti, M., Cantelli-Forti, G., Berninger, B., Conzelmann, K.K., Götz, M., et al. (2013). Inflammation-induced alteration of astrocyte mitochondrial dynamics requires autophagy for mitochondrial network maintenance. *Cell Metab* 18, 844-859.
- Nagai, J., Rajbhandari, A.K., Gangwani, M.R., Hachisuka, A., Coppola, G., Masmanidis, S.C., Faselow, M.S., and Khakh, B.S. (2019). Hyperactivity with disrupted attention by activation of an astrocyte synaptogenic cue. *Cell* 177, 1280-1292. e1220.
- Nagyoszi, P., Wilhelm, I., Farkas, A.E., Fazakas, C., Dung, N.T., Haskó, J., and Krizbai, I.A. (2010). Expression and regulation of toll-like receptors in cerebral endothelial cells. *Neurochem Int* 57, 556-564.
- Nava Catorce, M., and Gevorkian, G. (2016). LPS-induced murine neuroinflammation model: main features and suitability for pre-clinical assessment of nutraceuticals. *Current neuropharmacology* 14, 155-164.
- Nemzek, J.A., Hugunin, K., and Opp, M.R. (2008). Modeling sepsis in the laboratory: merging sound science with animal well-being. *Comparative medicine* 58, 120-128.
- Nishioku, T., Dohgu, S., Takata, F., Eto, T., Ishikawa, N., Kodama, K.B., Nakagawa, S., Yamauchi, A., and Kataoka, Y. (2009). Detachment of brain pericytes from the basal lamina is involved in disruption of the blood-brain barrier caused by lipopolysaccharide-induced sepsis in mice. *Cell Mol Neurobiol* 29, 309-316.

- Norden, D.M., Trojanowski, P.J., Villanueva, E., Navarro, E., and Godbout, J.P. (2016). Sequential activation of microglia and astrocyte cytokine expression precedes increased Iba-1 or GFAP immunoreactivity following systemic immune challenge. *Glia* 64, 300-316.
- Nunnally, M.E., and Patel, A. (2019). Sepsis-What's new in 2019? *Current Opinion in Anesthesiology* 32, 163-168.
- Oliet, S.H., Piet, R., and Poulain, D.A. (2001). Control of glutamate clearance and synaptic efficacy by glial coverage of neurons. *Science* 292, 923-926.
- Ozment, T.R., Ha, T., Breuel, K.F., Ford, T.R., Ferguson, D.A., Kalbfleisch, J., Schweitzer, J.B., Kelley, J.L., Li, C., and Williams, D.L. (2012). Scavenger receptor class a plays a central role in mediating mortality and the development of the pro-inflammatory phenotype in polymicrobial sepsis.
- Pan, W., and Kastin, A.J. (2002). TNF α transport across the blood–brain barrier is abolished in receptor knockout mice. *Experimental neurology* 174, 193-200.
- Parajuli, B., Horiuchi, H., Mizuno, T., Takeuchi, H., and Suzumura, A. (2015). CCL11 enhances excitotoxic neuronal death by producing reactive oxygen species in microglia. *Glia* 63, 2274-2284.
- Patani, R., Hardingham, G.E., and Liddelow, S.A. (2023). Functional roles of reactive astrocytes in neuroinflammation and neurodegeneration. *Nat Rev Neurol* 19, 395-409.
- Paukert, M., Agarwal, A., Cha, J., Doze, V.A., Kang, J.U., and Bergles, D.E. (2014). Norepinephrine controls astroglial responsiveness to local circuit activity. *Neuron* 82, 1263-1270.
- Rebola, N., Simões, A.P., Canas, P.M., Tomé, A.R., Andrade, G.M., Barry, C.E., Agostinho, P.M., Lynch, M.A., and Cunha, R.A. (2011). Adenosine A2A receptors control neuroinflammation and consequent hippocampal neuronal dysfunction. *J Neurochem* 117, 100-111.
- Pedata, F., Pugliese, A.M., Coppi, E., Dettori, I., Maraula, G., Cellai, L., and Melani, A. (2014). Adenosine A2A receptors modulate acute injury and neuroinflammation in brain ischemia. *Mediators of inflammation* 2014, 805198.
- Pekny, M., and Nilsson, M. (2005). Astrocyte activation and reactive gliosis. *Glia* 50, 427-434.
- Peng, W., Wu, Z., Song, K., Zhang, S., Li, Y., and Xu, M. (2020). Regulation of sleep homeostasis mediator adenosine by basal forebrain glutamatergic neurons. *Science* 369.
- Prescott, H.C., and Angus, D.C. (2018). Enhancing recovery from sepsis: a review. *Jama* 319, 62-75.
- Prescott, H.C., Osterholzer, J.J., Langa, K.M., Angus, D.C., and Iwashyna, T.J. (2016). Late mortality after sepsis: propensity matched cohort study. *bmj* 353.
- Prescott, H.C., Sussman, J.B., and Wiersinga, W.J. (2020). Postcritical illness vulnerability. *Current Opinion in Critical Care* 26, 500-507.
- Profaci, C.P., Munji, R.N., Pulido, R.S., and Daneman, R. (2020). The blood–brain barrier in health and disease: Important unanswered questions. *J Exp Med* 217.
- Qin, L., Wu, X., Block, M.L., Liu, Y., Breese, G.R., Hong, J.S., Knapp, D.J., and Crews, F.T. (2007). Systemic LPS causes chronic neuroinflammation and progressive neurodegeneration. *Glia* 55, 453-462.
- Ramakers, B.P., Riksen, N.P., van der Hoeven, J.G., Smits, P., and Pickkers, P. (2011). Modulation of innate immunity by adenosine receptor stimulation. *Shock* 36, 208-215.

- Reinhart, K., Daniels, R., Kissoon, N., Machado, F.R., Schachter, R.D., and Finfer, S. (2017). Recognizing sepsis as a global health priority—a WHO resolution. *New England Journal of Medicine* 377, 414-417.
- Rhee, C., Dantes, R., Epstein, L., Murphy, D.J., Seymour, C.W., Iwashyna, T.J., Kadri, S.S., Angus, D.C., Danner, R.L., and Fiore, A.E. (2017). Incidence and trends of sepsis in US hospitals using clinical vs claims data, 2009-2014. *Jama* 318, 1241-1249.
- Rieder, P., Gobbo, D., Stopper, G., Welle, A., Damo, E., Kirchhoff, F., and Scheller, A. (2022). Astrocytes and Microglia Exhibit Cell-Specific Ca. *Front Mol Neurosci* 15, 840948.
- Riff, R., Naamani, O., Mazar, J., Haviv, Y.S., Chaimovitz, C., and Douvdevani, A. (2021). A1 and A2A adenosine receptors play a protective role to reduce prevalence of autoimmunity following tissue damage. *Clinical & Experimental Immunology* 205, 278-287.
- Rittiner, J.E., Korboukh, I., Hull-Ryde, E.A., Jin, J., Janzen, W.P., Frye, S.V., and Zylka, M.J. (2012). AMP is an adenosine A1 receptor agonist. *Journal of Biological Chemistry* 287, 5301-5309.
- Robba, C., Crippa, I.A., and Taccone, F.S. (2018). Septic encephalopathy. *Current neurology and neuroscience reports* 18, 1-9.
- Rocheteau, P., Chatre, L., Briand, D., Mebarki, M., Jouvion, G., Bardou, J., Crochemore, C., Serrani, P., Lecci, P., and Latil, M. (2015). Sepsis induces long-term metabolic and mitochondrial muscle stem cell dysfunction amenable by mesenchymal stem cell therapy. *Nature communications* 6, 10145.
- Rudd, K.E., Johnson, S.C., Agesa, K.M., Shackelford, K.A., Tsoi, D., Kievlan, D.R., Colombara, D.V., Ikuta, K.S., Kissoon, N., and Finfer, S. (2020). Global, regional, and national sepsis incidence and mortality, 1990–2017: analysis for the Global Burden of Disease Study. *The Lancet* 395, 200-211.
- Rummel, C., Inoue, W., Poole, S., and Luheshi, G.N. (2010). Leptin regulates leukocyte recruitment into the brain following systemic LPS-induced inflammation. *Mol Psychiatry* 15, 523-534.
- Sankowski, R., Mader, S., and Valdés-Ferrer, S.I. (2015). Systemic inflammation and the brain: novel roles of genetic, molecular, and environmental cues as drivers of neurodegeneration. *Frontiers in cellular neuroscience* 9, 28.
- Sanz, E., Yang, L., Su, T., Morris, D.R., McKnight, G.S., and Amieux, P.S. (2009). Cell-type-specific isolation of ribosome-associated mRNA from complex tissues. *Proc Natl Acad Sci U S A* 106, 13939-13944.
- Scammell, T.E., Arrigoni, E., Thompson, M.A., Ronan, P.J., Saper, C.B., and Greene, R.W. (2003). Focal deletion of the adenosine A1 receptor in adult mice using an adeno-associated viral vector. *J Neurosci* 23, 5762-5770.
- Schmidt, S.I., Bogetofte, H., Ritter, L., Agergaard, J.B., Hammerich, D., Kabiljagic, A.A., Wlodarczyk, A., Lopez, S.G., Sørensen, M.D., Jørgensen, M.L., et al. (2021). Microglia-Secreted Factors Enhance Dopaminergic Differentiation of Tissue- and iPSC-Derived Human Neural Stem Cells. *Stem Cell Reports* 16, 281-294.
- Sebastiao, A.M., and Ribeiro, J.A. (2009). Adenosine receptors and the central nervous system. *Adenosine receptors in health and disease*, 471-534.
- Semmler, A., Okulla, T., Sastre, M., Dumitrescu-Ozimek, L., and Heneka, M.T. (2005). Systemic inflammation induces apoptosis with variable vulnerability of different brain regions. *Journal of chemical neuroanatomy* 30, 144-157.

- Shankar-Hari, M., Ambler, M., Mahalingasivam, V., Jones, A., Rowan, K., and Rubenfeld, G.D. (2016). Evidence for a causal link between sepsis and long-term mortality: a systematic review of epidemiologic studies. *Critical Care* 20, 1-13.
- Shankar-Hari, M., Saha, R., Wilson, J., Prescott, H.C., Harrison, D., Rowan, K., Rubenfeld, G.D., and Adhikari, N.K. (2020). Rate and risk factors for rehospitalisation in sepsis survivors: systematic review and meta-analysis. *Intensive care medicine* 46, 619-636.
- Shemer, A., Scheyltjens, I., Frumer, G.R., Kim, J.S., Grozovski, J., Ayanaw, S., Dassa, B., Van Hove, H., Chappell-Maor, L., Boura-Halfon, S., et al. (2020). Interleukin-10 Prevents Pathological Microglia Hyperactivation following Peripheral Endotoxin Challenge. *Immunity* 53, 1033-1049.e1037.
- Shimada, A., and Hasegawa-Ishii, S. (2017). Histological architecture Underlying Brain-immune Cell-Cell interactions and the Cerebral response to systemic inflammation. *Front Immunol* 8, 17.
- Shulyatnikova, T., and Verkhatsky, A. (2020). Astroglia in sepsis associated encephalopathy. *Neurochem Res* 45, 83-99.
- Singer, M., Deutschman, C.S., Seymour, C.W., Shankar-Hari, M., Annane, D., Bauer, M., Bellomo, R., Bernard, G.R., Chiche, J.-D., and Coopersmith, C.M. (2016). The third international consensus definitions for sepsis and septic shock (Sepsis-3). *Jama* 315, 801-810.
- Sofroniew, M.V. (2009). Molecular dissection of reactive astrogliosis and glial scar formation. *Trends in neurosciences* 32, 638-647.
- Sofroniew, M.V. (2020). Astrocyte Reactivity: Subtypes, States, and Functions in CNS Innate Immunity. *Trends Immunol* 41, 758-770.
- Song, G., Liang, H., Song, H., Ding, X., Wang, D., Zhang, X., and Sun, T. (2022). Metformin Improves the Prognosis of Adult Mice with Sepsis-Associated Encephalopathy Better than That of Aged Mice. *Journal of Immunology Research* 2022.
- Sonneville, R., de Montmollin, E., Poujade, J., Garrouste-Orgeas, M., Souweine, B., Darmon, M., Mariotte, E., Argaud, L., Barbier, F., Goldgran-Toledano, D., et al. (2017). Potentially modifiable factors contributing to sepsis-associated encephalopathy. *Intensive Care Medicine* 43, 1075-1084.
- Sonneville, R., Verdonk, F., Rauturier, C., Klein, I.F., Wolff, M., Annane, D., Chretien, F., and Sharshar, T. (2013). Understanding brain dysfunction in sepsis. *Annals of intensive care* 3, 1-11.
- Stopper, G., Caudal, L.C., Rieder, P., Gobbo, D., Stopper, L., Felix, L., Everaerts, K., Bai, X., Rose, C.R., Scheller, A., et al. (2023). Novel algorithms for improved detection and analysis of fluorescent signal fluctuations. *Pflugers Arch*.
- Stortz, J.A., Raymond, S.L., Mira, J.C., Moldawer, L.L., Mohr, A.M., and Efron, P.A. (2017). Murine models of sepsis and trauma: can we bridge the gap? *ILAR journal* 58, 90-105.
- Terayama, R., Tabata, M., Maruhama, K., and Iida, S. (2018). A 3 adenosine receptor agonist attenuates neuropathic pain by suppressing activation of microglia and convergence of nociceptive inputs in the spinal dorsal horn. *Experimental brain research* 236, 3203-3213.
- Tian, M., Qingzhen, L., Zhiyang, Y., Chunlong, C., Jiao, D., Zhang, L., and Li, W. (2019). Attractylone attenuates sepsis-associated encephalopathy and cognitive dysfunction by inhibiting microglial activation and neuroinflammation. *Journal of Cellular Biochemistry* 120, 7101-7108.

- Vachharajani, V., Russell, J.M., Scott, K.L., Conrad, S., Stokes, K.Y., Tallam, L., Hall, J., and Granger, D.N. (2005). Obesity exacerbates sepsis-induced inflammation and microvascular dysfunction in mouse brain. *Microcirculation* 12, 183-194.
- van der Poll, T. (2012). Preclinical sepsis models. *Surgical infections* 13, 287-292.
- van der Poll, T., van de Veerdonk, F.L., Scicluna, B.P., and Netea, M.G. (2017). The immunopathology of sepsis and potential therapeutic targets. *Nature Reviews Immunology* 17, 407-420.
- Van Gool, W.A., Van de Beek, D., and Eikelenboom, P. (2010). Systemic infection and delirium: when cytokines and acetylcholine collide. *The Lancet* 375, 773-775.
- Varatharaj, A., and Galea, I. (2017). The blood-brain barrier in systemic inflammation. *Brain, behavior, and immunity* 60, 1-12.
- Verkhatsky, A., Matteoli, M., Parpura, V., Mothet, J.P., and Zorec, R. (2016). Astrocytes as secretory cells of the central nervous system: idiosyncrasies of vesicular secretion. *The EMBO journal* 35, 239-257.
- Verkhatsky, A., Nedergaard, M., and Hertz, L. (2015). Why are astrocytes important? *Neurochem Res* 40, 389-401.
- Vidal-Itriago, A., Radford, R.A.W., Aramideh, J.A., Maurel, C., Scherer, N.M., Don, E.K., Lee, A., Chung, R.S., Graeber, M.B., and Morsch, M. (2022). Microglia morphophysiological diversity and its implications for the CNS. *Front Immunol* 13, 997786.
- Villeda, S.A., Luo, J., Mosher, K.I., Zou, B., Britschgi, M., Bieri, G., Stan, T.M., Fainberg, N., Ding, Z., and Eggel, A. (2011). The ageing systemic milieu negatively regulates neurogenesis and cognitive function. *Nature* 477, 90-94.
- Vutukuri, R., Brunkhorst, R., Kestner, R.I., Hansen, L., Bouzas, N.F., Pfeilschifter, J., Devraj, K., and Pfeilschifter, W. (2018). Alteration of sphingolipid metabolism as a putative mechanism underlying LPS-induced BBB disruption. *J Neurochem* 144, 172-185.
- Wang, H., Ardiles, A.O., Yang, S., Tran, T., Posada-Duque, R., Valdivia, G., Baek, M., Chuang, Y.A., Palacios, A.G., Gallagher, M., et al. (2016). Metabotropic Glutamate Receptors Induce a Form of LTP Controlled by Translation and Arc Signaling in the Hippocampus. *J Neurosci* 36, 1723-1729.
- Wang, H., Hong, L.-J., Huang, J.-Y., Jiang, Q., Tao, R.-R., Tan, C., Lu, N.-N., Wang, C.-K., Ahmed, M.M., and Lu, Y.-M. (2015). P2RX7 sensitizes Mac-1/ICAM-1-dependent leukocyte-endothelial adhesion and promotes neurovascular injury during septic encephalopathy. *Cell research* 25, 674-690.
- Wang, X., and Chen, D. (2018). Purinergic Regulation of Neutrophil Function. *Front Immunol* 9.
- Wei, C., Li, W., and Chen, J. (2011). Normal and abnormal functions of adenosine receptors in the central nervous system revealed by genetic knockout studies. *Biochimica Et Biophysica Acta-Biomembranes* 1808, 1358-1379.
- Welsh, T.G., and Kucenas, S. (2018). Purinergic signaling in oligodendrocyte development and function. *J Neurochem* 145, 6-18.
- Widmann, C.N., and Heneka, M.T. (2014). Long-term cerebral consequences of sepsis. *The Lancet Neurology* 13, 630-636.

- Wolf, S.A., Boddeke, H., and Kettenmann, H. (2017). Microglia in physiology and disease. *Annual review of physiology* 79, 619-643.
- Wu, K.C., Lee, C.Y., Chern, Y., and Lin, C.J. (2021). Amelioration of lipopolysaccharide-induced memory impairment in equilibrative nucleoside transporter-2 knockout mice is accompanied by the changes in glutamatergic pathways. *Brain Behav Immun* 96, 187-199.
- Wu, Y., Li, P., Goodwin, A.J., Cook, J.A., Halushka, P.V., Zingarelli, B., and Fan, H. (2020). miR-145a Regulation of Pericyte Dysfunction in a Murine Model of Sepsis. *J Infect Dis* 222, 1037-1045.
- Wu, Z., Cui, Y., Wang, H., Wu, H., Wan, Y., Li, B., Wang, L., Pan, S., Peng, W., Dong, A., et al. (2023). Neuronal activity-induced, equilibrative nucleoside transporter-dependent, somatodendritic adenosine release revealed by a GRAB sensor. *Proceedings of the National Academy of Sciences* 120, e2212387120.
- Wu, Z., He, K., Chen, Y., Li, H., Pan, S., Li, B., Liu, T., Xi, F., Deng, F., Wang, H., et al. (2022). A sensitive GRAB sensor for detecting extracellular ATP in vitro and in vivo. *Neuron* 110, 770-782.e775.
- Xin, Y., Tian, M., Deng, S., Li, J., Yang, M., Gao, J., Pei, X., Wang, Y., Tan, J., Zhao, F., et al. (2023). The Key Drivers of Brain Injury by Systemic Inflammatory Responses after Sepsis: Microglia and Neuroinflammation. *Molecular Neurobiology* 60, 1369-1390.
- Yamazaki, Y., Shinohara, M., Shinohara, M., Yamazaki, A., Murray, M.E., Liesinger, A.M., Heckman, M.G., Lesser, E.R., Parisi, J.E., and Petersen, R.C. (2019). Selective loss of cortical endothelial tight junction proteins during Alzheimer's disease progression. *Brain* 142, 1077-1092.
- Yazdan-Ashoori, P., Liaw, P., Toltl, L., Webb, B., Kilmer, G., Carter, D.E., and Fraser, D.D. (2011). Elevated plasma matrix metalloproteinases and their tissue inhibitors in patients with severe sepsis. *Journal of critical care* 26, 556-565.
- Ye, B., Tao, T., Zhao, A., Wen, L., He, X., Liu, Y., Fu, Q., Mi, W., and Lou, J. (2019). Blockade of IL-17A/IL-17R pathway protected mice from sepsis-associated encephalopathy by inhibition of microglia activation. *Mediators of inflammation* 2019.
- Yu, G., Wang, L.-G., Han, Y., and He, Q.-Y. (2012). clusterProfiler: an R package for comparing biological themes among gene clusters. *Omics: a journal of integrative biology* 16, 284-287.
- Zeng, H., He, X., Tuo, Q.H., Liao, D.F., Zhang, G.Q., and Chen, J.X. (2016). LPS causes pericyte loss and microvascular dysfunction via disruption of Sirt3/angiopoietins/Tie-2 and HIF-2 α /Notch3 pathways. *Sci Rep* 6, 20931.
- Zhao, G.-J., Li, D., Zhao, Q., Lian, J., Hu, T.-T., Hong, G.-I., Yao, Y.-M., and Lu, Z.-Q. (2016). Prognostic value of plasma tight-junction proteins for sepsis in emergency department: an observational study. *Shock* 45, 326-332.
- Zhao, N., Huang, W., Cătălin, B., Scheller, A., and Kirchhoff, F. (2021). L-Type Ca²⁺ channels of NG2 glia determine proliferation and NMDA receptor-dependent plasticity. *Frontiers in Cell and Developmental Biology* 9, 759477.
- Zhao, Y.-Z., Gao, Z.-Y., Ma, L.-Q., Zhuang, Y.-Y., and Guan, F.-L. (2017). Research on biogenesis of mitochondria in astrocytes in sepsis-associated encephalopathy models. *European Review for Medical & Pharmacological Sciences* 21.

Zhao, Z., Shang, X., Chen, Y., Zheng, Y., Huang, W., Jiang, H., Lv, Q., Kong, D., Jiang, Y., and Liu, P. (2020). Bacteria elevate extracellular adenosine to exploit host signaling for blood-brain barrier disruption. *Virulence* 11, 980-994.

Zhou, Y., Zhou, B., Pache, L., Chang, M., Khodabakhshi, A.H., Tanaseichuk, O., Benner, C., and Chanda, S.K. (2019). Metascape provides a biologist-oriented resource for the analysis of systems-level datasets. *Nature communications* 10, 1523.

11. ACKNOWLEDGEMENTS

I would like to express my heartfelt gratitude to everyone who contributed to the successful progress of my project.

First and foremost, I would like to express my deepest gratitude to my mentor, Prof. Frank Kirchhoff, for his unwavering support and encouragement during the entire research process. I am incredibly thankful for giving me the opportunity to work in your lab and for teaching me the history and knowledge in research, as well as for showing me the healthy lifestyle with cycling and running which inspired my academic and daily life.

I am filled with gratitude towards my supervisor, Dr. Wenhui Huang, for guiding me, motivating me, and providing me with invaluable feedback during the entire research process. Your expertise and support have played a crucial role in shaping this thesis into its final form which not only helped me grow professionally but also personally. I sincerely appreciate your guidance and encouragement along my way.

I would also like to thank all the current and former members of the Kirchhoff team for their collaboration and dedication. Special thanks to Dr. Davide Gobbo for helping with 2P-LSM imaging and data analysis, Dr. Na Zhao for patch-clamp, Dr. Gebhard Stopper for developing MSparkles, Dr. Laura Caudal for helping of LPC injection, Dr. Xianshu Bai for teaching me many experiments, Dr. Phillip Rieder for introducing 2P-LSM setup, and Dr. Anja Scheller for the support and stimulating discussions. I am grateful to Dr. Laura Stopper and Dr. Carmen Vanessa Kasakow for the first birthday hug in my life and sorry for all the inconvenience I caused. Many thanks to Seth Rhea, Buttigieg Emeline, Frank Rhode, Daniel Schauenburg, Ting Zhang, Nana-Oye Awuku, Dr. Erika Meyer, Paula Gelonch-Capell, Dr. Mariza Bortolanza, Dr. Naielly Rodrigues da Silva, and Ute Legler for their invaluable insights, critiques, and enthusiasm in sharpening my ideas and pushing me to think more deeply about my research. Your friendship and encouragement have made my academic journey more fulfilling and enjoyable.

To my friends, Dr. Qing Liu, Dr. Lipao Fang, Xiangda Zhou, and Dr. Xiaoyu Cai, thank you for your unwavering support, encouragement, and understanding during this demanding period of my life. Your presence has helped me keep my sanity and balance my academic pursuits with my personal life. Your unwavering belief in me has been a constant source of motivation, and I am deeply grateful for your friendship.

Finally, to my family and my girlfriend, thank you for your love, encouragement, and unwavering support. Your sacrifices and support have made it possible for me to pursue my academic dreams, and I am forever grateful for your unwavering belief in me. Your support has been the foundation of my academic journey, and I am blessed to have you in my life.

To each one of you, I extend my heartfelt thanks for your valuable contributions and companionship. I wish you all the best.

12. CURRICULUM VITAE AND LIST OF PUBLICATIONS

The curriculum vitae was removed from the electronic version of the doctoral thesis for reasons of data protection.

